MULTIPHASE FLOW DISPLACEMENT APPLICATION OF NOVEL GREEN NANOPARTICLE SYNTHESIS IN GLYCEROL AND RECONFIGURABLE NANOEMULSIONS IN RESERVOIR-ON-A-CHIP

A THESIS SUBMITTED TO

THE GRADUATE SCHOOL OF ENGINEERING AND SCIENCE

OF BILKENT UNIVERSITY

IN PARTIAL FULFILLMENT OF THE REQUIREMENTS FOR

THE DEGREE OF

MASTER OF SCIENCE

IN MATERIAL SCIENCE AND NANOTECHNOLOGY

By

Robab Jahangir

January 2024

Multiphase Flow Displacement Application of Novel Green Nanoparticle Synthesis in Glycerol and Reconfigurable Nanoemulsions in Reservoir-on-a-Chip
By Robab Jahangir
January 2024

We certify that we have read this thesis and that in our opinion it is fully adequate, in scope and in quality, as a thesis for the degree of Master of Science.

Bülend Ortaç(Advisor)

Gürkan Yeşiloz(Co-Advisor)

Wonmi Ahn

Işıl Gerçek Beşkardeş

Approved for the Graduate School of Engineering and Science:

Orhan Arıkan
Director of the Graduate School

ABSTRACT

MULTIPHASE FLOW DISPLACEMENT APPLICATION OF NOVEL GREEN NANOPARTICLE SYNTHESIS IN GLYCEROL AND RECONFIGURABLE NANOEMULSIONS IN RESERVOIR-ON-A-CHIP

Robab Jahangir
M.S. in Material Science and Nanotechnology
Advisor: Bülend Ortaç
Co-Advisor: Gürkan Yeşiloz
January 2024

Nanofluids and oil in water (O/W) nano/micro emulsions have been extensively investigated for their potential in multiphase displacement applications such as enhanced oil recovery (EOR). However, the potential of metal nanofluids and water-in-oil nanoemulsions (W/O) has not been readily studied and the underlying mechanisms are yet to be investigated. Moreover, most nanofluids pose toxicity risks to reservoirs, and a high polydispersity index of conventionally synthesized nanofluids adversely impacts displacement efficiencies. Hence, in this study, we synthesized two injection fluids including, a novel green nanofluid comprising of ultra-small silver nanoparticles (NPs) in glycerol and reconfigurable nanoemulsions to investigate their impact on displacement efficiencies. We have carried out the synthesis of green nanofluid comprising silver NPs in a customized microfluidic (Mf) chip, with 18 omega-shaped micromixers, by using glycerol as a promising green solvent and reducing agent at various concentrations (10-80 %), and simultaneous comparison of the results from batch synthesis. Interestingly, the experimental findings depicted that by varying different parameters, the spherical silver nanoparticles with an average ultra-small particle diameter of $<$ 2nm were obtained at all glycerol concentrations (10-80 %) and variables, as compared to batch synthesis (giving a yield of 10-fold larger particles). The synthesis was then confirmed by Dynamic Light scattering (DLS), UV-visible spectroscopy, and Tunnelling Electron Microscope (TEM). Subsequently, the displacement efficiencies were then investigated in a reservoir-on-a-chip platform (filled with fluorescence-doped oil) for real-time visualization, quantification and pore-scale investigation. The measurement data for green nanofluid revealed the wettability alteration and IFT reduction with the increase in viscosity and size of

NPs. No significant effect of the IFT on sweep efficiencies was observed, however, the contact angle of the injection fluids shifted from an oil-wet state (101°-113°) towards an intermediate wettability state (90°-97°) over 2 minutes. A shift towards intermediate wettability in a short time indicated the influence of AgNPs in displacing oil ganglia by structural disjoining pressure. It was reported that a critical glycerol viscosity (30 %) was essential to increase the sweep efficiency by 5 % in microfluidics-synthesized nanofluid (1.7 nm) and by 8 % in benchtop synthesized nanofluid (3.3 nm). Finally, the NPs-surfactant assemblies between SiO_2 and Poly[dimethylsiloxane-co-(3-aminopropyl)methylsiloxane] copolymer were investigated for the synthesis of reconfigurable nanoemulsions. The buckling phenomena was confirmed between pH 5 and 6 and nanoemulsions were synthesized with 3 different Oil: NPs concentrations i.e., 80:20, 70:30 and 60:40 at pH 3, 5, 6, and 8 (pH 3 and 8 taken as control groups). The sweep efficiency gradually increased in the order of 60:40 < 70:30 < 80:20, with the highest sweep efficiency obtained in the case of 80:20 nanoemulsions at pH 5, pH 6 and pH 5 in case of 70:30 nanoemulsions respectively, due to the displacement of oil because of formation of wedge film and in-situ emulsification.

Keywords: Multiphase flow displacement, green nanofluid, reconfigurable nanoemulsions, silver nanoparticles, glycerol, green synthesis, omega-shaped microfluidics mixer, coaxial microreactor, T-shaped droplet microfluidics chip, reservoir-on-a-chip.

ÖZET

GLİSEROL İÇERİSİNDE YENİ YEŞİL NANOPARÇACIK SENTEZİNİN VE YENİDEN ŞEKİLLENDİRİLEBİLİR NANOEMÜLSİYONLARIN ÇİP-ÜSTÜ-REZERVUAR PLATFORMUNDA ÇOK FAZLI AKIŞA UYGULANMASI

Robab Jahangir
Malzeme Bilimi ve Nanoteknoloji, Yüksek Lisans
Tez Danışmanı: Bülend Ortaç
Ikinci Tez Danışmanı: Gürkan Yeşiloz
Ocak 2024

Nanoparçacılar (NP), nanoakışkanlar ve su içerisinde yağ (O/W) nano/mikro emülsiyonları, ileri petrol kazanımı (EOR) gibi çok fazlı akış sürülme (akış yer değiştirmesi) uygulamalarındaki potansiyel kullanımları olduğu için yoğun bir şekilde araştırılmıştır. Bununla birlikte, metal nanoparçacıkların ve yağ içinde su nanoemülsiyonlarının (W/O) potansiyeli, altta yatan mekanizmaların yeterince incelenmemesi nedeniyle tam olarak açığa çıkarılmamıştır. Dahası, çoğu nanoakışkan rezervuarlarda toksisite riski oluşturur ve geleneksel olarak sentezlenen nanoakışkanların yüksek polidispersite indeksi, yer değiştirme verimliliğini olumsuz etkiler. Bu calısmada, akış sürülme verimliliklerinin etkisini araştırmak icin ultra-küçük gümüş nanopartiküllerden (NP'ler) olusan yeni nesil bir yesil nanoakışkan ve yeniden şekillendirilebilir nanoemulsiyonları iceren iki enjeksiyon sıvısı sentezlendi. Gümüş NP'lerin sentezi, özel tasarlanmış bir mikroakışkan (MF) çip içinde, 18 omega şekilli mikro-mikser kullanılarak gerçekleştirildi. Bu sentezde, umut vadeden yeşil çözgen ve çeşitli konsantrasyonlarda (% 10-80) indirgeyici madde olarak gliserol kullanıldı ve aynı anda toplu sentezden elde edilen sonuçların karşılaştırılması yapıldı. İlginç bir şekilde, deney bulguları, farklı parametreleri değiştirerek, küresel gümüş nanoparçacıklarının ortalama çapının <2 nm olduğunu gösterdi; bu durum tüm gliserol konsantrasyonlarında (% 10-80) ve değişkenlerde gözlemlendi ve geleneksel sentezle karşılaştırıldığında (10 kat daha büyük parçacıklar veren) ultra-küçük nanoparçacıklar elde edildi. Sentez daha sonra Dinamik Işık Saçılması (DLS), UV-görünür spektroskopisi ve Geçirimli Elektron Mikroskobu (TEM) ile doğrulandı. Ardından, yer değiştirme

verimlilikleri, gerçek zamanlı görselleştirme, nicelendirme ve gözenek ölçeğinde araştırma için floresans ile doldurulmuş bir çip platformunda (rezervuar üzerinde) incelendi. Nanoakışkan için ölçüm verileri, viskozitenin ve NP'lerin boyutunun artması ile ıslanabilirlik değişikliği ve IFT azalmasını ortaya çıkardı. IFT'nin sürükleme verimlilikleri üzerinde belirgin bir etkisi gözlemlenmedi, ancak enjeksiyon sıvılarının temas açısı, 2 dakika içinde bir yağlı-ıslanabilir durumdan (101°-113°) orta derecede ıslanabilir bir duruma (90°-97°) kaydı. Kısa bir süre içinde orta derecede ıslanabilirliğe doğru bir kayma, AgNPs'nin yapısal ayırma basıncı ile yağ gangliyonlarını yerinden etme etkisini gösterdi. Kritik bir gliserol viskozitesinin (%30) mikroakışkanlarda sentezlenen nanosıvıda (1.7 nm) sürülme verimini % 5 artırmak için ve masaüstü sentezlenen nanosıvıda (3.3 nm) % 8 artırmak için önemli olduğu gözlemlendi. Son olarak, bu tez çalışması kapsamında, SiO_2 ve Poli[dimetilsiloksan-ko-(3-aminopropil)metilsiloksan] kopolimer arasındaki NP-sürfaktan birimleri, yeniden şekillendirebilir nanoemülsiyonların sentezi için araştırıldı. Buckling olayı pH 5 ile 6 arasında doğrulandı ve nanoemülsiyonlar, pH 3, 5, 6 ve 8'de (pH 3 ve 8 kontrol grupları olarak alındı) 3 farklı Yağ: NP konsantrasyonu olan, yani 80:20, 70:30 ve 60:40 oranlarında sentezlendi. Sürülme verimliliği, sırasıyla 60:40 < 70:30 < 80:20, olarak giderek arttı; en yüksek sürülme verimliliği, 80:20 nanoemülsiyonlarının pH 5, pH 6 ve pH 5 durumlarında sırasıyla elde edildi.

Anahtar sözcükler: Çok fazlı akışlar, yeşil nanoparçacık sentezi, yeniden şekillendirilebilir nanoemülsiyonlar, gümüş nanoparçacıklar, glycerol, mikroakışkan mikromikserler, çip-üst-rezervuar.

Acknowledgement

First and foremost, I am thankful for the opportunities and blessings Allah Almighty has granted me. In particular, I would like to express my deepest appreciation to my supervisor, Dr. Gürkan Yeşilöz, for his unwavering support, invaluable guidance, and enthusiasm throughout my Master's journey in Material Science and Nanotechnology. His trust in welcoming me to the Yeşiloz Research Group, despite my initial inexperience in this specialized field, has been fundamental to my development. His insightful feedback on scientific matters, and motivational support during challenging times have been incredibly influential.

I extend my gratitude to my thesis committee members Dr. Wonmi Ahn and Dr. Işıl Gerçek Beşkardeş whose constructive comments and feedback significantly enhanced the quality of my work. Their expertise and guidance have been instrumental in shaping my research. A special acknowledgement goes to the National Nanotechnology Research Institute (UNAM), Bilkent University, and The Scientific and Technological Research Institution of Turkiye (TUBİTAK) for their exceptional research facilities and financial support, which were crucial for the successful completion of my research.

I am grateful to all members of the Yeşiloz Research Group: Dr. Iqra Munir, Eylul Tabel, Aslı Gizem Çınar, Faiqa Nazir Ahmed, Ali Vardin, Servin, Ceren Yılmaz, Safa Mintaş, Aybala Topçu, Erkin Köseoğlu, Damla Uzun, and Eda Demirdoğan. Their camaraderie, support, and collaboration have significantly enriched my research experience. A heartfelt thanks to Dr. Iqra Munir for being an especially supportive partner for her valuable guidance in scientific discourse and unwavering support during my pursuit of the Master's degree.

My sincere appreciation goes out to all my friends from Bilkent University, who have been a constant source of support, trust, and companionship. Their presence has made my time at the university more enjoyable and memorable. Special thanks to Ali Sheraz, Hamid Ali, Samar Batool, Syed Asad Shah, Rabia Ali, Muhammad Ilyas, Asfandyar Khan, Arooj Fatima, Reham Elshurafa, Salahudin

Zafar and Shakir for their wonderful friendship. A special thanks is reserved for Imran Nawaz's family, whose kindness made Bilkent feel like home. The delightful meals prepared by Arooj Bhabi and the affection shared by Abeeha, Minsa, Mustufa, and Hussain will be dearly missed. Throughout my pursuit of my dreams, I am profoundly thankful for the support of my dearest friend Faiqa Amjad Nizami and my cousins in Pakistan serving as my steadfast support system, they've offered not just encouragement but also moments of happiness.

Above all, my deepest gratitude is reserved for my parents, Jahangir Hussain and Shabana Kousar, and my siblings Afaq, Abubakar, Abdullah and Laiba Jahnagir. I'd never been able to fulfill my dream without my parents support. Their encouragement, sacrifices, and belief in me were the foundation of my journey towards realizing my aspirations. My profound appreciation goes to my grandparents, Jan Muhammad, Gareeb Bibi and Rasheed Beigham, for their prayers and unwavering love which have been my pillars of strength and the reason that I am able to reach my goal. This achievement is as much theirs as it is mine. Their belief in my potential was the catalyst that turned my aspirations into tangible achievements, creating a foundation upon which I could build my future. My family's support remains an integral part of my success, underscoring the significance of their role in the realization of my dreams. Thank you all for your endless love and support. I am grateful for not giving up on my dreams.

Contents

1 Introduction **1**

1.1 Multiphase Displacement in Porous Media 1

1.1.1 Displacement Mechanisms of Chemicals in Oil Recovery: Insights and Challenges 3

1.1.2 Nanoparticle Flooding 4

1.1.3 Emulsion Flooding 6

1.1.4 Glycerol in Multiphase Flow 8

1.2 Nanoparticle Injection For Multiphase Flow Displacement Application 9

1.2.1 Synthesis of Metal Nanoparticles 9

1.2.2 Synthesis of Metal Nanoparticles in Glycerol 10

1.2.3 Silver Nanoparticles 11

1.2.4 Benchtop Synthesis of silver Nanoparticles in glycerol . . . 12

1.2.5 Microfluidic Synthesis of Silver Nanoparticles in Glycerol . 13

1.3 Emulsions For Multiphase Displacement Applications 16

1.3.1 NPs-Surfactant assemblies: An Interfacial Phenomena . . . 16

1.3.2 Reconfigurable Emulsions 19

1.4 Microfluidics Reservoir-on-a-Chip 20

1.5 Objective 22

2 Materials and Methods 24

2.1 Materials 24

2.2 Device Fabrication 25

2.3 Experimental Setup for Silver Nanofluid synthesis 26

2.4 Mixing Mechanism in Microfluidic Omega-Shaped Micromixers . . 27

2.5 Preparation of Analyte Solutions 28

2.6 AgNPs Synthesis using the Microfluidic Chip 29

2.7 Characterization of Silver Nanofluid and Reconfigurable Nanoemulsions 30

2.8 Synthesis of Reconfigurable Nanoemulsions 32

2.9 Geometrical Design of Reservoir-on-a-chip 32

2.10 Flooding Experiments and Visualization of Fluid Displacement in Reservoir Micro-model 34

2.11 Data acquisition and image analysis for Flooding Experiments . . 35

3 One-Step Synthesis of Ultra-Small Nanoparticles in Glycerol as a Promising Green Solvent at Room Temperature using Omega-Shaped Microfluidic Micro-mixers 37

3.1 Results and Discussion 37

3.1.1 Analysis of mixing efficiency of the Omega-shaped micromixers 37

3.1.2 Synthesis of AgNPs in Glycerol 40

3.1.3 Microfluidics synthesis of AgNPs 41

3.1.4 Effect of Peclet number and mixing efficiency on AgNPs synthesis 43

3.1.5 Effect of Higher Flow Rates on AgNPs Size 46

3.1.6 Effect of PVP concentration on AgNPs size 48

3.1.7 Effect of reactant concentration on AgNPs size 50

3.1.8 Comparison of the AgNPs produced in the microfluidic reactor and batch reactor 51

3.2 Conclusion 53

4 Multiphase Flow Displacement: Silver Nanoparticles and Reconfigurable Nanoemulsions 55

4.1 Multiphase Displacement Application of Silver Nanofluid 55

4.1.1 Interfacial Activity of Nanofluids 55

4.1.2 Wettability Alteration by Nanofluid 57

4.1.3 Oil Displacement Efficiency and Nanofluid Recovery Mechanism in Reservoir-on-a-chip 59

4.1.4 Analysis of Trapped Oil Movement 63

4.2 Multiphase Displacement Application of Reconfigurable Nanoemulsions 67

4.2.1 Effect of pH on NPs-Surfactant Assemblies 67

4.2.2 Preliminary Investigation on the Potential EOR capacity of the Reconfigurable Nanoemulsions 69

4.2.3 Distribution of the Reconfigurable Nanoemulsion in porous media 73

4.2.4 Conclusion 75

5 Conclusions and Future Prospects **77**

5.1 Conclusions and Future Work 77

A Data **98**

B Code **99**

List of Figures

1.1 A depiction of two-phase flow in a porous media [1] 2

1.2 Effect of Nanofluid Flooding on Oil Displacement [2]. 5

1.3 Schematics of the oil displacement test setup by emulsions [3]. . . 7

1.4 Silver NPs with different shapes [4]. 12

1.5 Benchtop synthesis of silver NPs in glycerol [5]. 13

1.6 Schematic description of the omega-shaped microfluidic mixer and the nanoparticle synthesis process in glycerol [6]. 15

1.7 NP-interfacial assemblies and reduction and IFT energy from E_0 to E_1. b) SiO_2 and Poly[dimethylsiloxane-co-(3-aminopropyl)methylsiloxane] copolymer at water and silicon oil interface. 17

1.8 Figure 2: NPs- Poly[dimethylsiloxane-co-(3-aminopropyl)methylsiloxane] copolymer assemblies at the water and silicon oil interface at, a) pH 3, b) pH 5, c) pH 6, and d) pH 8. 18

1.9 A simplified schematic of observation of microfluidic reservoir-on-a-chip under microscope [7]. 21

2.1 PDMS microfluidics chip fabrication process 25

2.2 a)The imaging setup includes Microscope and Microfluidic Chip, b) A detailed snap of the microfluidic chip, c) A close-up image of experiment setup without microscope for nanoparticle synthesis . 27

2.3 Mixing characterization of 10 % glycerol at $Pe = 12{,}236$ and 61,184 (a and b, respectively) and 80 % glycerol at $Pe = 12{,}236$ and 61,184 (c and d, respectively). 28

2.4 a) A Droplet microfluidics synthesis of SiO_2 1 % (v) in silicon oil (containing 20 % (v) Poly[dimethylsiloxane-co-(3-aminopropyl)methylsiloxane] copolymer) to confirm buckling b) An illustration of reconfigurable emulsion synthesis process by ultrasonication. 33

2.5 Microfluidic chip filled with fluorescence doped oil 34

2.6 Experimental setup for flooding experiments, with inset representing binary and fluorescence image of injection fluid flooding at time t. 34

3.1 Mixing Index of 10 % and 20 % glycerol solutions at $Pe = 12{,}236$ and 61,184 inside an Omega-shaped Micromixer 39

3.2 a,b) TEM images of AgNPs synthesized in 50 % glycerol at a Pe number of 12,236. The histogram in the inset (a) depicts the size distribution, b) UVvisible spectroscopy results of AgNPs synthesised in 10 %, 50 %, and 80 % glycerol buffer at $Pe = 36{,}710$ in omega-shaped micromixers 42

3.3 Synthesis of nanoparticles in a microfluidic chip at $Pe = 12{,}236$, $Pe = 36{,}710$, and $Pe = 61{,}184$ for 10 % to 80 % glycerol buffer. . 44

3.4 Energy Dispersive X-ray (EDX) of the AgNPs on a Copper (Cu) grid 45

3.5 Schematic representation of AgNPs synthesis in a Y-piece flow reactor and a capillary tube. 47

3.6 Reynolds number for 10 %-80 % glycerol buffer at *Pe* numbers = 12,236 36,710 and 61,184. 48

3.7 Effect of PVP molarity, 0.001 and 0.003 M, on size of AgNPs synthesized in 10 %, 50 %, and 80 % glycerol buffer with respect to *Pe* = 12,236, 36,710, and 61,184. 49

3.8 a) PDI variation of AgNPs synthesized in 10 %, 50 %, and 80 % glycerol buffer with 0.375 M PVP at *Pe* numbers = 12,236 36,710 and b) PDI variation of AgNPs synthesized in 10 %, 50 % and 80 % glycerol buffer with 0.75 M PVP at *Pe* numbers = 12,236 36,710 and 61,184 and 61,184. 50

3.9 Effect of reactant concentration on particle size synthesized at *Pe* = 36,710 in 10 % to 80 % glycerol buffer. 51

3.10 Comparison of microfluidic synthesis of AgNPs at *Pe* = 12,236, 36,710, and 61,184 and benchtop synthesis for 10 % to 80 % glycerol. 52

4.1 a) The surface tension of injection fluids, b) Dynamic Light Scattering results of AgNPs/glycerol (10-30 %) synthesized in microfluidics (Mf) and Benchtop (Bt) settings, c) Graphs showing IFT between displaced oil and injection fluids 56

4.2 a) Contact angle variation for 10 % gly solutions, b) Contact angle variation for 20 % gly solutions, c) Contact angle variation for 30 % gly solutions. 58

4.3 a) Graphs showing the viscosity of glycerol % and nanofluids with glycerol % a) 10 % glycerol, b) 20 % and c) 30 % glycerol. 59

4.4 Injection fluids; water, 10 % gly and 10 % gly based nanofluids (Mf and Bt): a) Sweep efficiencies till BT, b) Sweep efficiencies after BT, till 20 PV; c) Visual representations of fluid flow within a reservoir-on-a-chip, captured at the breakthrough point (BT) and various PV specifically, 5, 10, 15, and 20 PV. 61

4.5 Injection fluids; water, 20 % gly and 20 % gly based nanofluids (Mf and Bt): a) Sweep efficiencies till BT, b) Sweep efficiencies after BT, till 20 PV; c) Visual representations of fluid flow within a reservoir-on-a-chip, captured at the breakthrough point (BT) and at various PV specifically, 5, 10, 15, and 20 PV. 62

4.6 Injection fluids; water, 30 % gly and 30 % gly based nanofluids (Mf and Bt): a) Sweep efficiencies till BT, b) Sweep efficiencies after BT, till 20 PV; c) Visual representations of fluid flow within a reservoir-on-a-chip, captured at the breakthrough point (BT) and at various PV specifically, 5, 10, 15, and 20 PV. 63

4.7 a and d) Oil ganglia displacement by 30 % nanofluid (Mf) up to 21 PV after BT, b and c) Oil ganglia displacement by 30 % nanofluid (Bt) in a period of 21 PV after BT. 64

4.8 a) Adsorbed oil displacement by 30 % nanofluid (Mf) up to 21 PV after BT, b) Adsorbed oil and ganglia displacement by 30 % nanofluid (Bt) in a period of 21 PV after BT. 66

4.9 IFT measurement of 1 % SiO_2 dispersion in silicon oil containing 20% Poly[dimethylsiloxane-co-(3-aminopropyl)methylsiloxane] copolymer at pH 3, 5, 6, and 8. 68

4.10 Injection fluids: deionized water, 80:20 (Oil: NPs) at pH 3, 5, 6, and 8, a) Sweep efficiencies till BT, b) Sweep efficiencies after BT, till 20 PV; c) Visual representations of fluid flow within a reservoir-on-a-chip, captured at the breakthrough point (BT) and at various PV specifically, 5, 10, 15, and 20 PV. 70

4.11 Injection fluids: deionized water, 70:30 (Oil: NPs) at pH 3, 5, 6, and 8, a) Sweep efficiencies till BT, b) Sweep efficiencies after BT, till 20 PV; c) Visual representations of fluid flow within a reservoir-on-a-chip, captured at the breakthrough point (BT) and at various PV specifically, 5, 10, 15, and 20 PV. 71

4.12 Injection fluids: deionized water, 60:40 (Oil: NPs) at pH 3, 5, 6, and 8, a) Sweep efficiencies till BT, b) Sweep efficiencies after BT, till 20 PV; c) Visual representations of fluid flow within a reservoir-on-a-chip, captured at the breakthrough point (BT) and at various PV specifically, 5, 10, 15, and 20 PV. 72

4.13 a) Displacement of oil fraction by 80:20 (Oil: NPs) nanoemulsions at pH 5 and in-situ emulsification. b) Movement of oil by in-situ emulsion 60:40 (Oil: NPs) nanoemulsions at pH 6, c) Process of oil ganglia formation and displacement by 80:20 (Oil: NPs) nanoemulsions at pH 8. 74

List of Tables

3.1 The values of each inlet flow rate for 10 %, 50 %, and 80 % glycerol buffer at Reynold number = 0.1, 0.3, and 0.5. 46

4.1 Details about the fluid viscosity, density, mobility ratios, and sweep efficiency at 25 °C. 60

Chapter 1

Introduction

1.1 Multiphase Displacement in Porous Media

Multiphase displacement in a porous media is a complicated phenomenon, encountered in many industrial and natural prognoses, such as soil and groundwater remediation, solar water splitting, carbon dioxide sequestration, fabrication of biomaterials in microfluidics chip and hydrocarbon recovery or enhanced oil recovery (EOR) [8, 9, 10]. In these porous mediums, a wide range of hydraulic heterogeneity exists, which causes the injection fluid to bypass the matrix region, forming a preferential flow pathway [9, 11, 12, 13], as shown in figure 1.1. A preferential flow pathway is naturally formed in heterogeneous porous media when a fluid prefers to travel via low-resistance regions creating an uneven flow pattern and a no-net fluid flow [9]. These uneven flow patterns have attracted significant attention because of their existence in many natural and engineering processes [14]. However, the hydraulic properties and heterogeneity of micro-structures pose a substantial technical issue for the economy and efficiency of multiphase displacement. For example, in reservoir engineering, the displacing fluid or injection fluid evades low-permeable matrix regions, causing a significant amount of oil entrapment in the unswept formation. These multiphase processes are extensively affected by the fluid properties and the geometry of porous media. Hence,

to optimize and improve the multiphase displacement efficiency, it is necessary to suppress the preferential flow in these diverse porous structures.

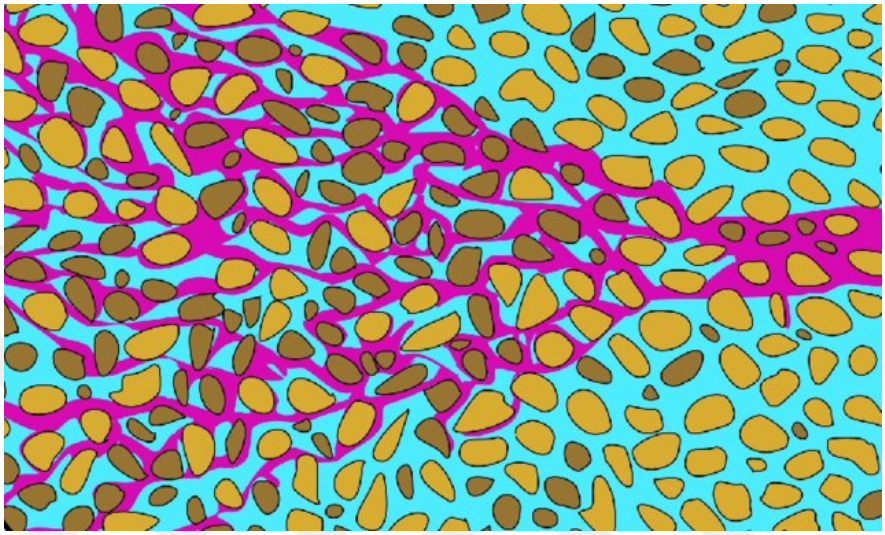

Figure 1.1: A depiction of two-phase flow in a porous media [1]

.

Extensive investigation has been conducted to reveal the mechanism of preferential flow at macro and micro scales [14]. In a study involving the drainage process in a micro-model, it was reported that the competition between capillary and viscous forces regulates the fluid-fluid interfacial stability, which results in the formation of macroscopic patterns such as viscous fingering, capillary fingering and compact displacement [14]. Capillary and viscous fingering are the two types of fluid displacement methods which can occur when a wetting fluid is displaced by a non-wetting fluid [15]. The ratio between viscous to capillary forces can be described by a dimensionless number known as a capillary number. Viscous fingering arises at a high capillary number when a more viscous fluid is displaced by a less viscous fluid [16]. On the contrary, capillary fingering involves thin finger growth and is influenced by diffusion-limited aggregation and invasion percolation [17]. However, the addition of chemicals to the injection fluid has shown a remarkable impact on displacement efficiency during multiphase interaction [8].

1.1.1 Displacement Mechanisms of Chemicals in Oil Recovery: Insights and Challenges

Numerous chemicals such as surfactants, nanofluids, polymers and micro and nanoemulsions have been effectively implemented to restrain the preferential flow [8, 18]. These chemicals generally work on the mechanism of enhancing the capillary number and displacement efficiency by changing wettability, reducing interfacial tension (IFT), and mobility ratio [8, 9, 18, 19]. The mobility ratio (M) is defined as the ratio between the viscosity of displaced fluid to displacing fluid (M = μdisplacing solution/μdisplaced solution), close to one, taking into consideration that the relative permeabilities of both solutions are nearly equal [20]. A low mobility ratio, close to 1, is a prerequisite for optimal displacement efficiencies [20].

Similarly, IFT is a measure of miscibility and a thermodynamic property of an interface [21]. In the case of high IFT between reservoir fluids, the capability of displacing fluid to retrieve oil from porous media is very low, leaving a substantial amount of oil behind, consequently resulting in low sweep efficiency [20]. Whereas, Wettability is the property of a liquid to adhere to or spread on a solid surface in the presence of another liquid [22]. It is also a significant parameter in multiphase flow as it not only affects relative permeability, capillary pressure and oil sweep efficiency but also governs the residual oil saturation, fluid flow and oil distribution in the reservoir [22, 23]. Wettability can be distinguished into water-wet ($0° \leq \theta \leq 90°$), oil-wet ($90° \leq \theta \leq 180°$) and intermediate wettability ($\theta = 90°$) [23, 24, 25]. In general, a positive correlation between water-wet surfaces and recovery factor exists due to the presence of capillary forces in water-wet pores, reducing oil adhesion to reservoir walls, and ultimately enhancing oil recovery [22].

To suppress the preferential flow by increasing the viscosity of injection fluid, the use of high molecular polymer dispersion in water has been reported in the literature [26]. Polymer flooding can reduce the displacement efficiency and water mobility ratio by increasing solution viscosity [18]. However, only increasing the

fluid viscosity may not increase the multiphase displacement efficiency. Additionally, shear degradation, injection capacity reduction and dilution effect can result in unreliable results. Surfactants can decrease the interfacial tension (IFT) and alter the wettability, which consequently diminishes the capillary force of fluid and retrieves the trapped oil [18]. However, the utilization of polymers and surfactants in EOR is limited due to exorbitant cost, loss by adsorption to mineral sites as well as their instability in harsh reservoir conditions (high temperatures and salinity) [27, 18].

1.1.2 Nanoparticle Flooding

With interest peeking in 2013, the application of nanoparticles (NPs) in various sectors including oilfields, has drawn immense attention due to their several remarkable properties, i.e. ultra-small size, mechanical strength, high surface area-to-volume ratio, low toxicity, interfacial properties and environmental friendliness [8, 7, 28]. Nanoparticles (NPs) with a size range between 1 and 100 nm act as a bridge between atomic/molecular-level structures and bulk particles. NPs are usually classified based on their dimensions, morphology, uniformity, and composition. As the dimensions of NPs decrease, their physicochemical properties significantly increase [10]. For instance, thermal conductivity, optical properties, melting point, toughness, quantum effect, and reactivity are directly related to the morphology and size of NPs, and due to these splendid properties, they have gained huge popularity in various fields of science. Additionally, NPs are chemically and thermally more stable than polymers and surfactants hence, they can be successfully employed in harsh reservoir conditions [27, 29, 30, 31]. Nanofluids are colloidal solutions containing NPs which can alter the chemical properties of the base fluid [27]. Injecting nanofluids into low-permeability reservoirs facilitates their penetration into micro and nano-sized pore throats, changes IFT and modifies the wettability of the reservoir by adsorbing on rock surface hence improving overall oil displacement efficiency in pore throats [32], shown in figure 1.2. Numerous researchers have reported that the addition of various NPs to injection fluid has positive effects on EOR due to their unique characteristics [27, 33, 34].

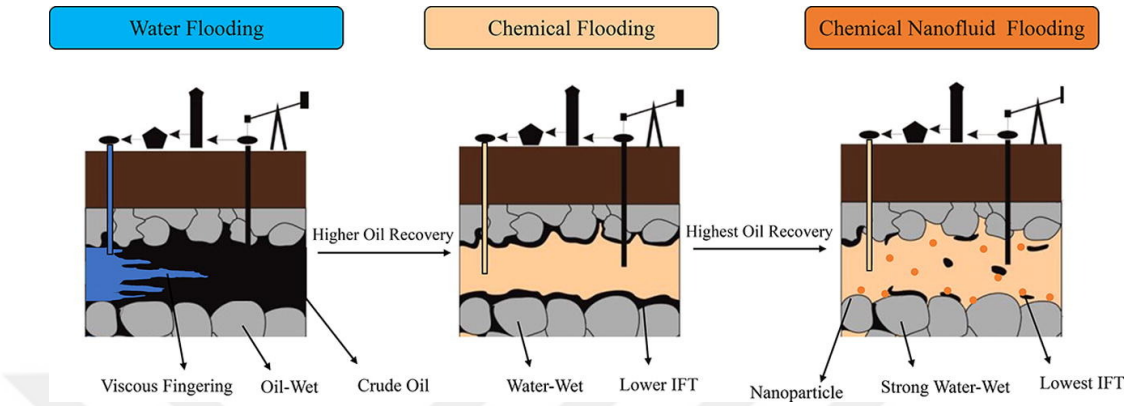

Figure 1.2: Effect of Nanofluid Flooding on Oil Displacement [2].

However, only a few NPs such as Organic NPs (GO, nano-clay), NiO_2, Al_2O_3, TiO_2, and, ZnO etc. have been successfully employed for pilot tests to evaluate their actual practicality [27]. The diverse effects of these nanoparticles on EOR are still under investigation. Ehtesabi et al. investigated the anatase and amorphous titanium dioxide NPs in core flooding experiments and observed that oil recovery was increased by 80 % as compared to water flooding where only 49 % recovery was achieved [35]. In addition, the effect of the simultaneous use of magnetic iron core-carbon shell nanoparticles and a mixture of hydrophilic surfactant (S1) and hydrophobic surfactant (S2) on oil recovery via a rock-on-a-chip technology was also investigated [36]. The oil recovery was reported to be highest (84 %) for nanoparticle-surfactant flooding as compared to surfactant and water flooding. In another study it was reported that adding only 0.1 wt % of silica NPs in Polyacrylamide solution can alter the rheological behaviour of solution by enhancing the pseudo-plasticity of polymers in low shear rate values, ultimately increasing the oil recovery [33]. However, most nanofluids including silica NPs are unstable and agglomerate under reservoir conditions such as pressure, temperature and salinity [13]. To evaluate the potential of various nanoparticles, including magnetic, inorganic and metallic ones, in enhancing oil production processes, further experimental investigations are required. Additionally, due to the abundance of silica, experimental studies showcasing metallic oxide NPs as effective EOR agents, are less compared to extensive research on silica nanoparticles [37].

1.1.3 Emulsion Flooding

The early execution of microemulsions in EOR applications dates back to the 1940s, yet an elevated interest was witnessed in the 1960s [38]. The main objective of microemulsions implementation is to remove the oil at pore and large scale by altering the wettability and IFT characteristics without changing the reservoir's uniqueness [38]. However, it leads to surfactant loss by adsorption to the rock surfaces [38]. In this regard, NPs injection in the form of nanodispersions has attracted immense attention for its potential in multiphase displacement applications such as EOR because of its small size and other promising IFT characteristics [39]. It is widely known that NPs can adsorb onto the immiscible fluid-fluid interface and form stable Pickering emulsions [39]. Pickering emulsions such as oil-in-water (O/W) and their stabilisation with NPs have been immensely investigated because of their good resistance under harsh reservoir conditions as compared to surfactants. These emulsions can enhance mobility control under high salinity conditions. However, most of the present studies focus on inorganic NPs which need custom surface alterations including polymer chains grafting to form stable Pickering emulsions that can resist harsh conditions. These alterations notably increase the production time and cost [39]. Apart from polymer-grafted NPs, the alternative lies in hybrid polymer nanofluid suspensions formed by directly amalgamating nanoparticles into the polymer. While this method is deemed easily achievable, achieving a consistent dispersion is still challenging due to significant nanoparticle aggregation within the polymer matrix.

To be precise, nanotechnology is approaching the petroleum industry through other types of emulsion appliances i.e., nanoemulsions [38]. A nanoemulsion is a homogeneous solution of two immiscible liquids having a size range of nanometers. When compared with microemulsions, nanoemulsions require a small number of surfactants and a reduced particle size makes it remarkable in its rheological properties and stability [38]. According to Anton et al., the greatest advantage of nanoemulsions is their driblet suspension stability. That is, the kinetic stability of these emulsions is not affected by physiochemical changes such as pH and temperature [38]. Kumar and Mandal stated that SiO_2 and surfactant-stabilized

nanoemulsions can result in additional oil recovery of 26.40 % over water flooding [40]. However, until now, the majority of nanotechnology studies are limited to the laboratory scale, and field applications with new and improved methodologies are highly desirable in industry [38]. An example of a laboratory setup for flooding of emulsions in a core model in an oven is shown in figure 1.3

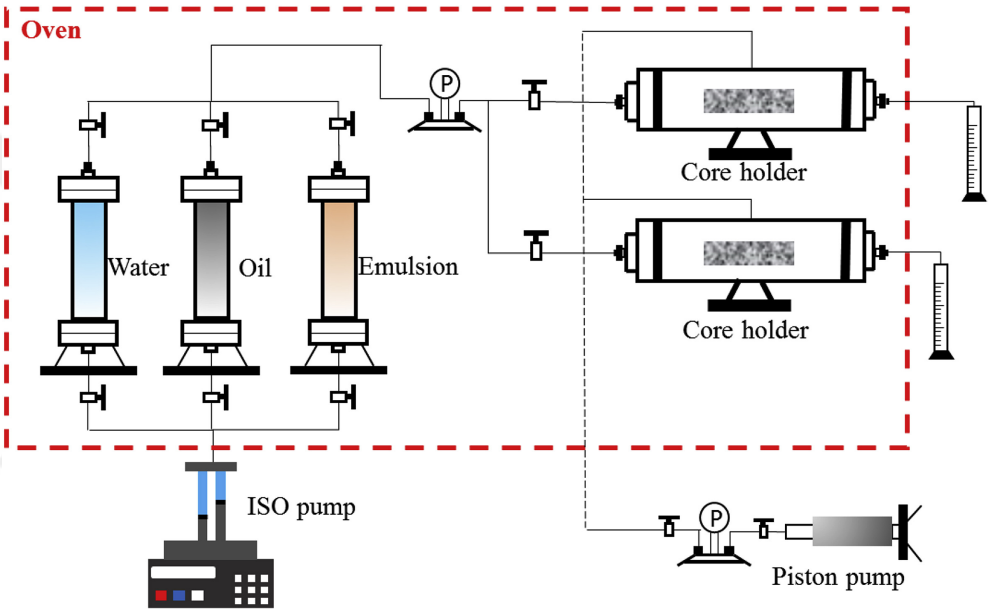

Figure 1.3: Schematics of the oil displacement test setup by emulsions [3].

Additionally, the advantage of NPs and the trade-off associated with using a polymer as a surface active agent to increase emulsification needs further investigation [41]. Kumar et al. reported the impact of polymer (carboxyl methyl cellulose), SiO_2 NP, and surfactant (sodium dodecyl benzenesulfonate) assisted Pickering emulsions formulation with light mineral oil and successfully retrieved an additional oil recovery of 24.81 % due to enhanced rheological behavior, IFT reduction, and minimization in droplet coalescence [42]. However, a critical insight reveals that W/O emulsions receive less consideration as compared to integrated studies associated with emulsion stability and tertiary oil recovery [43]. To the best of our knowledge, the effect of pH on W/O reconfigurable nanoemulsions flooding in reservoir-on-a-chip remains unexplored and demands critical scrutiny to discern its impact on sweep efficiency.

1.1.4 Glycerol in Multiphase Flow

Another interesting and novel solvent is glycerol which has been used in two-phase flow studies for more than 80 years [44]. The combined use of NPs and glycerol presents an appealing approach as they can simultaneously enhance the water viscosity and reduce the interfacial tension, both of which are highly advantageous for oil recovery. Glycerol is a trihydric alcohol, colourless, odourless, and non-toxic solvent with 15.0 poise viscosity at room temperature, immiscible in hydrocarbons and miscible in water and ethanol in all proportions [44, 45]. The viscosity of glycerol decreases with the increase in water content and temperature and increases with the addition of electrolytes to its aqueous solution. At room temperature, the surface tension of glycerol (63.2 dyn/cm) is close to water (72.5 dyn/cm) but significantly greater than the surface tension of the majority of the organic solvents [44]. Interestingly, due to the rising use of glycerol as a bio-based fuel, a surplus supply of glycerol is provided in the market, compelling an economic and environmental opportunity for investigating its potential as a substitute for polymers in oil recovery [46].

In oil reservoirs, glycerol can act as a viscosifier agent and can help to obtain a higher recovery factor [20, 44, 47, 48]. In a recent study by Fabiola et al., the effect of glycerol on surfactant adsorption in sandstone core was reported [20]. The viscosity of glycerol-non-ionic surfactant saponified coconut oil (SCO) solution, was close to displaced oil with a good mobility ratio. A higher recovery factor (53 %) was obtained for the glycerol-SCO solution, as compared to the glycerol-free surfactant solution. The overall oil recovery was reported to be 33 % more due to an increase in the solution's viscosity but a significant surfactant loss of 49 % was reported for the glycerol-SCO solution. Also, an alternative for alkali-polymer-surfactant flooding is available to overcome the reservoir limitations [46, 47]. The investigation highlights the potential of an aqueous glycerol solution and AOS+FC surfactant blend to enhance oil recovery in a core flooding experiment, which reports an increase in the oil recovery factor by flooding the glycerol-surfactant solution. In light of these findings, it becomes even more crucial to emphasize that the pore-scale exploration of alternative and

environmentally sustainable methods for oil recovery remains a priority within the industry. Hence, glycerol emerges as a novel green solvent and a promising candidate which needs further investigation and in-depth research in the context of multiphase displacement.

1.2 Nanoparticle Injection For Multiphase Flow Displacement Application

1.2.1 Synthesis of Metal Nanoparticles

Regardless of the continued progress in the synthesis of metal NPs, designing a single protocol for the controlled size tunability and uniform size distribution of particles remains a critical factor [5]. For example, the shape, size and polydispersity index (PDI) of NPs are the major components for the effectiveness in multiphase displacement applications. However, the current literature on NP synthesis methods needs further improvement in simple one-step protocols to generate ultra-small NPs with high reproducibility. Among well-known NP synthesis protocols, the reduction of metal is preferred either by citrate, hydroxylamine, $NABH_4$, dextrose, NaOH or acid. The major issue with these reducing agents is none of the reagents is capable of producing highly monodispersed NPs concerning the size and shape of NPs in a simple single step [5]. Additional steps such as heating, centrifugation, pH or temperature adjustment and sonication are required during the reaction to get the desired NP size during the synthesis. Besides that, density gradient centrifugation techniques can also be used for the purification of such heterogeneous colloidal mixtures. However, none of the existing approaches entirely meet the critical requirement for achieving monodisperse NPs [49].

Theoretically, for homogeneous monodisperse particle size, a selective heat profile and quick homogeneous nucleation and growth time are required [50]. For years, the process of nucleation and growth of NPs have been described via

LaMer burst nucleation theory and Ostwald ripening (to describe the particle size change) [51]. This model was presented by the Lifshitz-Slyozov-Wagner, LSW theory, and was considered the sole theory until Watzky and Finke presented another approach describing consistent slow nucleation followed by autocatalytic growth [52]. Nucleation is a process in which nuclei act as a template for the growth of crystals. As defined by Mullin, primary nucleation occurs in the absence of other crystalline matter and can be used to describe the nucleation process of various chemical syntheses. Nucleation can be further divided into homogeneous nucleation and heterogeneous nucleation. Homogeneous nucleation happens when uniform nuclei are formed throughout the parent phase, while heterogeneous nucleation occurs at structural inhomogeneities such as container surfaces, grain boundaries and impurities. Heterogeneous nucleation forms much more often in liquids because of a stable nucleating surface. Interestingly, homogeneous NPs with ultra-small size can be achieved by following a simple protocol using the impact of glycerol solvent in the presence of PVP as a stabilising agent, thus monitoring the nucleation profile at variable solvent concentration to achieve homogeneous NPs [5].

1.2.2 Synthesis of Metal Nanoparticles in Glycerol

To date, various studies have reported the synthesis of metal NPs; however, most of them are limited to the reduction of metal ions at alkaline pH conditions, ultraviolet light irradiance, and high temperatures [53]. In some cases, the utilization of glycerol as a reducing agent facilitates the selectivity, catalysis, and effectiveness of reactions [54]. Syntheses of various metal particles (e.g., copper, platinum, silver, and gold) in glycerol (at 230 and 100 °C) have been reported previously, wherein glycerol was used both as a reducing agent and a solvent medium [55]. It has also been stated that synthesis in glycerol can be done at room temperature without the addition of any further reducing agent [56]. Similarly, a recent study reported that for nanoparticle synthesis in glycerol, alkaline conditions, as well as high temperatures, are not necessary [53]. Perhaps, at neutral pH conditions and room temperature, reducing species such as free radicals and aldehydes

are generated in glycerol, which can yield NPs with different size distributions. In another recent study, the synthesis of bimetallic nanoparticles was reported in microfluidics, where the whole synthetic processes were accessible in ambient conditions and without a chemical reducer [57]. Similarly, the synthesis of tunable metal nanoparticles in glycerol as a reducing medium at room temperature was reported [5]. However, so far, no investigation has been conducted in microfluidics using glycerol as a reducing solvent medium for the synthesis of nanoparticles and benchtop synthesis as a counterpart in the same conditions at room temperature.

1.2.3 Silver Nanoparticles

Among several metal sources, silver nanoparticles (AgNPs) are one of the paramount NPs that have been widely utilized commercially in healthcare products, food storage, packaging, textile coating, and cleaning agents [6]. They have also been effective against various antibiotic-resistant bacterial and viral strains and have expanded applications in bio-therapeutics like cancer treatment, bioimaging, diagnostics, and drug delivery [58, 59, 4]. The reason is its exceptional conductivity, plasmon light scattering, and catalysis [60]. Particularly, ultra-small AgNPs (size less than 5 nm) have been utilized in economically printed electronics because of their unique catalytic activity possessed due to their low surface-to-volume ratio. However, these characteristics significantly depend on the average size, overall size distribution, and shape of NPs figure 1.4, which are directly affected by the fabrication procedures [61, 62]. Therefore, enormous efforts have been made to gain better control over the shape and size of these NPs. However, the potential utilizatiın of AgNPs in multiphase displacement applications such as EOR has not been reported earlier and needs critical investigation.

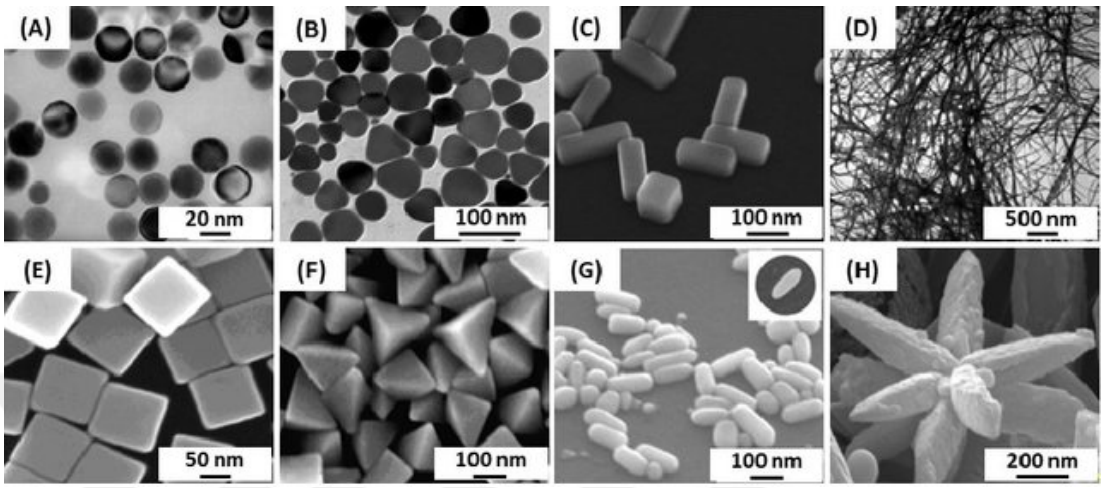

Figure 1.4: Silver NPs with different shapes [4].

1.2.4 Benchtop Synthesis of silver Nanoparticles in glycerol

Conventional macro-scale/batch reactors use standard synthetic methods for the production of NPs. Despite the comprehensibility of traditional approaches, there are substantial disadvantages such as waste production, low reproducibility, considerable quality variation, and undue resource consumption [60]. The lack of control on spatial and temporal variation of physical conditions such as the pressure, reactant concentration, and temperature has an adverse effect on the nucleation and growth state [63]. As a result, the agglomeration of particles and size variation have been the major challenges in getting reproducible results in each batch. Accordingly, it was necessary to establish considerable means for AgNP synthesis to ease the ecological footprints and subdue the constraints of traditional approaches [64, 65, 66].

It has been reported that the reduction stage for AgNPs is less than 200 ms, and the mixing of reactants is a crucial stage to affirm uniform reaction conditions [67]. In addition to the type of synthesis approach, the synthesis abides by a step-wise process initiated from the input of a metal ion: nucleation, coalescence, ripening, and growth, where the nucleation stage determines the shape of NPs

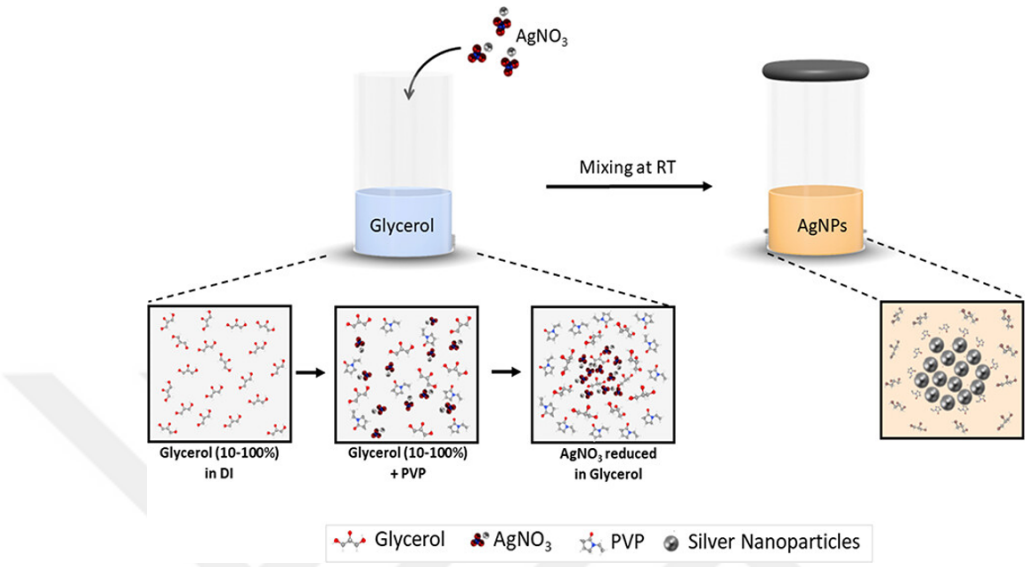

Figure 1.5: Benchtop synthesis of silver NPs in glycerol [5].

[61]. Sophisticated experimental techniques along with comprehensive quantitative knowledge are required for the analysis of the nucleation and growth stage [63]. However, macroscale techniques are unable to provide complete information regarding the nucleation and growth of NPs. Hence, in our previous study, we reported a one-step synthesis of tunable AgNPs in glycerol at room temperature as shown in figure 1.5.

1.2.5 Microfluidic Synthesis of Silver Nanoparticles in Glycerol

In order to achieve such properties, the advent of microfluidics in chemical synthesis has acquired substantial attention as a forerunner technology. Reducing the reactor dimensions enables high reactant conversion and minimizes the byproduct and waste production [65]. Therefore, it alleviates the environmental impact and improves the control over NP synthesis. Microfluidic systems also provide better control over the spatiotemporal separation of nucleation and growth stages of the synthesis process. The spatial separation of such a phase gives the advantage of having better control over mixing, reaction time, size, and reproducibility as well

as the sensitivity of particles due to their high surface-to-volume ratio [64, 65]. Furthermore, the regulated flow of reactants controls the local ion concentration and gives rise to homogeneous and regulated reduction rates among different nucleation sites providing consistent particle size, vouching for reproducibility, automation, and consequently fewer manual errors [57, 68]. To recapitulate, microfluidics provides the integration with optimization interfaces and feedback control, which is otherwise not possible in batch reactors [64]. However, microfluidic devices render laminar flow due to the low Reynolds numbers. The Reynolds number gives the ratio of inertial to viscous flow; hence, the mixing efficiency is significantly affected by channel dimensions, flow rate (Q), density (ρ), and viscosity (μ) of the reactants as shown in eq: [69, 70, 71]

$$Re = \frac{\rho\, UL}{\mu} \tag{1.1}$$

where U denotes the velocity of the flow and L is the characteristic length. As diffusion and convection-assisted diffusion (advection) are the main mixing mechanisms in microfluidic chips, having a laminar flow profile in microfluidic channels makes the mixing more challenging. The effect of diffusion and convection on mixing can be described by the Peclet (Pe) number. The Pe number gives the ratio between longitudinal convection and diffusion as depicted in equation 2: [72, 73]

$$Pe = \frac{UL}{D} \tag{1.2}$$

where L is the hydraulic diameter, U is the velocity of the flow, and D is the diffusion coefficient, herein taken as 2.27×10^{-11} m^2/s [72]. At low flow rate conditions, the velocity of the flow is low, and normally, a low value of the Pe number indicates a more uniform mixing [73]. However, the no-slip boundary condition causes fouling, blockage, and particle deposition on the channel walls [68]. Hence to decrease the mixing length, over the past decade, both active and passive micromixers have been studied under observation for chaotic mixing

at higher *Pe* numbers. As compared to bulk synthesis, the large surface-to-volume ratio of micromixers enhances the reaction kinetics and efficiency and the controllability of the products [71, 74, 75, 76]. In addition, the majority of microfluidic chips are traditionally fabricated with elastomeric polymers such as polydimethylsiloxane (PDMS). However, it is incompatible with many organic solvents, so it either necessitates the coating of a polymer, solgels, and parylene or fabrication with fluoroelastomers, for instance, photocurable perfluoropolyethers (PFPEs) or the thermally curable perfluoropolyether (SI-FELS) [77].

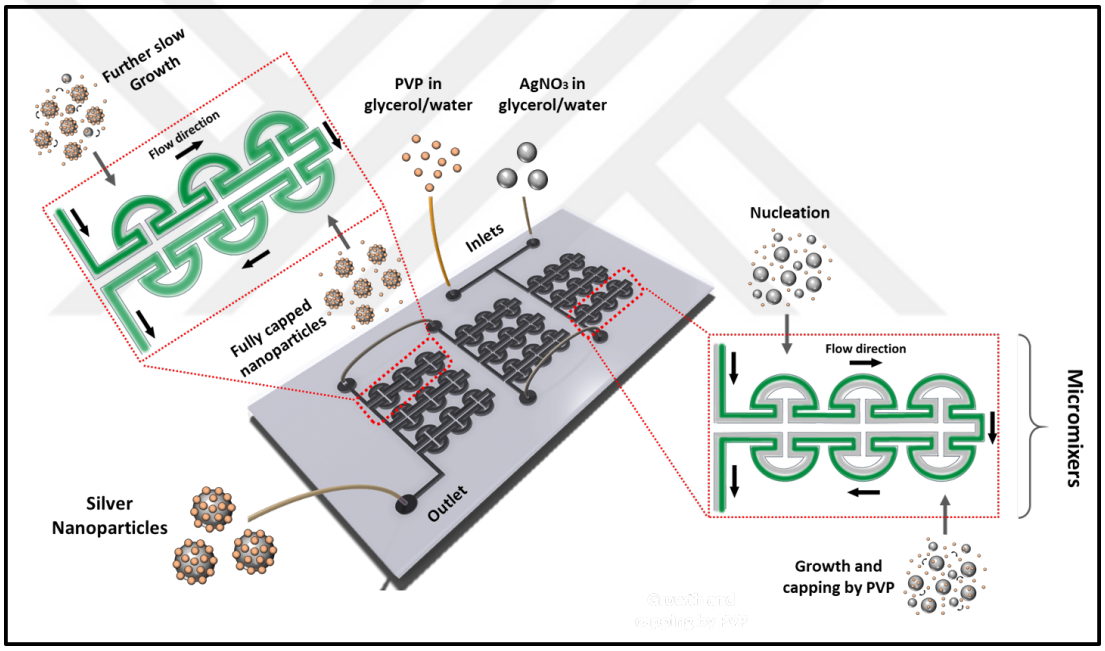

Figure 1.6: Schematic description of the omega-shaped microfluidic mixer and the nanoparticle synthesis process in glycerol [6].

The compatibility of glycerol with PDMS makes it an excellent candidate for the chemical synthesis inside microfluidic chips shown in figure 1.6. Utilizing the same approach, in the current study, we elucidate a simple co-flow microfluidic device adapted from the literature for the synthesis of AgNPs [78]. Cumulatively, 3 sets of micromixers each with 18 omega-shaped micromixers were used for the synthesis of AgNPs by using glycerol and polyvinylpyrrolidone (PVP) as reducing and stabilizing agents, respectively. Such an approach displayed great potential for generating ultra-small AgNPs at varying glycerol concentrations (10-80 %) [6].

1.3 Emulsions For Multiphase Displacement Applications

1.3.1 NPs-Surfactant assemblies: An Interfacial Phenomena

The liquid-liquid interface serves as a multi-functional platform for fabricating structures and advanced materials [79]. The oil-water interfacial assembly of nanomaterials with diverse geometric shapes such as nanosheets, nanoparticles and nanorods have sophisticated applications in pharmaceuticals, polymer composites, coatings, magnetic data storage, oil and mineral refining, foam and emulsions stabilization [79, 80, 81, 82, 83]. The reduction of interfacial energy between two fluids is the paramount factor for efficiently assembling nanoparticles (NPs) at the interface, which can act as a barrier between fluids [79]. These interfacial assemblies can either be a spontaneous aggregation of NPs at the interface or the interfacial interaction between functionalized ligands dispersed in one liquid and NPs with complementary functionality dissolved in another liquid, achieving 'NP-surfactants' by successively converting the NPs, shown in Figure 1b [79]. To describe the Pickering emulsions, the theory of the active assembly process was first elucidated by Pieranski, and extends its applicability to NPs as well [79, 81].

In an aqueous solution, NPs with a suitable size and surface chemistry adsorb on a liquid-liquid or liquid-solid interface due to decreased Helmholtz free energy [84, 29, 85]. To reduce the total free energy, the energy difference ΔE should be negative [85, 86, 87]. For instance, the adsorption of a single spherical particle with a radius r, at the oil-water interface can decrease the initial interfacial energy ΔE_0 to ΔE_1, resulting in an energy difference of (ΔE_1) as shown in figure 1.7: [79]

$$E_0 - E_1 = \Delta E_1 = \frac{\pi r^2}{\gamma_0/W)}[\frac{\gamma_0}{W} - (\frac{\gamma^P}{W} - \frac{\gamma^P}{O})]^2 \tag{1.3}$$

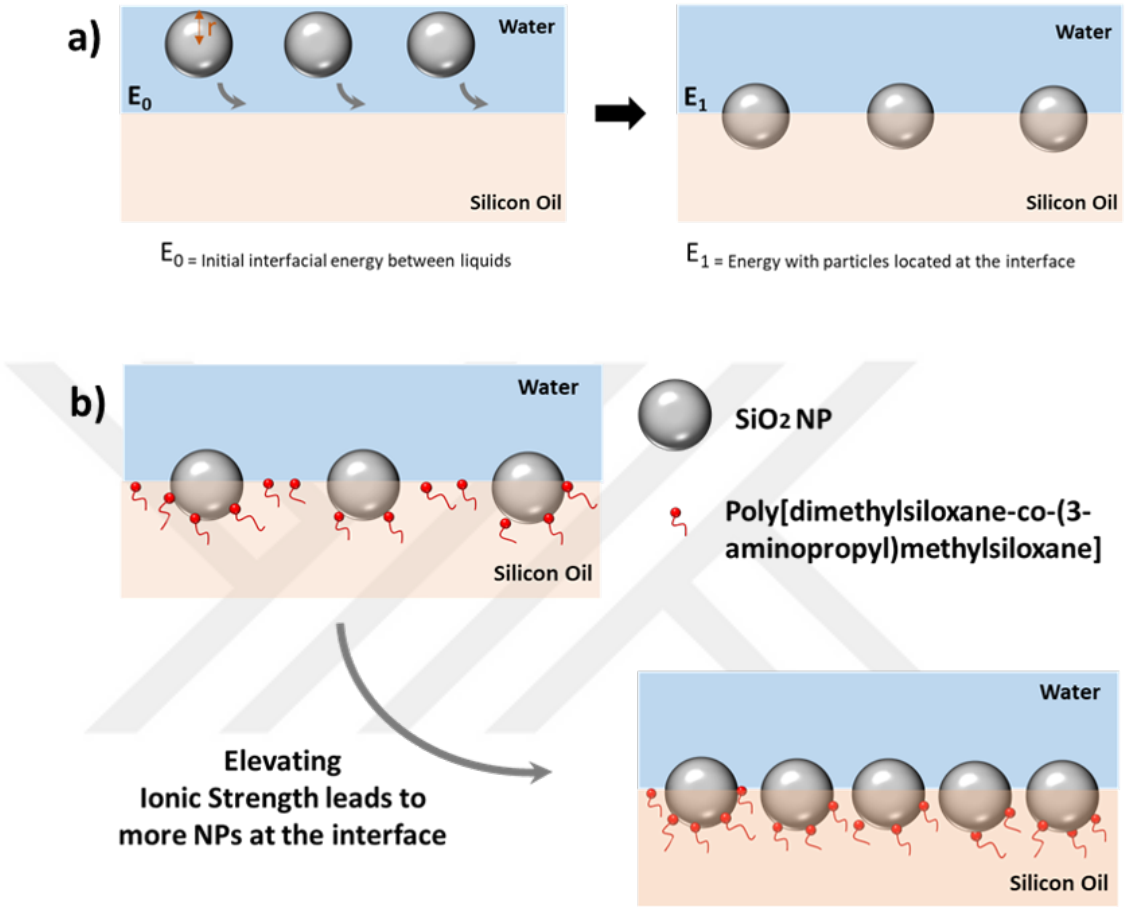

Figure 1.7: NP-interfacial assemblies and reduction and IFT energy from E_0 to E_1. b) SiO_2 and Poly[dimethylsiloxane-co-(3-aminopropyl)methylsiloxane] copolymer at water and silicon oil interface.

Here, E_1 is the energy with particles adsorbed at the interface. Considering the NPs size to be small here, ΔE_1 is also less and thermal energy is comparable with the ΔE_1, this results in the packing of NPs to be liquid-like forming dynamic interfacial assemblies where NPs are continuously adsorbed and desorbed at the interface [79]. However, by the formation of NP-surfactant assemblies at the interface, ΔE_1 is increased because of multiple surfactants wrapping around one species, as shown in figure 1.7 a. At the interface, the adsorption energy of the particles can be much higher than that of thermal fluctuations [88]. Thus, the particle adsorption at the oil-water interface is conceivably stable and could buckle upon interfacial compression, [88], shown in figure 1.8 (c and d). Additionally, the number of ligands attaching with a single NP is self-regulated and results

in a maximum decrease in the interfacial energy per NP, eliminating the need to precisely alter the surface functionality of NPs to increase the IFT energy reduction per NP.

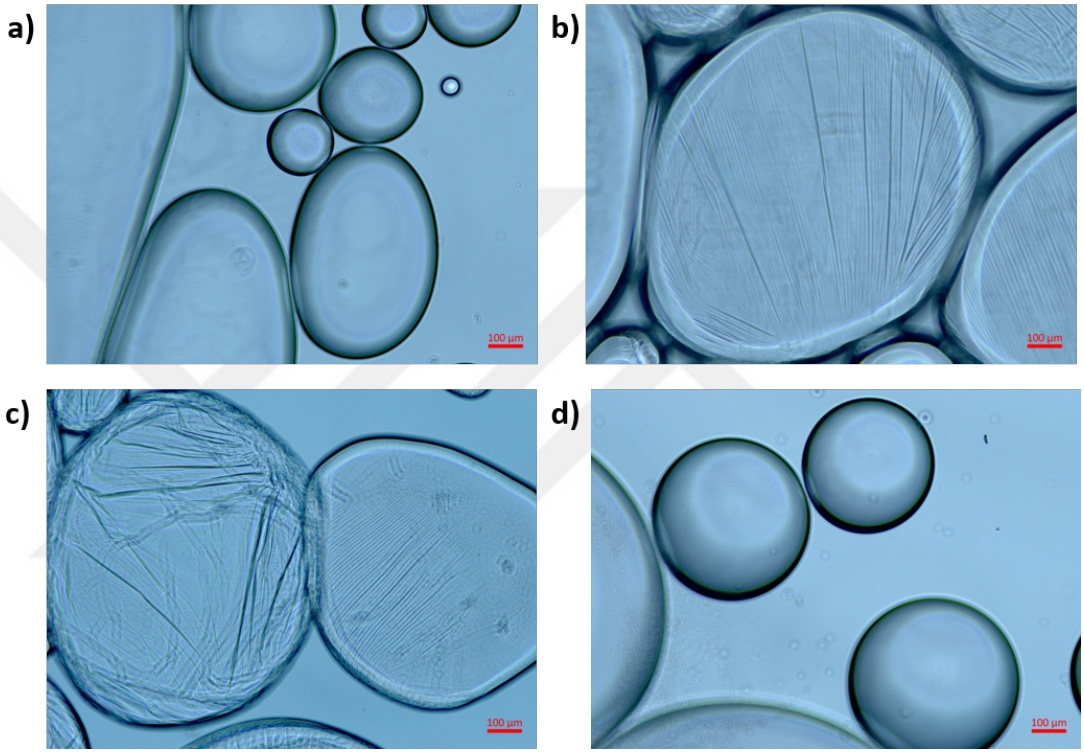

Figure 1.8: Figure 2: NPs- Poly[dimethylsiloxane-co-(3-aminopropyl)methylsiloxane] copolymer assemblies at the water and silicon oil interface at, a) pH 3, b) pH 5, c) pH 6, and d) pH 8.

Remarkably, by controlling the interaction strength of NPs and ligands these assemblies can be made responsive to external stimuli such as pH [79]. Huang et al. explored the effect of pH on electrostatic interaction in a system having water (containing carboxylated polystyrene nanoparticles) and silicon oil (containing amine-terminated polydimethylsiloxane, PDMS-NH_2) followed by the application of electric field at 4.8 kV/cm [89]. They found that at pH $>$ 5, the ellipsoidal shape was maintained by the droplet due to a strong interaction between amine groups and carboxylates. However, for pH $<$ 5 the interaction strength decreased which resulted in the droplet deforming into its original spherical shape. Hence, pH can be used to trigger changes in the NP-surfactant interfacial assemblies which as a result will change the shape and macroscopic properties depending on

the fluid phase and complementary functionalities of NPs and surfactants.

As previously stated, the significance of NP-surfactants interfacial assemblies expands to a broader application spectrum [79, 80, 81, 82, 83]. Unlike, Pickering emulsions, colloidosomes, and colloidal capsules, where microparticles are used for stabilization, NP-surfactant interfacial assemblies can also be employed for emulsions stability [85, 89]. This versatility of NP-surfactant stability of emulsions makes it applicable in various scenarios involving multiphase displacement. Colloidal systems such as emulsions and particle suspensions have been extensively used for multiphase flow in porous media, among others [90, 91, 92]. Hence, the application of NP-surfactant stabilized reconfigurable emulsions as an injection fluid is a prerequisite to exploring its impact on multiphase displacement.

1.3.2 Reconfigurable Emulsions

Emulsions are comprised of droplets of one liquid phase dispersed in another immiscible liquid phase [91]. The process of emulsification typically occurs due to a decrease in Gibbs free energy between two fluids [90]. Based on their sizes, emulsions can be categorized as microemulsions and nanoemulsions. Nanoemulsions (NEs) are kinetically more stable and have $\Delta G > 0$ while, microemulsions are thermodynamically stable, have $\Delta G \leq 0$ and are usually synthesized when interfacial tensions are very low [90, 92].

Apart from natural emulsification, EOR has been reported to generate stable W/O and O/W emulsions [93]. In general, emulsions have high viscosity as compared to surfactants and exhibit sufficient sweep efficiency even in the absence of polymers [18]. It is rather a cost-effective method, as only one component of emulsions is a surfactant and others are water, oil, or amphiphiles [18]. Despite that, the success of emulsion flooding in improving oil displacement depends on the appropriate selection of chemicals for the synthesis of emulsions [18]. Lately, the application of Nanoemulsions (NEs) to EOR has gained the consideration of researchers [92]. NEs comprise small particles and are far more stable than conventional Pickering emulsions [92]. Some clues of emulsion's stability with

NPs and surfactants with a similar charge can be found in the literature, however, most stable O/W emulsions are obtained in a system with the oppositely charged NPs and surfactants [94]. In these cases, at a specific surfactant concentration, the electrostatic attraction between surfactant molecules and NPs results in favourable interfacial stability of emulsions. The assembly of co-polymers and nanoparticles at the liquid-liquid interface has been reported to structure liquids [95] and stabilize foam and emulsions. In a recent study, it was reported that partially oxidized graphene oxide NPs with hydrophilic edges (such as COOH and OH) can irreversibly adsorb to immiscible fluid interface and create Pickering emulsions for EOR applications [96].

Some clues of emulsion stability with NPs and surfactants with a similar charge can be found in the literature, however, most stable O/W emulsions are obtained in a system with the oppositely charged NPs and surfactants/ligands [94]. In these cases, at a specific surfactant concentration, the electrostatic attraction between surfactant molecules and NPs results in favorable interfacial stability of emulsions [89, 94]. Thus, the particle adsorption at the oil-water interface is conceivably stable and could buckle upon interfacial compression, resulting in reconfigurable structures, shown in figure 2a [88].

1.4 Microfluidics Reservoir-on-a-Chip

Traditional laboratory tests such as core flooding and sand-pack experiments are often limited due to challenges associated with the visualization of residual oil and need magnetic resonance imaging (MRI), positron emission tomography (PET) and micro-computed tomography (micro-CT) [7]. However, a fundamental understanding of injection fluid on displacement efficiency requires pore-scale visualization and real-time flow in porous media [7]. These issues can be partially resolved by using lab-on-a-chip platforms. Recently, microfluidic devices have gained massive applications across various sectors of industry such as microelectronics, cosmetics, biotechnology, pharmaceuticals, oil and chemical industry.

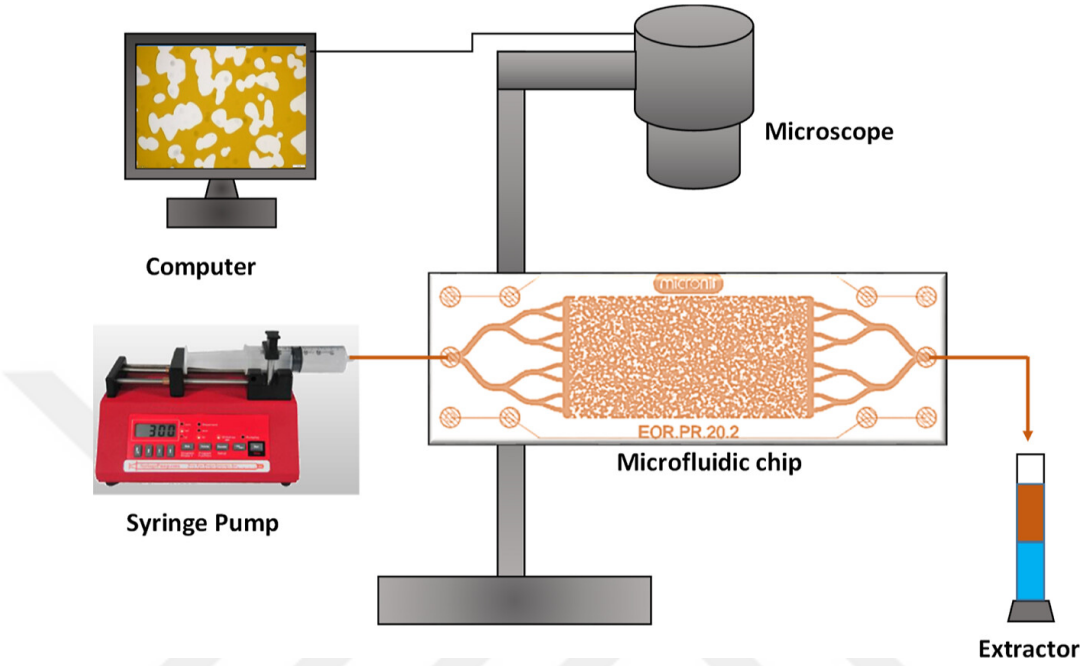

Figure 1.9: A simplified schematic of observation of microfluidic reservoir-on-a-chip under microscope [7].

As compared to traditional laboratory tests, where pore scale analysis and visualization are an issue, microfluidic platforms are an effective alternative to visualise the flow dynamics, pore throats and grain size in real-time in porous media to stimulate multiphase flow and solid-fluid interactions [97, 7] as shown in figure 1.9 and 2.6 . These devices provide a significant reduction in experiment time and material usage. The microscopic visualization of the interplay between viscous and capillary forces at the micro-scale is essential in designing the EOR process. In this regard, microfluidic devices make it possible to provide valuable insight into different phenomena such as the distribution of fluid in the porous matrix during flooding as well as microemulsion production, pore blockage and surfactant retention [98, 99]. Because of these advantages, microfluidic devices are a cost-effective alternative to performing a treatment before their usage in the oilfield. Microfluidic devices of different types have been extensively used to investigate the displacement of oil in porous media because of their ability to imitate the porous structures of the oil reservoir. The first glass micro model was created by Mattax and Kyte to investigate the fluid-fluid interface in a porous matrix and wettability impact on oil displacement during water flooding [100].

Later, a complicated micro-model was created by Bonnet and Lenormand using a photo-etching method with pose size imitating a real oil reservoir [101]. Similarly, the impact of a nanofluid (synthesized from Tween 40 and silica gel emulsions) on emulsion stability and sweep efficiency in a microfluidics chip was reported [102]. Hence, understanding the complex mechanisms underlying oil displacement and testing Enhanced Oil Recovery (EOR) techniques are made possible in by microfluidics. Various factors, such as viscosity, wettability, and the composition of the displacing material, have a significant impact on oil retrieval. Through the use of microfluidics, researchers can better understand these factors, which can lead to the development of successful EOR techniques.

1.5 Objective

From the above discussion, the significance of novel injection fluids is obvious in many multiphase displacement industrial applications. Various nanofluids and O/W nanoemulsions have been investigated for their potential in multiphase displacement applications. Still, the underlying mechanisms of displacement by metal nanofluids and W/O nanoemulsions need to be further investigated. Additionally, various nanofluids are toxic and could harm the reservoir, hence necessitating alternatives such as green solvents/injection fluids for such applications.

This work aims to investigate the effects of metal nanoparticles and reconfigurable W/O nanoemulsions to investigate their potential in multiphase displacement applications. For this, ultra-small silver nanoparticles (AgNPs) in glycerol (reducing agent and solvent medium) were synthesized (using $AgNO_3$ as the metal source and PVP as a stabilizing agent) at room temperature in a novel Omega-shaped microfluidic chip for multiphase application. A comparative study with benchtop synthesized AgNPs was also conducted to evaluate the potential of increasing size. Similarly, reconfigurable nanoemulsions with SiO_2 (dispersion in water) and Poly[dimethylsiloxane-co-(3-aminopropyl)methylsiloxane] copolymer (dissolved in silicon oil) was synthesized by ultrasonication. The displacement

experiments were then conducted in a reservoir-on-a-chip for real-time quantification and visualisation. Different characterization techniques including Dynamic Light Scattering (DLS), Transmission Electron Microscope (TEM), UV-visible spectroscopy, Atension theta-pendant Drop Tensiometer, Contact angle and fluorescence Microscope were used in the study.

Chapter 2

Materials and Methods

2.1 Materials

For Nanofluid Synthesis: Glycerol ($C_3H_8O_3$, $\geq$ 99 %, Birpa), Silver nitrate ($AgNO_3$, Merck), and polyvinylpyrrolidone (PVP) (average MW 55,000, Sigma Aldrich) were used as received, and deionized water (DI, 18.2 MΩ cm/MilliPore) was used to synthesize silver nanoparticles. For Nanoemulsion Synthesis: Poly[dimethylsiloxane-co-(3-aminopropyl)methylsiloxane] copolymer and Ludox-HS-40 containing SiO_2 NPs with a diameter of 21 nm were purchased from Sigma Aldrich. For chip treatment in case of emulsions flooding, Tetraethyl Orthosilicate (TEOS) was received from Sigma Aldrich. Similarly, for displacement experiments, mineral Oil and silicon oil with a dynamic viscosity of 178 mPas and 40 mPas at 25 °C was purchased from Sigma Aldrich. Sodium Hydroxide (NaOH) and Hydrochloric acid (HCl) were used to prepare 0.1 M solutions of NaOH and HCl, to adjust the pH of nanofluids, which were also purchased from Sigma Aldrich. Deionized water was used to prepare all samples.

2.2 Device Fabrication

For AgNPs synthesis: The respective omega-shape mixer design was fabricated on a silicon wafer (used as a master) by the photolithography technique. The fabricated micro-reactors have a height of 40 µm and a width of 200 µm. Next, 10:1 of Polydimethylsiloxane (PDMS) and curing agent (SYLGARDTM 184 Silicone Elastomer Kit by Dow Inc.) were mixed and degassed in the vacuum oven before pouring onto the master. This mold was then kept at 95 °C for 2 hrs. using a hotplate to cure the PDMS. Once cured completely, PDMS was gently peeled from the silicon master, and 2 inlets and 1 outlet hole of 1.2 mm diameter were punched.

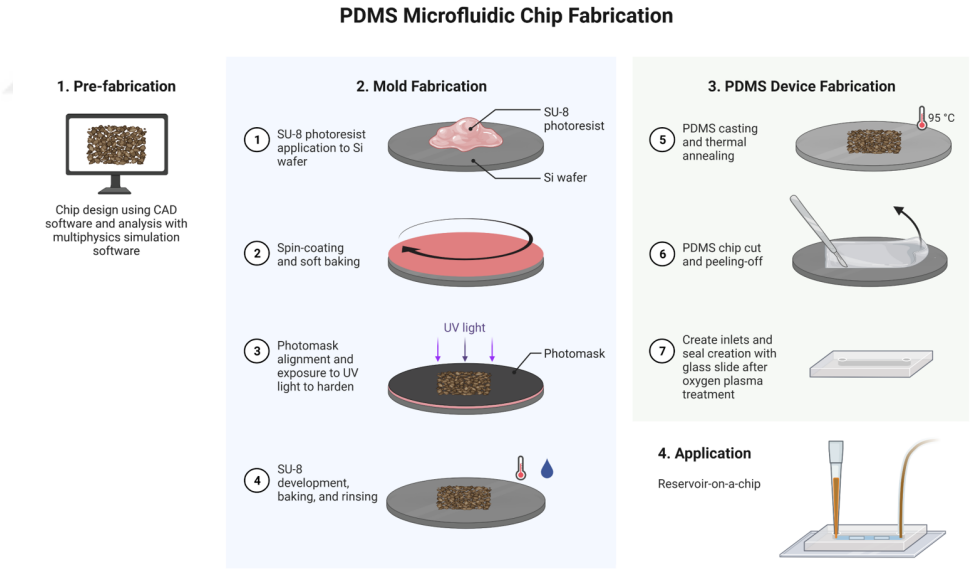

Figure 2.1: PDMS microfluidics chip fabrication process

.

A glass slide (used as a base) was cleaned with volatile solvents in the sequence of acetone-isopropanol and quickly air-dried to get rid of any dirt or contamination. Both the PDMS (having microfluidic chip imprints) as well as cleaned glass slides were subjected to oxygen plasma treatment for surface activation, to have an enhanced bonding of PDMS onto the glass substrate. The irreversible bonding

between PDMS and glass slide was obtained by sticking the activated surfaces together. Lastly, the chip was placed on a conduction hotplate for overnight post-baking at 95 °C. A droplet microfluidic platform was also fabricated with the same process and 1.2 mm punch with 2 inlets and 1 outlet.

For multiphase displacement application, a microfluidic device with an interconnected channel network imprint was fabricated with the same procedure, shown in figure 2.1. However, an inlet and outlet of 1.5 mm diameter were punched. For nanoemulsion flooding, post-fabrication, the microfluidic chip underwent a 15-minute saturation in a 1:2 solution of tetraethyl orthosilicate (TEOS) and Ethanol for chemical surface treatment. The residual solution from the chip was effectively removed by drying under a vacuum. Subsequent saturation with an Ammonium Hydroxide (NH_4OH) solution for 3 minutes was done to ensure prevention from swelling in contact with silicon oil W/O emulsions.

2.3 Experimental Setup for Silver Nanofluid synthesis

The experimental setup is comprised of a microfluidic chip containing a series of Omega-shaped micromixers (to ensure a favourable mixing efficiency), and a fluid pumping unit (NE-4000, syringe pump) integrated with an inverted microscope (Zeiss, Axio Observer 7) equipped with a CCD camera to visualize the mixing flow shown in figure 2.2. For mixing characterization, one of the streams was flooded with fluorescent dye, (Fluorescein, 90+%, Alfa Aesar), and the mixing efficiency was assessed using image J software.

The schematic depiction of the microfluidic chip used for AgNPs synthesis is illustrated in figure 1.6, where the co-flow of solutions A (silver nitrate in glycerol aqueous buffer) and B (PVP in glycerol aqueous buffer) were controlled via the syringe pump. An Actual image of the microfluidic chip is shown in figure 2.2. The aqueous solutions varied from a low viscous 10 % glycerol (w/w) to a high

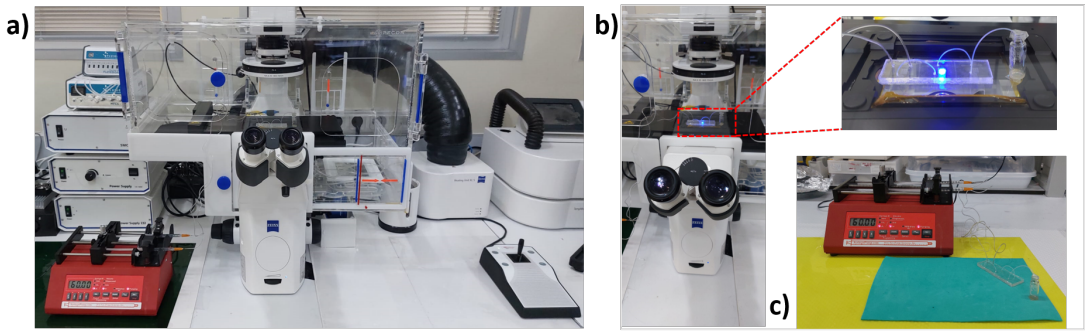

Figure 2.2: a)The imaging setup includes Microscope and Microfluidic Chip, b) A detailed snap of the microfluidic chip, c) A close-up image of experiment setup without microscope for nanoparticle synthesis

.

viscous 80 % glycerol (w/w) solution with a respective viscosity range between 1.2 mPas to 66.6 mPas at 25 °C. Inlet and outlet Teflon tubings with 1 mm internal diameter and 1.2 mm external diameter were used. The flow ratio between the injected stream was fixed at 1:1 for all of the experiments and the synthesized AgNPs were collected in a glass vial from the outlet after 2 hrs. Meanwhile, strict cleaning protocols such as washing and air purging the product collection vials, flushing the microfluidic device with DI water and ethanol after every run, and cleaning the tubing (with isopropanol and DI water) were adopted carefully to avoid any contamination.

2.4 Mixing Mechanism in Microfluidic Omega-Shaped Micromixers

When a stream of fluid is flowing via a straight channel in the absence of any external fluctuations, the cross-stream mixing is restrained due to symmetries in the flow caused by the creation of a uniform surface acting as a barrier for mixing [72]. Thorough mixing can only happen when these two apportions are perturbed. The working mechanism of mixing in omega-shaped mixers of the microfluidic chip is depicted in figure 1.6 and 2.3.

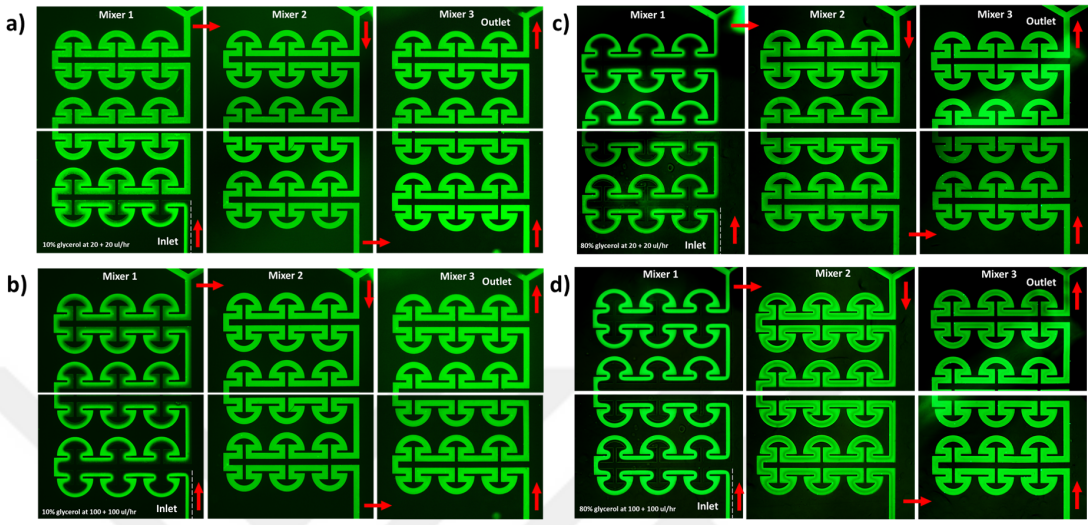

Figure 2.3: Mixing characterization of 10 % glycerol at Pe = 12,236 and 61,184 (a and b, respectively) and 80 % glycerol at Pe = 12,236 and 61,184 (c and d, respectively).

A series of 3 sets of micromixers were used in this study to overcome the mixing challenge. To ensure the complete mixing for all glycerol percentages, the mixing index was characterized by selecting the highest (80 %) and lowest (10 %) glycerol buffer. Solution 1 (80 % Glycerol in water) and Solution 2 (fluorescence dye in 80 % Glycerol in water) was pumped through the microfluidic chip at the lowest (12,236) and highest (61,184) Pe numbers. A similar process was repeated for 10 % glycerol. This percentage and Pe number values were selected after observing a range in multiple optimization experiments (figure 2.3) to ensure complete mixing is achieved.

2.5 Preparation of Analyte Solutions

For mixing characterization, the stock solution of fluorescence dye in 100 % glycerol was first prepared. From this stock, 10 % to 80 % of aqueous glycerol solutions were prepared using deionized water (w/w). For silver nanoparticle synthesis, silver nitrate was used as a metal ion source, PVP as a stabilizing agent, and glycerol as a green-reducing solvent medium. For mixing characterization, the

stock solution of fluorescence dye in 100 % glycerol was first prepared. From this stock, 10 % to 80 % of aqueous glycerol solutions were prepared using deionized water (w/w). For silver nanoparticle synthesis, silver nitrate was used as a metal ion source, PVP as a stabilizing agent, and glycerol as a green-reducing solvent medium. For all percentages of glycerol, i.e. 10 %, 20 %, 30 %, 40 %, 50 %, 60 %, 70 %, and 80 % (w/w); a set of 5 ml solution was prepared in the glass vials and mixed homogeneously using magnetic stirring at room temperature. Next, each 5 ml solution was labelled as Solution A and B, and 0.025 g of $AgNO_3$ and 0.005 g PVP were added separately to each vial. The vial containing $AgNO_3$ in glycerol was wrapped with aluminium foil to avoid any exposure to light. Depending on the viscosity, the solutions were stirred from 20 min to 1 hr. Once dissolved completely, the solutions were ready to be used for the synthesis of AgNPs in the microfluidic chip. For benchtop synthesises of nanofluids, in a glass with glycerol % solution 0.02 g of PVP was added, and mixed until homogeneously dissolved (1 hr), followed by the addition of 0.082 g of $AgNO_3$. The solution was then wrapped in an aluminium film and left on a mixer for overnight mixing.

2.6 AgNPs Synthesis using the Microfluidic Chip

Once the mixing was optimized with different % of glycerol (without $AgNO_3$ and PVP), the glycerol solutions (10 %-80 %) containing $AgNO_3$ and PVP were prepared to synthesize the AgNPs in the microfluidic chip at room temperature. The primary purpose of glycerol was to act as a solvent as well as a reducing medium by providing glyceraldehyde and free radicals for the reduction of silver salt [66] while the stability of NPs was achieved by PVP in the medium. The concentration of reducing agent (glycerol) and ligand (PVP) with respect to the concentration of precursor (silver nitrate) specifies the nucleation, growth and stabilization of AgNPs. As the concentration significantly affects the average size and distribution of the resultant NPs, the transfer of mass during the reaction plays a vital role in explaining the concentration at which a reaction takes place

at any given time. The reproducibility of AgNPs synthesis in microfluidics over a range of glycerol percentages and *Pe* numbers was evaluated by repeating the experiment several times. For each experiment, the synthesized silver NPs were collected after 2 hr and further analyzed for size and morphological characterization by using various techniques.

In order to see the effect of varying concentrations of $AgNO_3$ (metal ion source) and PVP (stabilizing agent) on the size and homogeneity of synthesized nanoparticles, different concentrations of the ingredients were also tested as: i) Concentration 1- Solution A: 1.875 mM $AgNO_3$ and Solution B: 0.75 mM PVP in 5 ml glycerol (%) were prepared as discussed previously; ii) Concentration 2 - Solution A: 7.5 mM $AgNO_3$ and Solution B: 3 mM PVP in 5 ml glycerol (%) were prepared in corresponding glycerol solutions providing the same reaction conditions as mentioned above.

2.7 Characterization of Silver Nanofluid and Reconfigurable Nanoemulsions

For the determination of NP size distribution, diameter measurement involved employing electron micrographs from a transmission electron microscope (TEM, Tecnai G2, FEI). Samples for TEM were prepared by dropping 2 µl of individual silver NPs in glycerol solution onto a Formvar-Carbon coated 400 mesh copper TEM grid (Agar Scientific, UK) at room temperature (RT) until dried and imaged on a FEI Tecnai TF20 FEG high-resolution TEM, functioning at 200 kV. For the calibration of magnification and the scale bar for TEM images, a standard cross-grating was employed. The determination of the average size and standard deviation of silver NPs involved the utilization of an image processing tool (Image J 1.50i), analyzing approximately 50 particles within the TEM images, shown in figure 3.2a.

Confirmation of silver NPs synthesis was carried out via a double-beam configured UV-Vis spectrophotometer (Cary 100 Bio). The assessment covered the wavelength range of 200 nm to 700 nm, comparing against glycerol as a reference.

Furthermore, the confirmation of silver NPs synthesis was confirmed using a double-beam configured UV-Vis spectrophotometer (Cary 100 Bio). The assessment covered the wavelength range of 200 nm to 700 nm, comparing against glycerol as a reference. For the analysis, 350 µl quartz cuvettes were used with a path length of 10 mm. Dynamic Light Scattering (Malvern Nanoseries-ZS) was used to measure the size and monodispersity of synthesized NPs in a microfluidic chip. The measurements were taken with respective refractive index and absorption values of the solutions using disposable plastic cuvettes, at room temperature. As DLS gives slightly large dimensions of NP size and distribution as compared to TEM [53], further studies of morphology, size, and composition of the NPs were performed by TEM and EDX (Energy Dispersive X-ray Analysis) using FEI Tecnai TF20 FEG high-resolution TEM, operating at 200 kV. To prepare the TEM samples, a drop of 10 µl AgNPs dispersed in ethanol was loaded on a copper grid and allowed to dry at room temperature. Histograms of size distribution were calculated from the TEM results using Image J software by measuring the diameters of at least 50 particles.

Further, for the displacement/flooding experiments, the viscosity of the nanofluids and nanoemulsions was measured by the Anton Paar Rheometer as mentioned in Table 4.1 and Fig 5. The Attension Theta (Biolin Scientific) instrument was used to analyze the interfacial tensions between injection fluids and oil. Briefly, the test droplet was suspended in model oil and static IFT between immiscible fluids was measured. Measurements of surface tension and contact angle were performed by using the pendant drop (1.8 mm syringe needle) and sessile drop technique (0.5 mm syringe needle) of the contact angle instrument, equipped with a camera. The operating principle of the pendant drop was based on the hanging droplet technique in which surface tension was calculated by measuring the geometrical properties of injection liquid droplets [103]. The surface tensions of glycerol-based (10 %-30 %) solutions were close to the surface tension of water 72.8 mN/m and varied between 73.2 mN/m and 66.5 mN/m as shown

in figure 4.1a. The contact angle measurements were taken between injection fluids and a PDMS substrate submerged in the oil phase for 1 hr. Briefly, after 1 hr. submersion in oil, the oil was wiped off of the surface of PDMS followed by cleaning with pressurized air. The contact angle measurements were then taken between injection fluids and fresh oil-wet PDMS substrate. Using a disposable capillary syringe, the droplet was placed onto the surface and the initial contact image was taken followed by capturing an image after 2 minutes. An average of 3 independent data values was taken to obtain the final result.

2.8 Synthesis of Reconfigurable Nanoemulsions

For the preparation of silica nanofluids, 1 % (v/v) silica NPs were added to the 5 ml of deionized water in 4 vials separately. After mixing the solutions for 15 minutes, the pH of the nanofluids was adjusted to pH 3, 5, 6, and 8 by using 0.1 M NaOH and HCl solutions until a stable pH was achieved (figure 2.6a). For nanoemulsions preparations, in a separate vial, a stock of 20 % Poly[dimethylsiloxane-co-(3-aminopropyl)methylsiloxane] copolymer in silicon oil was prepared. Then 12 nanoemulsions samples (2.5 ml each) containing 4 variable pH (3, 5, 6, 8) and oil: nanofluid, (80:20, 70:30, 60:40) were prepared. After initial mixing, each sample was then ultrasonicated at 85 watts for 15 minutes (figure 2.6b). The nanoemulsions samples were left for 1 hr to stabilize before being used for flooding experiments. The detailed procedure of the nanoemulsions formation is shown in figure 2.4.

2.9 Geometrical Design of Reservoir-on-a-chip

Keeping into consideration the importance of multiscale porous structures in acquiring an understanding of the immiscible fluid flow dynamics, in this study, to simulate the real process of oil displacement in porous media, an oil-wet, PDMS-based reservoir-on-a-chip model of size 5 $\times$ 5 mm containing a conglomerate rock

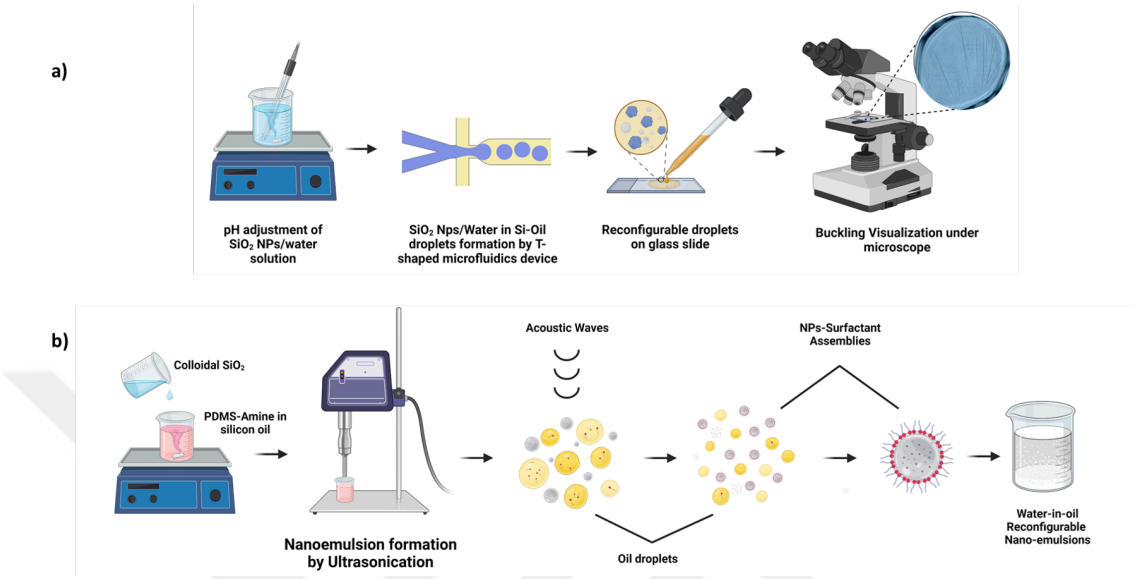

Figure 2.4: a) A Droplet microfluidics synthesis of SiO_2 1 % (v) in silicon oil (containing 20 % (v) Poly[dimethylsiloxane-co-(3-aminopropyl)methylsiloxane] copolymer) to confirm buckling b) An illustration of reconfigurable emulsion synthesis process by ultrasonication.

design was used for microscopic displacement visualization at ambient conditions. The displaced oil (viscosity 263 mPas and density 0.865 g/cm^3) was doped with an oil-based fluorescence dye for high-quality color contrast, facilitating a more precise determination of porosity and residual phase saturation via Image J analysis as shown in figure 2.5.

The porous structure design is the central component of the microfluidics multiphase displacement experiments [104]. Depending on the applications, the intricate geometrical variations can either closely imitate the structure of a natural reservoir or simplify the distinct porous media. Kumar Gunda et al. were the first ones to propose the reservoir-on-a-chip concept by transferring the statistic network information of natural rock to the microfluidic structural design by using Delaunay triangulation and a stochastic random network generator [104, 105]. Since then various heterogeneous porous microfluidics models such as fracture matrix model, dual permeability model and preferential flow models have been developed and reported in the literature [104, 106, 107, 14].

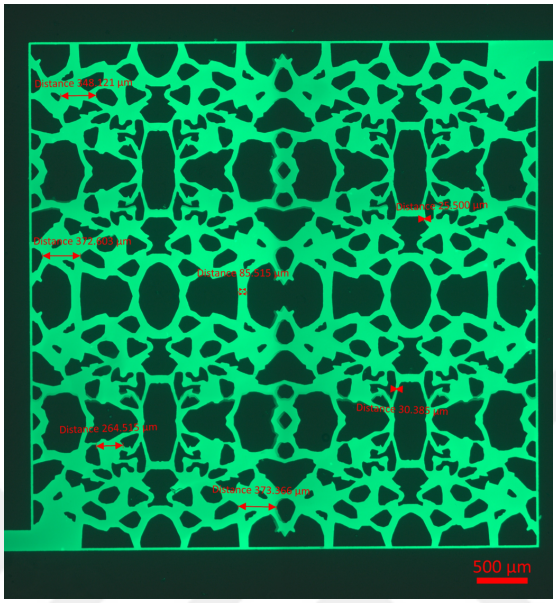

Figure 2.5: Microfluidic chip filled with fluorescence doped oil

2.10 Flooding Experiments and Visualization of Fluid Displacement in Reservoir Micromodel

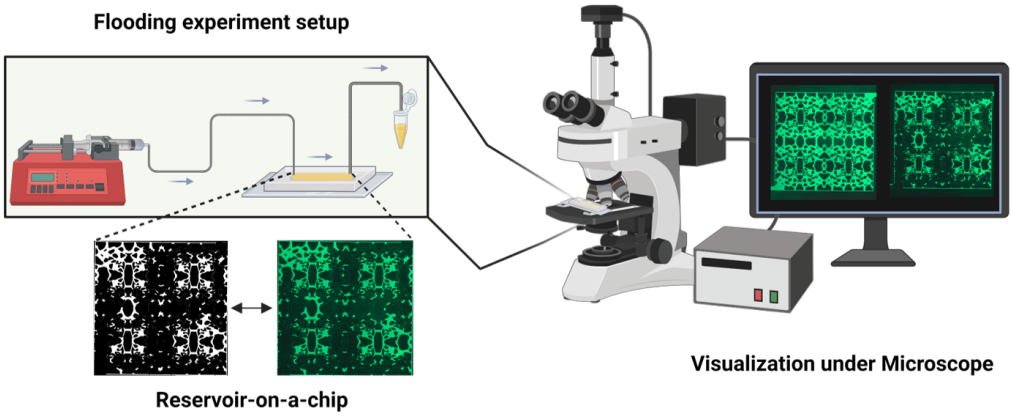

Figure 2.6: Experimental setup for flooding experiments, with inset representing binary and fluorescence image of injection fluid flooding at time t.

Before injecting displacing fluid, the reservoir-on-a-chip was manually filled

with the fluorescence-doped oil and left to rest for 1 hr to ensure uniform wettability. The chip was then placed on the microscope stage and a reference image was taken by using the 2×3 tiles setting of the Zeiss microscope with a 5X objective lens. During the flooding experiment, high-quality images of the chip were taken with the same microscopic setting every 1 minute (0.5 PV) until breakthrough (BT) was achieved, and every 2 minutes (1 PV) after BT till 20 PVs were reached. Then each flooding experiment was separately proceeded in a sequence of deionized water flooding, glycerol/water solutions (10 % to 30 %) and nanofluids (AgNPs/glycerol, 10 % to 30 % solutions synthesized in microfluidics (Mf) and benchtop (Bt) settings) flooding by pumping via a syringe pump (N400) at a constant flow rate of 10 µl/hr. The breakthrough time varies for each injection fluid. After the BT, 20 pore volumes (PVs) were injected for all cases, where a single PV was equivalent to 0.34 µl with an injection time of 2 minutes, shown in figure 2.6.

2.11 Data acquisition and image analysis for Flooding Experiments

Fluid occupancy maps of microfluidic chips were obtained by taking fluorescence images to investigate the accumulative sweep efficiency and pore-scale displacement. The grey scale data, shown in image 2 inset, of the all snaps was evaluated by Image J for analytical calculations. The black region depicts Voids and the white region shows the channels initially filled with oil and later displaced by an injection fluid also depicted in black. The obtained grey scale data gives information regarding the area fraction of the initial oil in place (IOIP). The recovery factor or sweep efficiency was calculated by following the equation:

$$\text{Sweep Efficiency} = \frac{\text{Initial oil in place - Final oil in place}}{\text{Initial oil in place}} \times 100 \qquad (2.1)$$

The porosity can be defined as the % volume in a structure that is a void

space [108]. The porosity of the reservoir-on-a-chip was calculated (0.4524) by finding the area fraction value by image J processing. The pore volume (PV) was calculated by the following equation,

$$\text{Pore Volume} = \text{Volume} \times \text{porosity} \tag{2.2}$$

Here, the overall volume of the reservoir is 0.75 mm^3 and a single PV is 0.34 µl.

Chapter 3

One-Step Synthesis of Ultra-Small Nanoparticles in Glycerol as a Promising Green Solvent at Room Temperature using Omega-Shaped Microfluidic Micro-mixers

3.1 Results and Discussion

3.1.1 Analysis of mixing efficiency of the Omega-shaped micromixers

The mixing of precursors with other reactants plays a crucial role in developing stable reaction conditions for the synthesis of NPs. Therefore, as a model, the synthesis of AgNPs in a passive microfluidic micro-mixer was conducted in this

study [78]. To validate the mixing efficiency inside a microfluidic omega-shaped micro-mixer (adapted and re-modelled for this work from Al-Halhouli et al. [78]), a co-flow stream of the highest glycerol percentage (80 %) with one-half doped with fluorescence dye was acquired in the microchannel. The channel height and width were fixed at 40 µm and 200 µm, respectively. As depicted in figure 2.3 (a-d), at the start of the inlet where two streams of fluid are combined in the main channel, the mixing was limited by lateral diffusion direction. As the fluid enters the micromixers, it enables an immediate swift in the flow direction. The flow is redirected six times by 90° inside each Omega mixing module which not only introduces dean vortices and promotes mixing but also reduces the footprint length for mixing. However, a mixing efficiency of 74 % and 66 % was observed for 80 % glycerol at Pe = 12,236 and 61,184 when only 1 micromixer was used. Under the same conditions, for 10 % glycerol, a mixing efficiency of 85 % and 77 % was achieved (figure 3.1). As illustrated in figure 2.3, we used glycerol (%) and a single set of micromixers did not yield a satisfactory mixing when it comes to higher percentages of glycerol (80 %); hence, we increased the number of omega-pattern sets in series to achieve complete mixing that 3 micromixer sets were provided excellent mixing (denoted as Mixer 1, 2 and 3 in figure 2.3). The quantification of the mixing index can be found in figure 3.1.

As compared to other Ag metal sources, $AgNO_3$ has a slower rate of particle formation due to the strong interaction between Ag+ and NO_3-[109].It emphasizes acquiring a good mixing efficiency in the microfluidic chip. In order to control the synthesis, in general, two conditions exist in the literature. First of it is to use a high flow rate to induce chaotic motion. This, however, would result in incomplete and inhomogeneous mixing in shorter channel length and the breakage of PDMS bonding (particularly due to high viscosity and higher Re number). Second, to enlarge the geometries of the design to promote mixing, but changing the channel dimensions could affect the reaction time and particle size, [110] in fact, this scenario means not to utilize the microfluidic advantages on microscale time and spatial length scale benefits. It is worth to emphasize herein that as it is discussed below, in this study, we have observed that the same synthesis parameters used for bulk benchtop experiments and microfluidic chip yield different results.

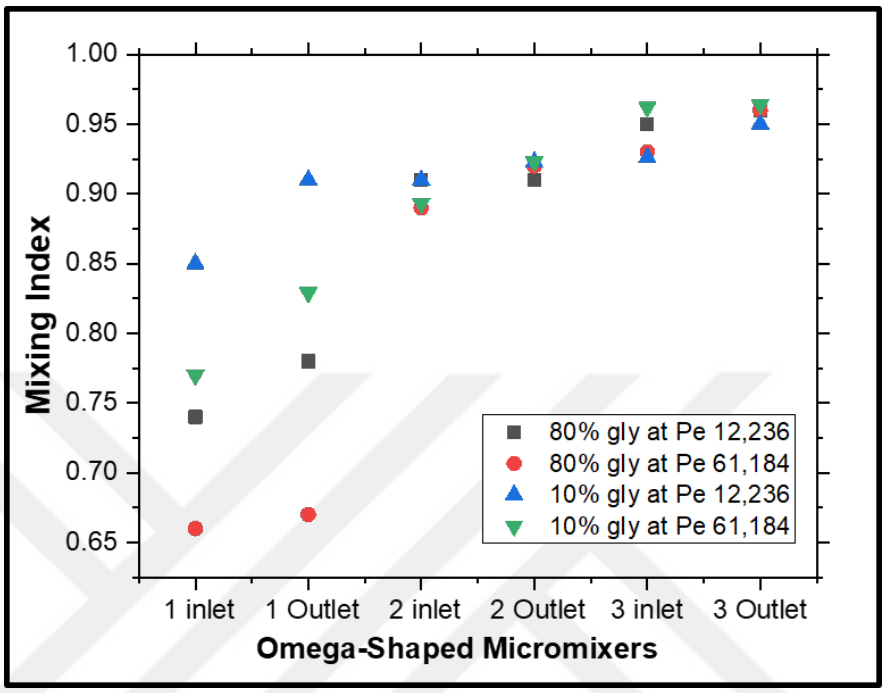

Figure 3.1: Mixing Index of 10 % and 20 % glycerol solutions at $Pe = 12{,}236$ and 61,184 inside an Omega-shaped Micromixer

.

Traditional benchtop synthesis yields nanoparticle sizes around 10-fold larger, while in almost all cases, interestingly, the microfluidic synthesis yield nanoparticle sizes less than 2 nm, which raises the significance of microfluidic reaction kinetics on time and length scales. Hence, to promote the mixing and reaction conditions, instead of changing channel dimensions or geometry, we integrated 3 sets of Omega-shaped mixers in series to get a better mixing index at a considerable Pe number and viscosity (figure 2.3). For the image processing and mixing index (MI) calculation, the chip was placed on the inverted microscope. To evaluate the degree of mixing (mixing efficiency), the distribution of intensity values for 10% and 80% glycerol solutions at Pe numbers 12,236 and 61,184 were conducted. The mixing efficiency is expressed by the homogeneity of the mixed product, and it can be studied by image processing techniques. The mixing efficiency can be described depending on the mixing index calculation by the given equation: [72, 110]

$$MI = 1 - \frac{\sqrt{\frac{1}{N}\sum_{i=1}^{N}(I_i - I_{ave})^2}}{I_{ave}} \tag{3.1}$$

where I_i and I_{ave} denote local and average values of fluorescent intensity across the channel cross-section. The light intensity data of the snaps taken for both Pe numbers, at the inlet and outlet of each set of micromixers were evaluated by Image J for analytical calculations. The obtained data gives information regarding the distribution of the intensity values, where mixing index 1 means complete mixing with 100 % efficiency while 0 means no mixing at all. At the end of the 2nd and 3rd micromixers set, a mixing efficiency of above 90 % and 95 % was obtained for 80 % and 10 % glycerol at respective Pe numbers of 12,236 and 61,184 (figure 3.1).

3.1.2 Synthesis of AgNPs in Glycerol

For the synthesis of AgNPs, glycerol has been used both as a reducing agent as well as a green solvent medium. As a reaction mechanism, glycerol when reacting with oxygen produces a reducing agent, i.e., glyceraldehyde [53]. In addition, under ambient thermal energy such as exposure to visible or UV light, glycerol also produces free radicals. Interestingly, the reduction of metal ions by glyceraldehyde yields larger NPs [53]. However, the reduction by free radicals results in small NPs due to their fast reactivity as compared to aldehydes [53]. Therefore, in our synthesis protocol, the reduction is predicted to be done by both glyceraldehyde and free radicals. However, for glycerol to have enough aldehydes a significant time for exposure to oxygen is required which in our case was limited to 1-2 hrs of solution preparation. Hence, it is expected that as compared to aldehydes a significant number of free radicals were involved in the reduction of Ag+.

As reported by Demcheko et al. a strong reducing agent facilitates instant nucleation hence decreasing the size of NPs. However, an agent with less redox potential will yield bigger NPs [111]. Therefore, a strong reducing agent and the

reduction stage play an important role in the synthesis of NPs. According to Polte et al. particularly for AgNPs, the reduction stage is quite fast, i.e., < 200 ms [67]. Thus, the mixing of silver precursors with other reactants plays a crucial role in developing stable reaction conditions, thereby affecting the size, shape as well as monodispersity of the synthesized product.

3.1.3 Microfluidics synthesis of AgNPs

For the one-step microfluidic synthesis of AgNPs in glycerol, firstly the PVP and $AgNO_3$ solutions in varying percentages of glycerol were prepared separately outside the microfluidics device. Then, the freshly made solutions were pumped into the microfluidic mixer at controlled *Pe* numbers. The product was collected at the outlet for 2 hrs. The change in the solution color from transparent to yellow and then a light grey confirmed the reduction of silver ions by glycerol and hence the production of AgNPs, while the stability of the nanoparticles was achieved due to the presence of PVP in the reaction mixture. Remarkably, in comparison to other AgNPs synthesis procedures including ultrasonication, high-temperature heating, pH variation and/or addition of surfactants, our protocol offers a synthesis of ultra-small silver nanoparticles in one-step procedure using a straightforward mixing strategy without complex procedures.

Nevertheless, the process of NPs formation depends on classical nucleation theory [112]. For years the process of nucleation and growth has been described by Lamer Burst nucleation until Watzky and Finke gave the approach of slow nucleation followed by autocatalytic growth [113]. Nucleation is a process in which a seed (nuclei) acts as a template for crystal growth. However, crystal-mediated nucleation is acknowledged as secondary nucleation. Homogeneous nucleation is associated with the formation of homogeneous nuclei and vice versa. It can be thermodynamically described by Gibb's free energy of the nanoparticles. As Gibb's free energy is the sum of volume-free energy and surface-free energy, [52, 114] the volume-free energy is persistently negative and the surface-free energy is eternally positive. So, there is maximal energy wherein a persistent

nucleus with a critical radius can be formed sans dissolving. To recapitulate, the nuclei serve as a template for crystal growth with varied diameters. However, the use of a strong stabilizing agent prevents the further growth of NPs and makes the solution kinetically stable [115].

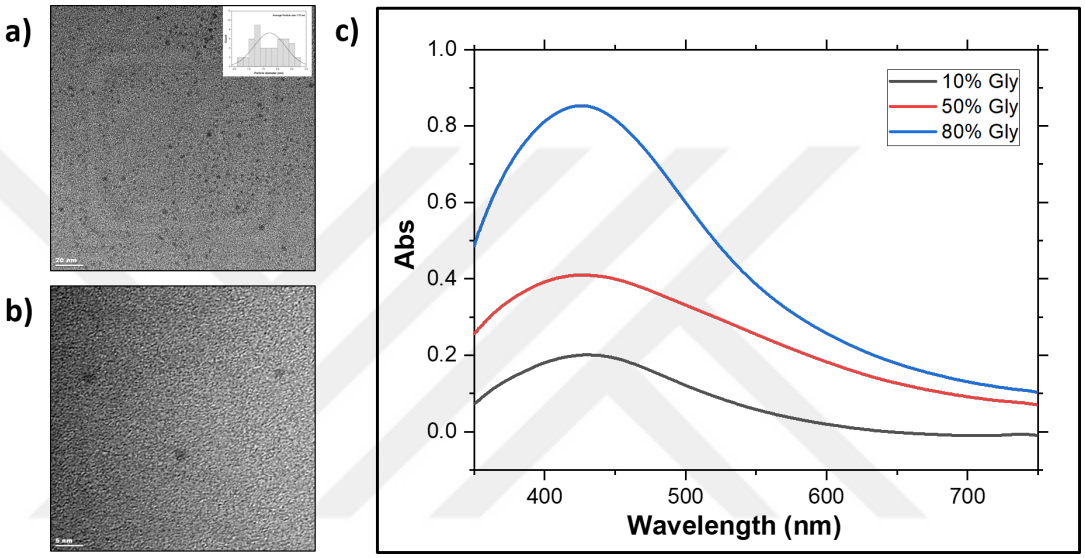

Figure 3.2: a,b) TEM images of AgNPs synthesized in 50 % glycerol at a *Pe* number of 12,236. The histogram in the inset (a) depicts the size distribution, b) UVvisible spectroscopy results of AgNPs synthesised in 10 %, 50 %, and 80 % glycerol buffer at $Pe = 36{,}710$ in omega-shaped micromixers

.

Microfluidics synthesis of AgNPs has been widely investigated, and the majority of the studies focus on NPs synthesis in droplet microfluidics [116]. Synthesis in a continuous flow reactor has also been reported, but in most of the protocols, the synthesis was limited by the temperature (100-140 °C) required for the reduction and stabilization of the NPs [117]. In droplet microfluidics, by changing the flow rate of dispersed and continuous phases the size of NPs can be controlled. It has been reported that the ultra-small AgNPs of 2.5 nm can be obtained in droplet-based microfluidics using Borane dimethylamine (DMAB)/PVA, tween 80 and $AgNO_3$ salt as a reducing agent, stabilizing agent and a silver precursor respectively [118]. Similarly, Xu et al. were able to synthesize AgNPs of 4.9 nm and 7.6 nm respectively in a T-junction microfluidic chip by using $NaBH_4$/PVP, EDTA, and $AgNO_3$ [116]. However, amongst various established NPs synthesis methods, the reduction of reduction is preferred by either citrate, $NaBH_4$ or

hydroxylamine hydrochloride, often in conjnction with ascorbic acid, dextrose and /or NaOH. Unfortunately, none of these approaches can consistently yield nanoparticles with high monodispersity/uniformity in shape and size in a single step. Additional techniques like centrifugation, heating, sonication, and the addition of surfactants in the reaction are key to reaching the desired size during this synthesis. Besides, in the search for environment-friendly solvents and processes for the synthesis of nanoparticles, glycerol has been notified as a "green chemistry solvent" due to its non-toxicity, biodegradability and renewable character. Glycerol also possesses the ability to dissolve a variety of compounds with ease, including inorganic salts, organic compounds, and acids/bases. Hence, in the current study, the significant reduction properties of glycerol combined with the microfluidics allowed fast reaction kinetics and rapid nucleation thus yielding ultra-small NPs in the range of 0.7 nm to 2.0 nm figure 3.2 and 3.3.

3.1.4 Effect of Peclet number and mixing efficiency on AgNPs synthesis

Since the *Pe* number can affect nanoparticle synthesis by affecting the mixing efficiency, [73, 114] under standard operating conditions, the corresponding *Pe* numbers for $AgNO_3$/glycerol solution and PVP/glycerol solution were studied for *Pe*=12,236, *Pe*=36,710 and *Pe*=61,184. Due to the large surface-to-volume ratio and small capillary dimensions, microfluidic devices permit rapid and consistent mass transfer, and as a result, provide exceptional control of the characteristics of nanoparticles [119]. In literature it is reported that the synthesis, reaction and nucleation of AgNPs have very fast kinetics [120]. For AgNPs synthesis, quick nucleation of less than 1 ms was observed by Takesue et al. [114]. Thus, the reaction is perceived to occur at the very initial part of the reactor where the interface between two fluids supplies necessary reagents for clustering and stabilization of AgNPs. Generally, higher flow rates can result in the appearance of large NPs [110]. If a significant amount of mixing is not achieved, then only a small amount of silver precursor is consumed in the synthesis and a substantial amount of silver precursor is left at the outlet of the microfluidic chip. The

recirculation pattern formed at the outlet causes a fast mass transfer causing a non-homogeneous concentration region. Hence, the resulting NPs will have a low surface charge and aggregate to form larger NPs causing polydispersity of NPs.

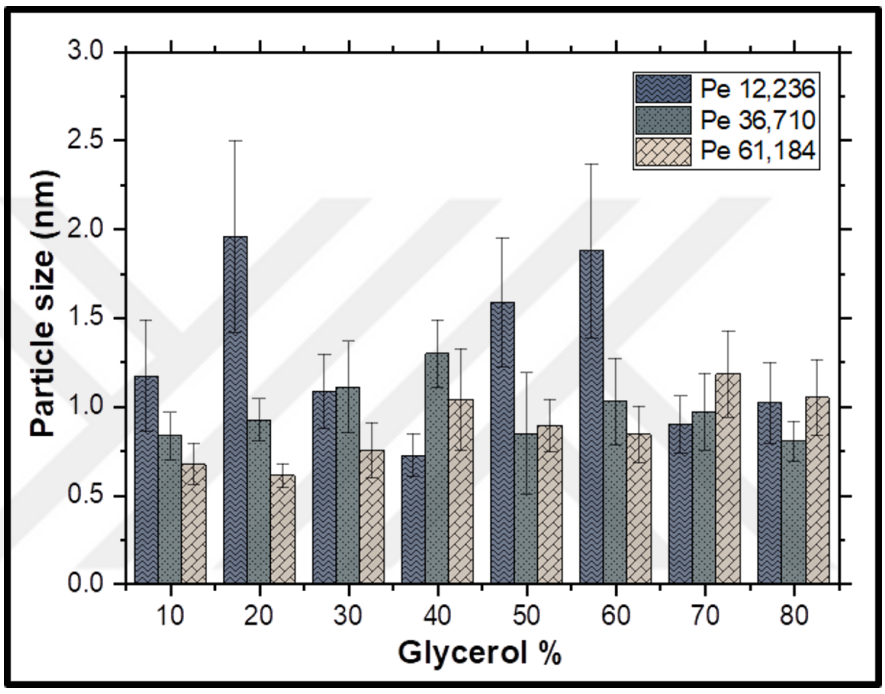

Figure 3.3: Synthesis of nanoparticles in a microfluidic chip at Pe = 12,236, Pe = 36,710, and Pe = 61,184 for 10 % to 80 % glycerol buffer.

For that reason, we first confirmed the mixing in the device figure 2.3, followed by the size measurements using figure 3.3. For three optimized Pe numbers, a gradual increase or decrease in the size of NPs with respect to Pe number was expected. However, for all of the glycerol %, the size of AgNPs was measured as < 2 nm, with a specific size range for Pe=61,184 between 0.61 nm (20 %) and 1.18 nm (70 %). While for Pe=36,710 highest size of 1.29 nm was obtained for 40% glycerol and the smallest AgNPs size of 0.80 nm was obtained for 80 % glycerol. Similarly, for Pe=12,236 a largest size of 1.95 nm was obtained for 20 % glycerol and 0.72 nm for 40 % glycerol. Thus, our findings highlight the appearance of similar size-ranged nanoparticles irrespective of the high or low flow rates/Pe numbers. However, it is important to note that the effect of flow rate on NPs size distribution is still not completely understood, and conflicting results have been reported in the literature [68]. For instance, it has been reported that the average

size of AgNPs decreases with an increase in volumetric flow rate.44 Furthermore, Liu et al. found that with the increase in the flow rate, the particle size increases to the maximum threshold (3.5 ± 0.9 nm, to 7.2 ± 2.0 nm at 200 and 400 µl/min) and then decreases with an increase in flow rate (3.0 ± 0.5 nm at 600 µl/min) [68]. One such study was conducted by Shin et al. where they investigated the effect of flow rate on the size distribution of nanoparticles (NPs) in a microfluidic channel.

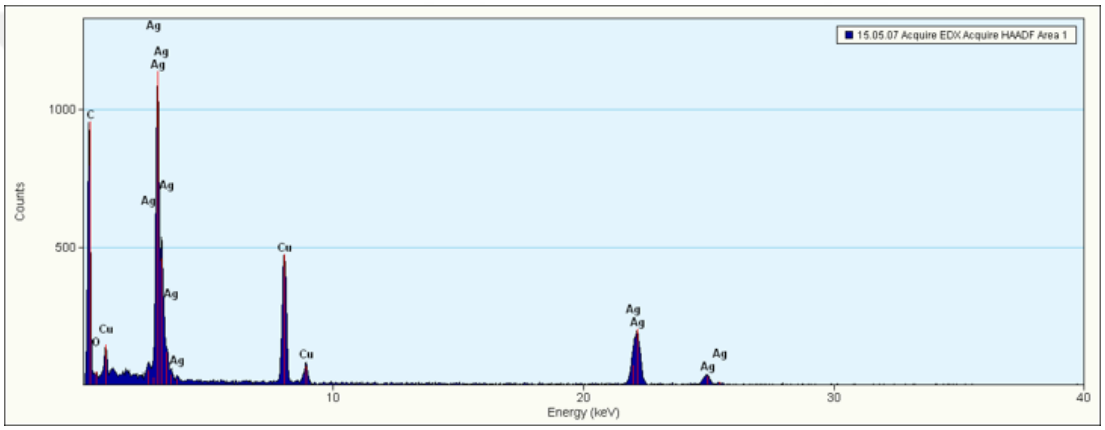

Figure 3.4: Energy Dispersive X-ray (EDX) of the AgNPs on a Copper (Cu) grid
.

Akin to our work, the authors found that similar ranged NPs were produced irrespective of the high or low flow rates/*Pe* numbers, which suggests that flow rate may not be the dominant factor affecting NPs size in a microfluidic system. Despite these conflicting results, it is clear that when designing a microfluidic system for the synthesis of nanoparticles, it is important to consider all of the factors such as channel geometry, channel dimensions, the flow rate ratio of precursor solution, and especially the different reaction mechanisms and kinetics which can lead to different NPs synthesis results and size [121, 122]. Our research findings provide new and additional insights into ultra-small AgNPs synthesis and contribute to the existing literature by elucidating the mechanisms driving NPs synthesis under varying glycerol concentrations as a reducing medium in omega-shaped microfluidic mixers. The synthesis of NPs is usually confirmed by a change in the color of the solution. To further confirm the synthesis of AgNPs, UV-Visible spectroscopic measurements were obtained. Since no significant change in size was observed for all of the *Pe* numbers, UV-Visible spectroscopy data was generated

Glycerol %	Flow rate (µl/hr) at Re no. 0.1	Flow rate (µl/hr) at Re no. 0.3	Flow rate (µl/hr) at Re no. 0.5
10	50	150	250
50	255	765	1785
80	2325	6984	11630

Table 3.1: The values of each inlet flow rate for 10 %, 50 %, and 80 % glycerol buffer at Reynold number = 0.1, 0.3, and 0.5.

for the lowest, intermediate, and highest glycerol percentages (i.e., 10 %, 50 % and 80 %) at *Pe* numbers of 36,710. An absorption peak between 427-430 nm approved the silver nanoparticles (figure 3.2c). Furthermore, TEM data was generated to observe the morphology of the obtained particles and compare the size with our DLS data. TEM images of AgNPs synthesized in 50 % glycerol buffer at *Pe* number 12,236 show uniform nanoparticle distribution (figure 3.2a and b). The particle size statistics plotted as a histogram were measured by selecting 50 random NPs from the population, which indicated that the average size of particles was 1.72 nm; similar to the DLS results (Figure 3a). Next, the energy dispersive X-ray (EDX) spectra were measured for the elemental analysis of the obtained particles. The results depicted a great amount of Ag from the reduction of $AgNO_3$, whereas the peaks of Cu were also observed from the copper-coated grid (figure 3.4).

3.1.5 Effect of Higher Flow Rates on AgNPs Size

In order to relate all the *Pe* numbers utilized in this study with their respective *Re* numbers, firstly, the values of Re number were calculated at various *Pe* number (*Pe*=12,236, *Pe*=36,710 and *Pe*=61,184) (figure 3.6a). At this point, we wanted to further confirm that the ultra-smaller size was truly originating due to controlled mass transfer and perfectly regulated experimental conditions (*Pe*

numbers and concentrations) in microchannels. Therefore, the effect of higher *Re* numbers 0.1, 0.3, and 0.5 on AgNPs size was also tested (corresponding flow rates are given in Table 3.1. However, since glycerol has been used as a solvent medium in the current study, owing to high viscosity at higher percentages, such a higher *Re* number damaged the microfluidic chip and the bonding strength was not possible to carry those flow rates. Therefore, as an alternative approach, a coaxial flow reactor setup [110] has been utilized as an additional tool to overcome the synthesis at a higher Re number [110].

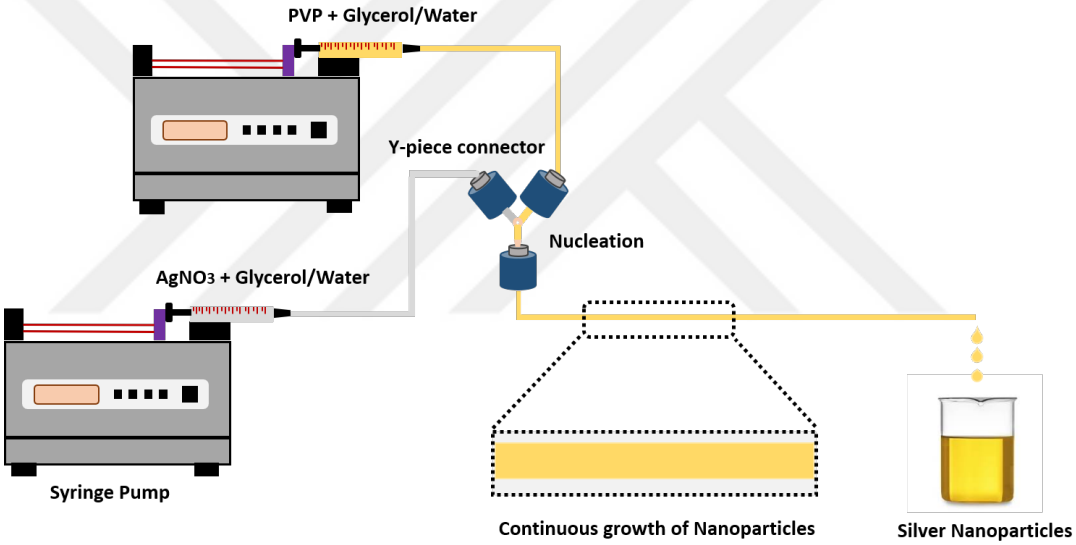

Figure 3.5: Schematic representation of AgNPs synthesis in a Y-piece flow reactor and a capillary tube.

In our system, the capillaries were connected by a Y-piece connector with the outer tube having an internal channel diameter of 100 µm (figure 3.5) being a similar length scale with the microfluidic device used (hydraulic diameter of the microfluidic channels is 70 µm). Three different glycerol percentages (10 %, 50 % and 80 %) were used to get an overall effect on size and size distribution. As shown in figure 3.6b, the size of AgNPs was in a range of 0.73 nm to 1.24 nm for 10 % to 80 % glycerol when synthesis was done with Re numbers, *Re*= 0.1, *Re*=0.3 and *Re*=0.5. Earlier studies also reported a decrease in channel diameter would yield an inherently large surface-to-volume ratio [123]. Hence, results in rapid mass transfer which could lead to good mixing efficiency and narrow size of particles. Hence, it was proved that as long as the design has

µm dimensions, a nearly perfect mass transfer between solution $AgNO_3$/glycerol and PVP/glycerol results in controlled nucleation and growth conditions which yield ultra-small AgNPs. In the following section, these findings in microfluidics are compared with benchtop synthesis which yields larger nanoparticle sizes at different degrees with varying glycerol concentrations.

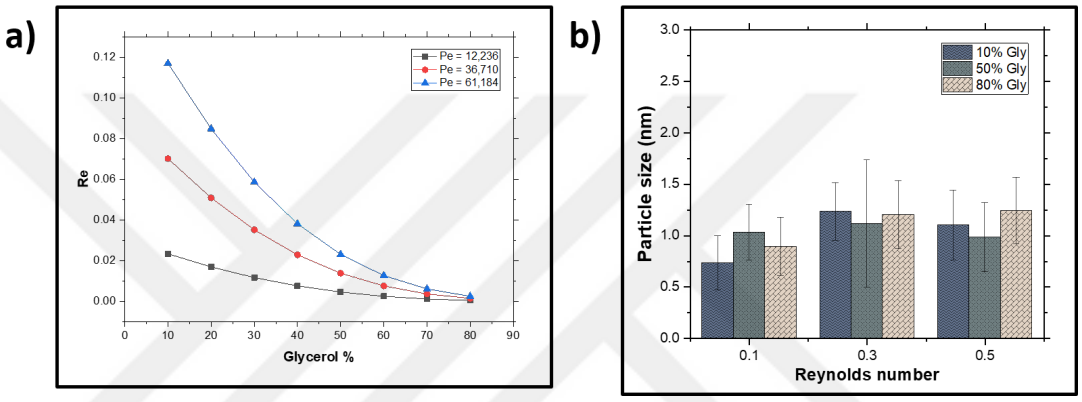

Figure 3.6: Reynolds number for 10 %-80 % glycerol buffer at *Pe* numbers = 12,236 36,710 and 61,184.

3.1.6 Effect of PVP concentration on AgNPs size

In order to observe the effect of PVP concentration on AgNPs size in 10 %, 50 %, and 80 % glycerol, two different concentrations of PVP 0.375 mM and 0.75 mM were prepared while keeping the concentration of $AgNO_3$ (3 mM) constant. As illustrated in figure 3.7, the DLS results for both PVP concentrations exhibit monodispersity of particles with an average size of less than 1.6 nm for all glycerol percentages at *Pe* numbers 12,236, 36,710, and 61,184. For instance, for 10% glycerol in both PVP concentrations, the size varied between 0.67 nm to 1.17 nm at all *Pe* numbers. While for 50 % glycerol a general size variation between 0.6 nm and 1.6 nm was obtained. Similarly, the largest size of 1.6 nm (0.375 mM PVP) at *Pe* =12,236 and the smallest size of 0.8 nm (0.75 mM PVP) at *Pe* = 36,710 was acquired in 80 % glycerol solution. Hence, the DLS results confirmed that the synthesized AgNPs were perfectly stabilized by both concentrations (0.375 mM and 0.75 mM) of PVP. Notably, the stability test for AgNPs synthesized with

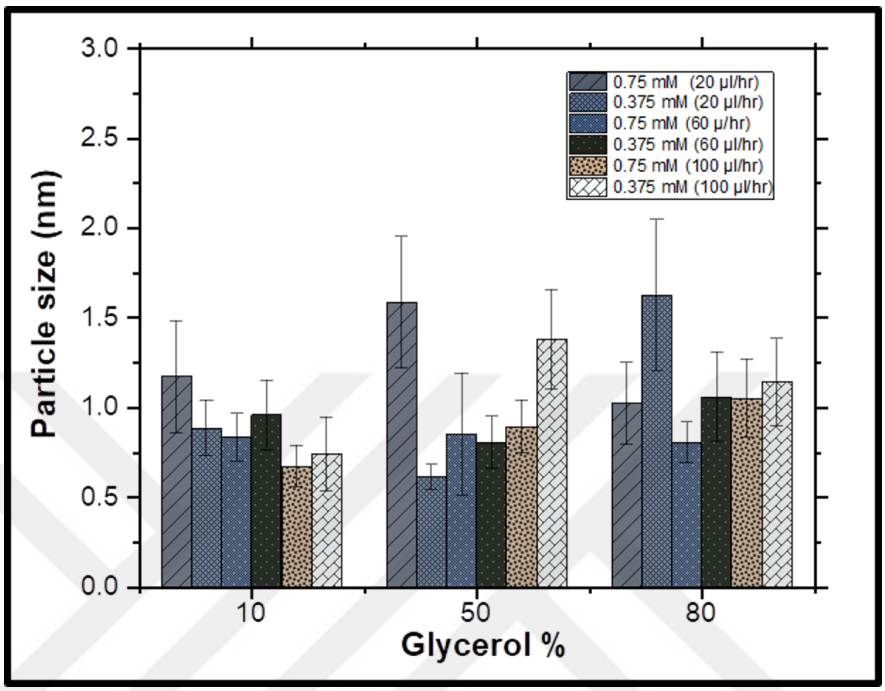

Figure 3.7: Effect of PVP molarity, 0.001 and 0.003 M, on size of AgNPs synthesized in 10 %, 50 %, and 80 % glycerol buffer with respect to Pe = 12,236, 36,710, and 61,184.

0.375 mM PVP reveals that the polydispersity index (PDI) of particles increased in a period of week as shown in figure 3.8a (where PDI 1 and PDI 2 represent PDI before and after the stability test).

However, AgNPs synthesized with 0.75 mM PVP had no significant variation in PDI over a span of a month (figure 3.8b). The results can be justified by the working mechanism of PVP where the oxygen and nitrogen atoms in a polar group of PVP have a strong affinity towards Ag+ [60]. It acts as a capping agent via electrostatic and steric stabilization of amide groups of pyrrolidone agents. Hence, its interaction with silver ions creates a capping layer and controls the size of nanoparticles. As depicted previously a significant amount of PVP prevents aggregation of AgNPs due to repulsion caused by the interaction of hydrophobic carbon chains and stabilizes the size of NPs [63]. However, in the case of 0.375 mM PVP figure 3.8b. The amount of PVP is not enough for full encapsulation of a smaller size AgNPs. Hence, the particles agglomerate and gradually grow into larger particles to reduce overall surface energy. On the other hand, a perfect

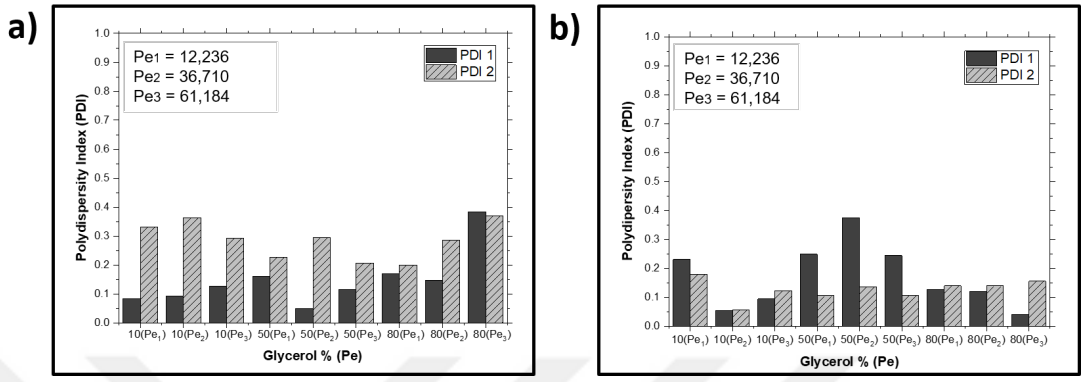

Figure 3.8: a) PDI variation of AgNPs synthesized in 10 %, 50 %, and 80 % glycerol buffer with 0.375 M PVP at *Pe* numbers = 12,236 36,710 and b) PDI variation of AgNPs synthesized in 10 %, 50 % and 80 % glycerol buffer with 0.75 M PVP at *Pe* numbers = 12,236 36,710 and 61,184 and 61,184.

encapsulation and an increase in stability of AgNPs with increasing the PVP concentration (0.75 mM) is evident because of an increase in steric repulsion which inhibits aggregation.

3.1.7 Effect of reactant concentration on AgNPs size

In general, in order to get small nanoparticle size, less concentration of silver precursor is used. Yet, for the large-scale synthesis, this is undesirable. Herein we tested the recipe (7.5 mM $AgNO_3$ and 3 mM PVP) in microfluidics, at an intermediate Pe number of 36,710. Interestingly, for 3 mM PVP and 7.5 mM $AgNO_3$ (figure 3.9) the size of NPs varied between 0.6 nm and 1.2 nm for 10 %-80 % glycerol. However, this concentration could easily clog the microchannel due to the adhesion of silver nuclei with the walls of micromixers because of its high surface-to-volume ratio. Hence, an optimized concentration of 1.8 mM of $AgNO_3$ and 0.75 mM of PVP was fixed throughout the study after testing various concentration combinations e.g. 3.75 mM, 2.5 mM, and 1.8 mM of $AgNO_3$ with 2 mM, 1 mM, and 0.75 mM of PVP, respectively (data not shown). When compared, no paramount effect of concentration on the size of NPs was observed, restricting the particle size between the range of 0.80 nm and 1.3 nm (figure 3.9), thus emphasizing the impact of microfluidics on the synthesis chemistry of NPs.

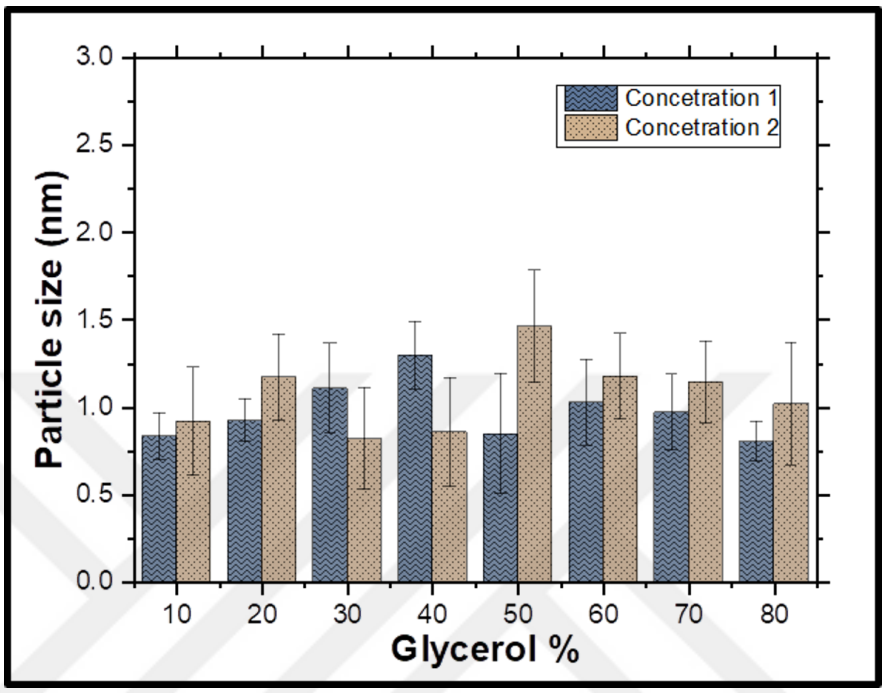

Figure 3.9: Effect of reactant concentration on particle size synthesized at Pe = 36,710 in 10 % to 80 % glycerol buffer.

3.1.8 Comparison of the AgNPs produced in the microfluidic reactor and batch reactor

Silver nanoparticles with a size of less than 5 nm have unique catalytic activity due to a high surface-to-volume ratio [124]. Existing studies require complex procedures such as heating, lengthy protocols, and multiple reagents for synthesis. In order to see the tremendous effect of microfluidics on the size of AgNPs, we compared our results with synthesizing silver NPs in glycerol through the conventional benchtop method [5]. For a representative comparison, initially the same ratio of Ag: PVP was used as in the batch reactor, and later 4 times less concentration of Ag : PVP in the batch reactor was also tested. As depicted in figure 3.10, in benchtop synthesis the size of AgNPs was in the range of 1 nm to 14 nm for 10 % - 80 % glycerol, giving a linear increase in the size of nanoparticles with an increase in glycerol percentage; thus, showing a tunable effect of reducing solvent medium on the size during the synthesis of silver nanoparticles.

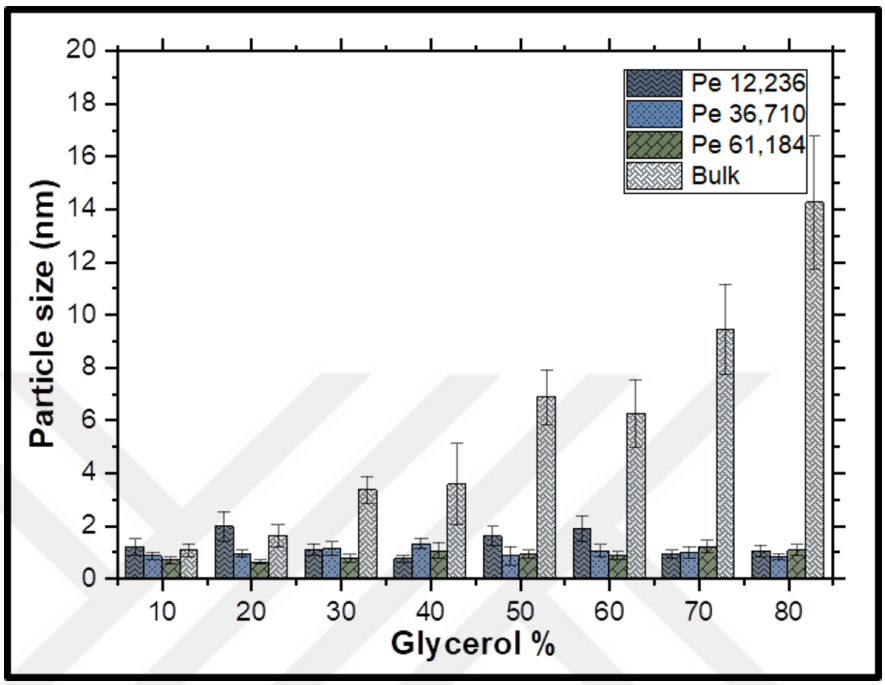

Figure 3.10: Comparison of microfluidic synthesis of AgNPs at Pe = 12,236, 36,710, and 61,184 and benchtop synthesis for 10 % to 80 % glycerol.

However, in order to obtain ultra-small nanoparticles (< 2 nm) in one single step microfluidic synthesis surpassed the benchtop synthesis; no significant effect of increasing glycerol percentage on AgNPs size was observed, giving a size variation between 0.7 nm to 1.95 nm, consequently confirming the effect of microfluidics on the size of NPs with respect to the synthesis kinetics discussed above. To further elaborate, over the past decade, microfluidic-assisted continuous NP synthesis has drawn significant attention due to several advantages over conventional bulk synthesis [125]. Both microfluidics and batch-type bulk synthesis use chemical reduction for the synthesis of NP. The advantages of microfluidics over batch synthesis can be understood by comparing the physics behind the mass/heat transport length scale with respect to micro and macroscale analogues [126]. Conventional bulk synthesis requires more sample volume and the reaction kinetics varies due to the large diffusion time for mass and heat transfer causing more batch-to-batch variation[76]. However, micromixers offer immense potential for high reproducibility, low batch-to-batch variation, and enhanced efficacy

[125]. Firstly, at the microscale, the surface-to-volume effects dominate as a result viscous forces dominate over inertial forces and flow prevails in the laminar regime ($Re < 2000$) [126].

Mixing in laminar flow regimes facilitates the analysis and control of molecular transport. Secondly, the paramount surface-to-volume ratio of microfluidic reactors results in better mass and heat transfer. The fast nucleation in microfluidics leads to small seed size hence yielding small NPs with better control on morphology and composition of the NPs as compared to bulk synthesis. The obtained results were compared with existing studies where microfluidics and benchtop synthesis of NPs was done. A difference in size was also observed based on synthesis in microfluidics and benchtop in a study of Tofighi et.al where Au: PVP NPs with an average size of 1.0 nm in the microfluidic reactor and 1.9 nm in the batch reactor was achieved [127]. Due to fast nucleation and regulated flow in microfluidics, a slightly small NPs size was obtained when compared to benchtop results.

3.2 Conclusion

This study examined the synthesis of ultra-small AgNPs (< 2nm) in glycerol as a promising green-reducing solvent medium by using a continuous flow configuration of customized omega-shaped microfluidic micromixers. As compared to traditional synthesis protocols, our strategy portrays a simple, easy and time-efficient, one-step green synthesis of AgNPs in glycerol as a solvent and reducing medium devoid of any additional conditions like high temperature, the addition of surfactants, ultrasonication and/or centrifugation. Synthesis parameters and conditions such as variable glycerol percentage (10 %-80 %), Pe number, concentration of reagents and molarity of PVP were investigated to observe the effect on the average size and size distribution of NPs. The rapid mass transfer and controlled reaction kinetics in a microfluidic reactor indicated the average size distribution of AgNPs for all reaction conditions is less than 2 nm. However, the controlled mixing conditions in omega-shaped micromixers provided long-term

monodispersity of particles as compared to benchtop synthesis. To recount, as long as the channel's dimensions are on a small scale (in micrometres) the particle size was less than 2 nm. Furthermore, the comparison with our batch synthesis showed a drastic effect of microfluidics on NPs size with respect to glycerol viscosity. The improvement and development of other NPs synthesis protocols in glycerol inside our customized microfluidic chip are still under investigation. Overall, with respect to the conventional benchtop-assisted NP synthesis, the current study opens the door to highlighting the profound effect of the microfluidic technique itself on synthesizing ultra-small as well as more homogeneous nanoparticles without any additional effort.

Chapter 4

Multiphase Flow Displacement: Silver Nanoparticles and Reconfigurable Nanoemulsions

4.1 Multiphase Displacement Application of Silver Nanofluid

4.1.1 Interfacial Activity of Nanofluids

IFT is a significant parameter in analysing the fluid movement and distribution in a porous matrix for multiphase displacement applications such as enhanced oil recovery (EOR) [7]. The importance of IFT lies in its capacity to extract oil from the reservoir pores by decreasing the capillary pressure within the reservoir channels. When the IFT between the reservoir oil and injection fluid is elevated, the lack of immiscibility between the two fluids obstructs the displacement of oil from the reservoir [7]. In the current analysis, the effect of interfacial tension between injection fluids /oil interface was measured at 25 °C under atmospheric pressure conditions. Figure 4.1c, shows a distribution graph for the static IFT between

oil and injection fluids including, water, 10-30 % bare glycerol and nanofluids containing AgNPs synthesised in 10-30% glycerol in benchtop and microfluidics settings, (preceding data in figure 1.5 and 1.6. Data from these experiments revealed that the IFT between oil and bare glycerol solutions (10 %-30 %) decreased, with the increase in viscosity [128].

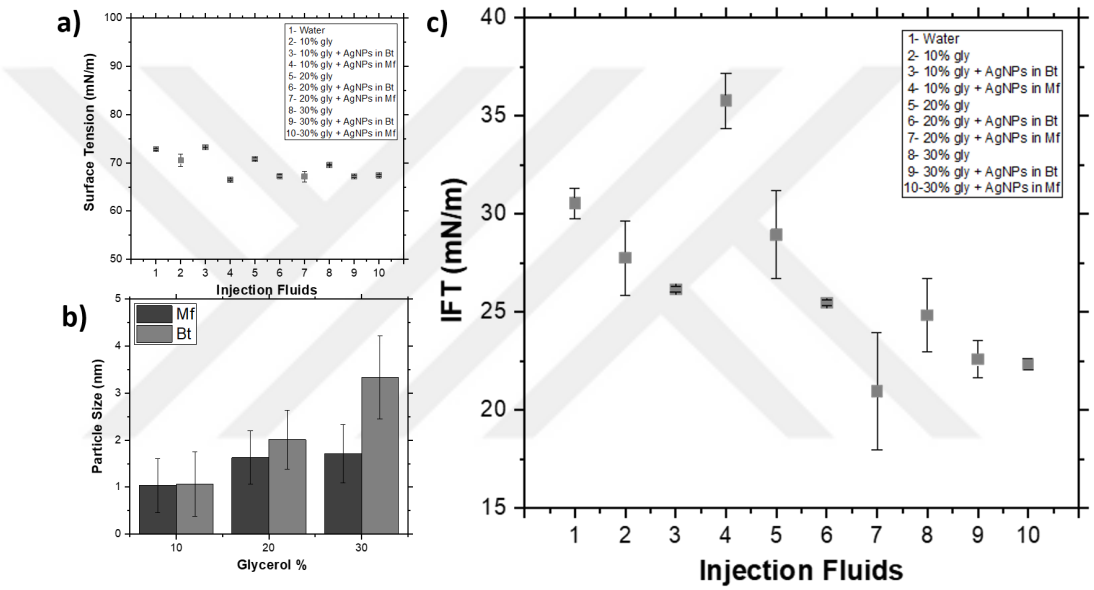

Figure 4.1: a) The surface tension of injection fluids, b) Dynamic Light Scattering results of AgNPs/glycerol (10-30 %) synthesized in microfluidics (Mf) and Benchtop (Bt) settings, c) Graphs showing IFT between displaced oil and injection fluids

.

After introducing AgNPs into the system (10 %-30 % glycerol solutions) it was observed that the adsorption of NPs at the interface led to a further reduction of system energy [84], resulting in a decrease of IFT from 30 mN/m (deionized water) to about 22.37 mN/m and 22.58 mN/m (30% glycerol with AgNPs synthesized Bt and Mf settings). Additionally, it was also noticed that NPs size influenced the interfacial tension between the oil/nanofluids interface. Figure 4.1b, illustrates the size of AgNPs synthesized in glycerol % in microfluidics and benchtop synthesis. It was observed that IFT decreased more uniformly in the case of Bt-synthesized AgNPs from 26.15 mN/m (1.2 nm in 10 % glycerol) to 22.58 mN/m (3.3 nm in 30% glycerol). A similar behavior of decreasing IFT

with NPs size was also observed in a study by A.V. Minakov et al. and Muhammad Adil et al. [103, 129]. However, for microfluidics-synthesized AgNPs, in 10 % glycerol, a slight increase in IFT to 35 mN/m was observed. In 20 % and 30 % glycerol, a decrease in IFT to 21 mN/m and 22.37 mN/m was observed. It was expected because, in our previous study, we used a reduced amount of reactants (by one-fourth) during microfluidic synthesis due to microchannel clogging issues experienced by using the same/higher concentration as Bt-synthesized NPs [6]. As IFT is susceptible to nanofluid concentration due to variations in the surface energy of the NPs [129], a variable IFT was obtained for Mf-synthesized AgNPs. Furthermore, the error bars express the variation in IFT measurements which can be caused by local variations of particle concentration during measurements. However, it is essential to note that a substantial reduction in IFT to 0.01 and 0.001 orders is required to be considered as an effective EOR mechanism which had been predominantly observed in surfactant-based EOR applications [24, 130, 131]. Additionally, the effect of NP size on IFT is less pronounced as compared to the contact angle [103]. Therefore, it is expected that IFT reduction by AgNPs nanofluid has less impact on EOR as compared to the wettability modification mechanism.

4.1.2 Wettability Alteration by Nanofluid

Wettability is the property of a liquid to adhere to or distribute across a solid surface in the presence of another liquid [22]. Wettability alteration caused by NPs is influenced by different factors including NPs concentration and size [22]. The effect of nanofluid with different sizes and concentrations on PDMS microfluidic surface wettability was studied as shown in figure 4.2. The initial contact angle (θ) of deionized water on an oil-aged PDMS surface was observed to be in an oil-wet state with $\theta = 108^\circ$ with a wettability reducing to $\theta = 97^\circ$ after 2 minutes. For all glycerol-based fluids, the initial contact angle varied between from oil-wet state $\theta = 107^\circ$ and $\theta = 113^\circ$ except 10% glycerol/AgNPs Bt-synthesized fluid and 30% glycerol/AgNPs Mf-synthesized nanofluid, where initial θ was 104° and 101°. Following two minutes, a noticeable shift in wettability emerged, indicating

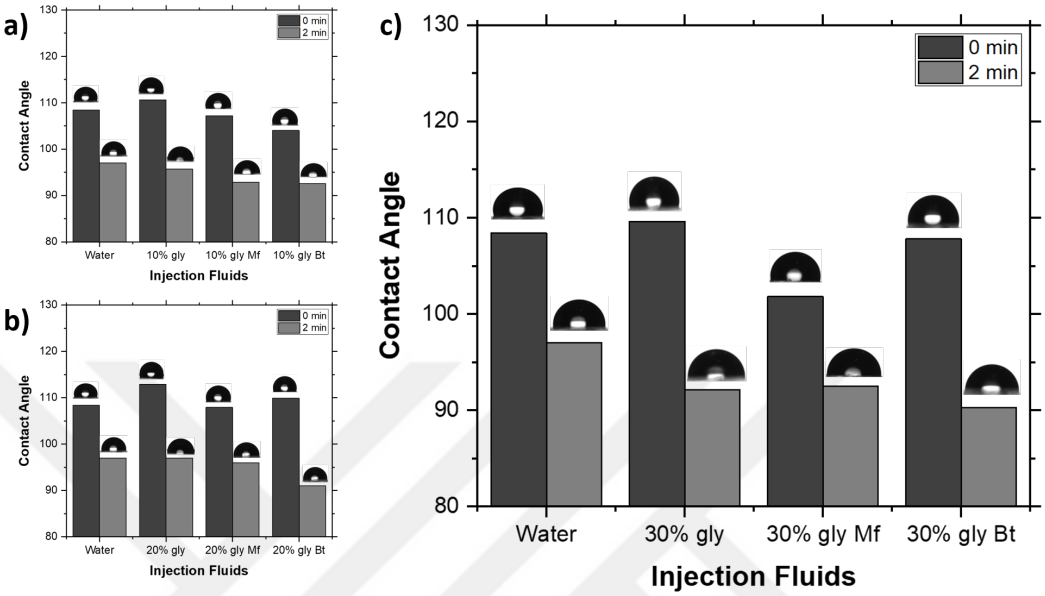

Figure 4.2: a) Contact angle variation for 10 % gly solutions, b) Contact angle variation for 20 % gly solutions, c) Contact angle variation for 30 % gly solutions.

a transition towards an intermediate wettability, with θ ranging from 96° to 90° for all fluids. It was also noticed that the increase in viscosity from 998 Kg/m^3 to 1106 Kg/m^3, along with the presence of AgNPs, have slightly influenced the wettability alteration towards the intermediate wettability state, subsequently leading to water-wet over time.

It is a significant parameter in multiphase flow as it not only affects relative permeability, capillary pressure and oil sweep efficiency but also governs the residual oil saturation, fluid flow and oil distribution in the reservoir [22, 23]. Wettability can be distinguished into water-wet ($0° \leq \theta \leq 90°$), oil-wet ($90° \leq \theta \leq 180°$) and intermediate wettability ($\theta = 90°$) [24, 23, 25]. In general, a positive correlation between water-wet surfaces and recovery factor exists due to the presence of capillary forces in water-wet pores, reducing oil adhesion to reservoir walls, and ultimately enhancing oil recovery [22]. Injecting nanofluids into low-permeability reservoirs facilitates their penetration into micro and nano-sized pore throats and modifies the wettability of the reservoir by adsorbing on rock surface hence improving overall oil displacement efficiency in pore throats [23].

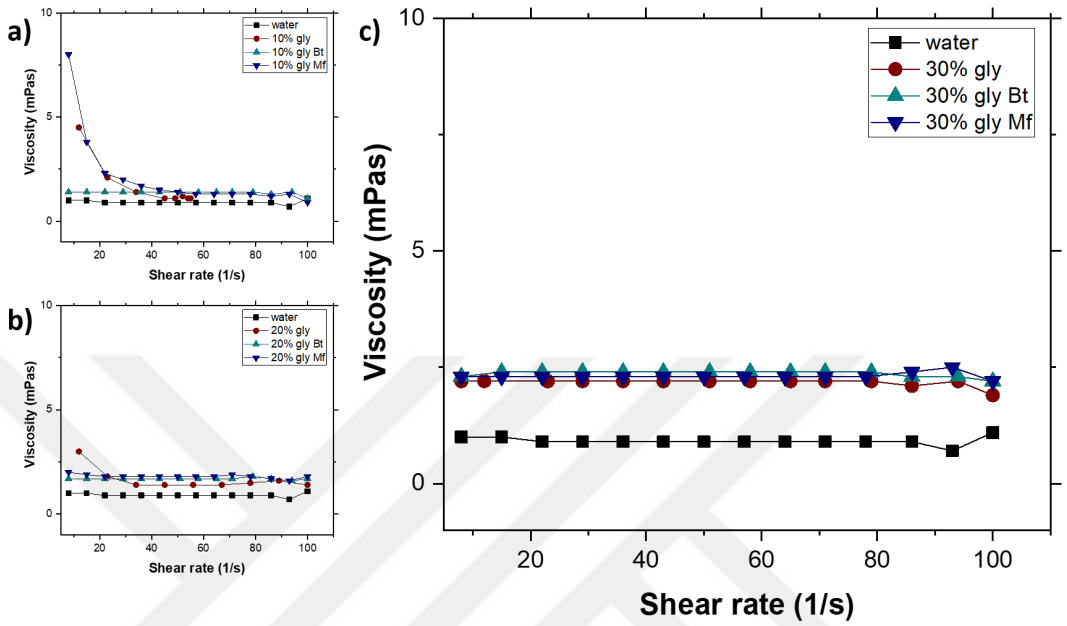

Figure 4.3: a) Graphs showing the viscosity of glycerol % and nanofluids with glycerol % a) 10 % glycerol, b) 20 % and c) 30 % glycerol.

4.1.3 Oil Displacement Efficiency and Nanofluid Recovery Mechanism in Reservoir-on-a-chip

For optimal displacement efficiencies, a very low mobility ratio is a prerequisite [20]. The mobility ratio (M) signifies the ratio between the viscosity of displaced fluid to displacing fluid (M = μdisplacing solution/μdisplaced solution), close to one, taking into consideration that the relative permeabilities of both solutions are nearly equal [20]. However, in this study, our primary objective is to explore the impact of significantly elevated mobility ratios between fluids on displacement efficiencies, as shown in Table 4.1. To investigate the real process of oil entrapment in porous media and the sweep efficiency of different injection fluids, a microscopic examination of oil displacement in a PDMS-based microfluidic chip was carried out. The microfluidic chip simulates a physical rock network to assess the areal sweep efficiency. The overall displacement efficiency of different fluids is provided in Table 4.1. The IOIP and sweep efficiency were quantified by carefully analysing the porosity and void fractions in a microfluidic chip using

Fluid	Viscosity mPas	Density Kg/m^3	Mobility ratio	Sweep Efficiency % (BT)	Sweep Efficiency %(overall)
Oil	263	865	----	----	----
0 % gly	0.917	998	286	36.9	52.4
10% gly	1.172	1035	224	45.8	50.7
20% gly	1.515	1043	173	30.4	52.7
30% gly	2.151	1077	122	47.4	51.8
10% gly + AgNPs/MF	1.377	1058	190	44.7	50.4
20% gly + AgNPs/MF	1.792	1066	146	38.1	52.2
30% gly + AgNPs/MF	2.271	1071	115	51.3	57.1
10% gly + AgNPs/BT	1.338	1046	196	35.0	49.2
20% gly + AgNPs/BT	1.703	1077	154	36.0	52.0
30% gly + AgNPs/BT	2.413	1106	109	43.5	60.5

Table 4.1: Details about the fluid viscosity, density, mobility ratios, and sweep efficiency at 25 °C.

Image J processing. The microscopic images of the sweep efficiency of different injection fluids are provided in figure 4.4, 4.5, and 4.6. For displacement experiments, initially, a dry and clean microfluidic chip was manually saturated with the oil to age at room temperature for 1 hr to change the wettability. Figure 4.2 depicts the contact angles of all injection fluids with the initial oil-wet state with θ varying between 101° to 113° for all fluids. A very low injection rate of 10 µl/hr was maintained to ensure accuracy and stability in the injection process because of the small size of the microfluidic channels.

Then oil-saturated microfluidic chips were flooded separately by control groups i.e. deionized water, 10 %, 20 % and 30 % glycerol solutions. It was noticed that a gradual increment in oil sweeping was achieved till breakthrough (BT) and a large oil fraction was displaced. A variable BT time of 9 PV, 14.5 PV, 7.5 PV and 20.5 PV with sweep efficiencies at 36.9 %, 45.8 %, 30.4 % and 47.4 % was observed for deionized water, and 10 % to 30 % gly, respectively. After BT, 20 PV were injected to increase the sweep efficiency but a uniform curve with a slight increment in sweep efficiency of 52.4 %, 50.7 %, 52.57 % and 51.8 % was achieved respectively, as shown in figure 4.4, 4.5, and 4.6. This could be due to an initial strongly oil-wet state causing an extremely high negative capillary pressure, consequently moving oil droplets towards the smaller pores due to decreasing oil permeability.

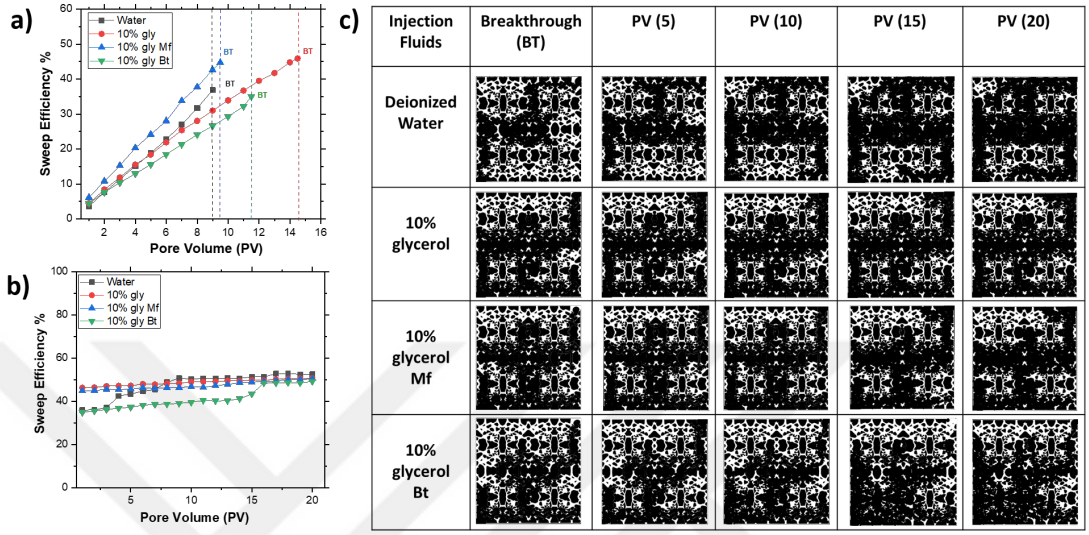

Figure 4.4: Injection fluids; water, 10 % gly and 10 % gly based nanofluids (Mf and Bt): a) Sweep efficiencies till BT, b) Sweep efficiencies after BT, till 20 PV; c) Visual representations of fluid flow within a reservoir-on-a-chip, captured at the breakthrough point (BT) and various PV specifically, 5, 10, 15, and 20 PV.

In addition, the recovery factors are closer to each other due to a slight variation in viscosity and density among control group solutions from 0.917 to 2.15 g/cm^3 as shown in Table 4.1 and figure 4.3. Finally, the chip was flooded with the glycerol-based nanofluids synthesized in microfluidics and benchtop setups. Due to the presence of AgNPs, a slight increment in the viscosity of glycerol-based solutions was achieved as seen in Table 4.1 and figure 4.3. BT for 10 % glycerol-based nanofluids was achieved at 9.5 PV (Mf), and 11.5 PV (Bt) with 44.7 % and 35 % sweep efficiencies respectively, shown in figure 4.4c. After injecting 20 PV an increment in sweep efficiency to 50.4 % and 49.17 % was observed. A relatively close yet low sweep efficiency of 10 % Mf-synthesized nanofluid can be due to its higher IFT. For 20 % gly-based nanofluids, BT at 18.5 PV (Mf) and 10 PV (Bt) was achieved with a recovery factor of 38.13 % and 35.9 % as shown in figure 4.5c. After the injection of 20 PV a visible increase in sweep efficiency to 52 % can be seen for both cases. However, it can be easily noticed as compared to other fluids, a relatively low IFT at 21 mN/m for 20 % Mf synthesized nanofluid, and a lower viscosity and small NPs size alone wouldn't bring a positive increment in the sweep efficiency, and overall displacement efficiency stayed around 52 % for 10 %

and 20 % silver-glycerol based nanofluids. This means ultra-low IFT reduction is required for observing more efficient displacement efficiency [24, 130, 131]. The results are consistent with the literature where Stefan Iglauer et al. reported that IFT reduction by silica nanofluids (9.3 mN/m, 0.5 wt.%) has less significant effects on EOR displacement hence limiting the oil recovery as compared to wettability alteration mechanism [24].

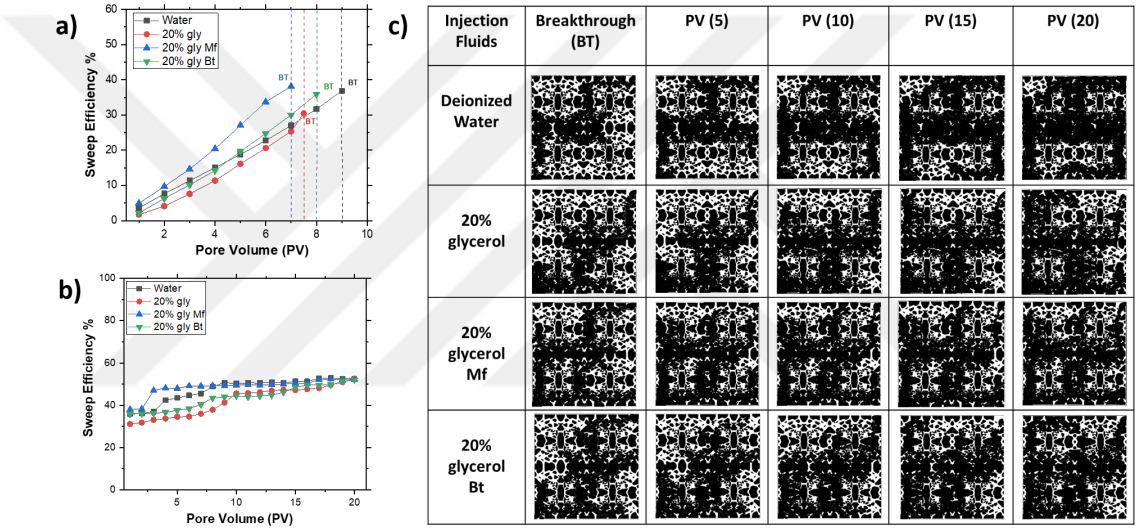

Figure 4.5: Injection fluids; water, 20 % gly and 20 % gly based nanofluids (Mf and Bt): a) Sweep efficiencies till BT, b) Sweep efficiencies after BT, till 20 PV; c) Visual representations of fluid flow within a reservoir-on-a-chip, captured at the breakthrough point (BT) and at various PV specifically, 5, 10, 15, and 20 PV.

At the same time, with the increase in glycerol % in nanofluids the viscosity increased slightly to 2.2 mPas (Mf) and 2.4 mPas (Bt). Mf-synthesized nanofluid had NPs (1.7 nm) with lower PDI than Bt-synthesized nanofluids and swept more oil fraction initially, by penetrating more regions. The BT was delayed and achieved a sweep efficiency of 51.3 %. at 18.5 PV. Similarly, Bt-synthesized silver nanofluid swept 43 % OOIP at 10 PV before BT. As illustrated in figure 4.6c the presence of slightly bigger AgNPs 1.7 nm (Mf) and 3.3 nm (Bt) had a visibly positive increment in sweep efficiency of 5 % (Mf) to 8 % (Bt) achieved after 20 PV injections. It explains widely reported phenomena in the literature [22] that the oil recovery factor correlates with the size and concentration of NPs,

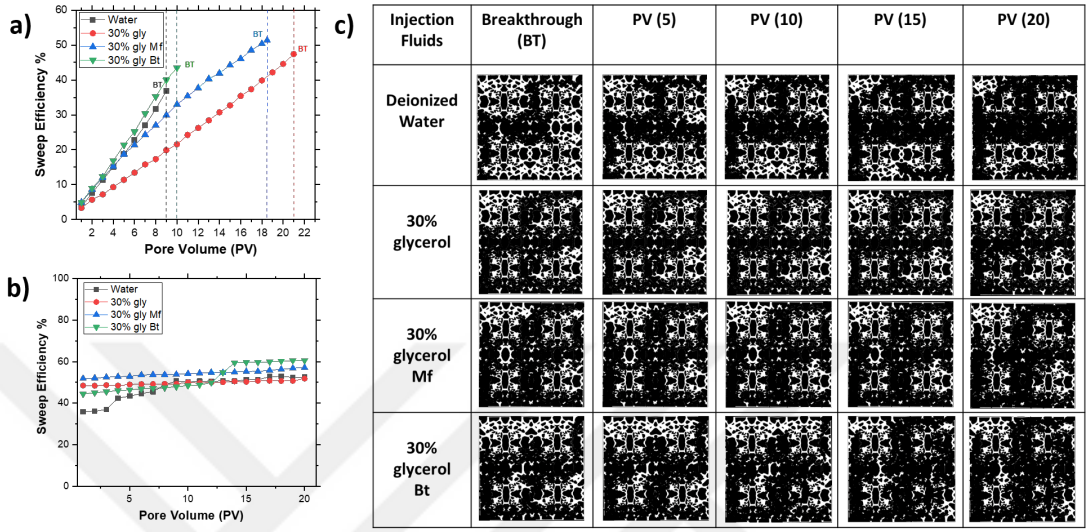

Figure 4.6: Injection fluids; water, 30 % gly and 30 % gly based nanofluids (Mf and Bt): a) Sweep efficiencies till BT, b) Sweep efficiencies after BT, till 20 PV; c) Visual representations of fluid flow within a reservoir-on-a-chip, captured at the breakthrough point (BT) and at various PV specifically, 5, 10, 15, and 20 PV.

where on one hand, small NPs can increase disjoining pressure due to electrostatic repulsion between NPs, yielding a good efficiency (observed for both 30 % AgNPs/glycerol nanofluids). On the other hand, a larger NP size can cause formation damage such as pore plugging, while a smaller NP size could lead to pore bridging, potentially diminishing the recovery factor (observed for the rest of AgNPs/glycerol nanofluids) [22]. During the experiments, it was observed that the flow of oil interrupted the injection fluid flow at the outlet between 13-16 PV for the 10% Bt nanofluid case and between 5-8 PV and 13-16 PV for the 20 % Bt case. This phenomenon happened due to the invasion of injection fluid into more pore matrix, pushing oil towards the outlet and gradually increasing the sweep efficiency.

4.1.4 Analysis of Trapped Oil Movement

The presence of flow heterogeneity and capillary forces in the porous media necessitates a thorough study of suspension flow dynamics and their relative response

during multiphase flow [104]. Microfluidic devices provide a controlled environment for studying fluid dynamics at the pore scale, which is crucial to help understand the fluid invasion pathways in porous media [132, 133]. Nanomaterials such as nanoparticles exhibit an elevated surface-to-volume ratio and a distinctive interfacial tension which allow them to remove trapped oil or ganglia by penetrating inaccessible non-aqueous fluid-saturated regions [104]. As explained earlier, the reported IFT for AgNPs might not be enough to influence the oil displacement. So here have focused more on the wettability modification and its effect on oil displacement. Generally, wettability modification happens due to two theories associated with wettability alteration: structural disjoining pressure and electrical double layer (EDL) [24]. PDMS has an inherently negative surface charge [134] as well as the surface charge of silver NPs is also strongly negative [135]. So, it is hard to provide any possibility of NPs adsorption by ionic interaction between AgNPs and PDMS. On the other hand, NPs can enhance structural disjoining pressure [24]. It has been reported, that the dispersion of NPs such as silica NPs in an aqueous phase causes structural disjoining pressure because of Brownian motion between NPs and electrostatic repulsion [24]. Similarly, it is expected that AgNPs also create a wedge film at the three-phase interaction (oil-solid-water) due to the influence of structural disjoining pressure.

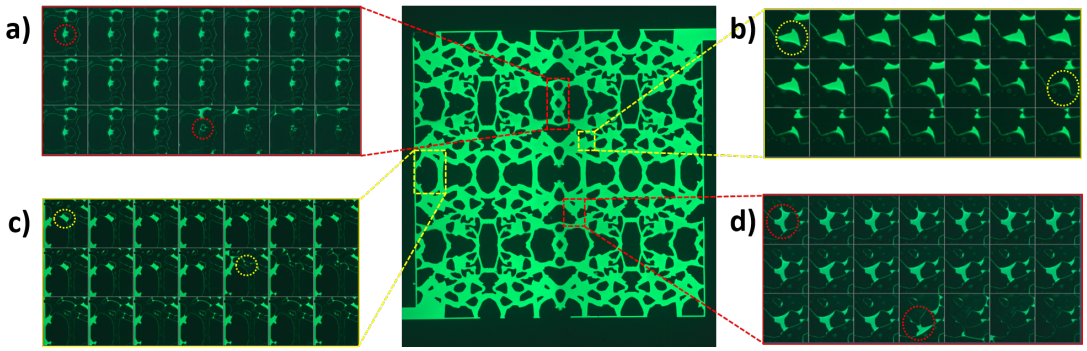

Figure 4.7: a and d) Oil ganglia displacement by 30 % nanofluid (Mf) up to 21 PV after BT, b and c) Oil ganglia displacement by 30 % nanofluid (Bt) in a period of 21 PV after BT.

The pore scale investigation was only performed for the 30 % AgNPs/glycerol synthesized in both settings because the recovery factor was relatively low for all

other fluids and limited the movement of trapped oil ganglia. However, the wettability alteration by NPs is not an immediate process and it is a time-dependent phenomenon [11]. For instance, the increased size of AgNPs to 3.3 nm in 30 % glycerol (Bt) notably altered the oil phase distribution, breaking large structures into smaller disconnected oil blobs, depicted in figure 4.7a. However, it took 18 PVs to displace the oil ganglia, indicating the enhanced disjoining pressure from the suspension influenced the gradual spreading of aqueous fluids [104]. Furthermore, under the influence of viscous forces and a receding contact angle due to structural disjoining pressure, the oil droplet can be released from the rock surface [24]. Similar behaviour was seen in figure 4.7d, where the increase in structural disjoining pressure caused a large oil ganglion trapped at a pore throat to be released by the Mf-synthesized silver nanofluid. Additionally, it can be seen that the silver nanofluid can reduce the size of trapped ganglia by forming a wedge film at three-phase contact (oil-solid-water) under the action of structural disjoining pressure as shown in figure 4.7b.

Further investigation on pore scale revealed the displacement of the oil adsorbed to the surface of the PDMS. In figure 4.8a, 30 % (Mf) nanofluid injection scenario, 2 oil ganglia's and an oil droplet (in the middle of pore) is adsorbed to the surface of the PDMS (in PV 1). After injection of 16 PV, the injection fluid pinches off oil ganglia 1, dividing it into two. Following the injection of 18 PV, a visible decrease in the size of pinched off oil ganglia 1 can been seen, indicating the movement of oil under structural disjoining pressure. Additionally, the adsorbed droplet and the oil ganglia 2 are also displaced. If noticed carefully from PV 1 to 18, a considerable amount of oil is adsorbed with the PDMS walls of reservoir in the form of oil film, which also ensures a visual contrast of channel walls with black channel/pore region. However, after injecting 18 PV, desorption of the oil from the PDMS reservoir walls can be seen, as contrast between channel walls and the pore reduces ensuring the oil film movement and also displacing a trapped oil from surrounding region under the influence of structural disjoining pressure [104].

Similarly, in figure 4.8b 30 % (Bt) nanofluid injection scenario, an oil droplet adsorbed in middle of the pore can be seen, as well as an oil trapped region

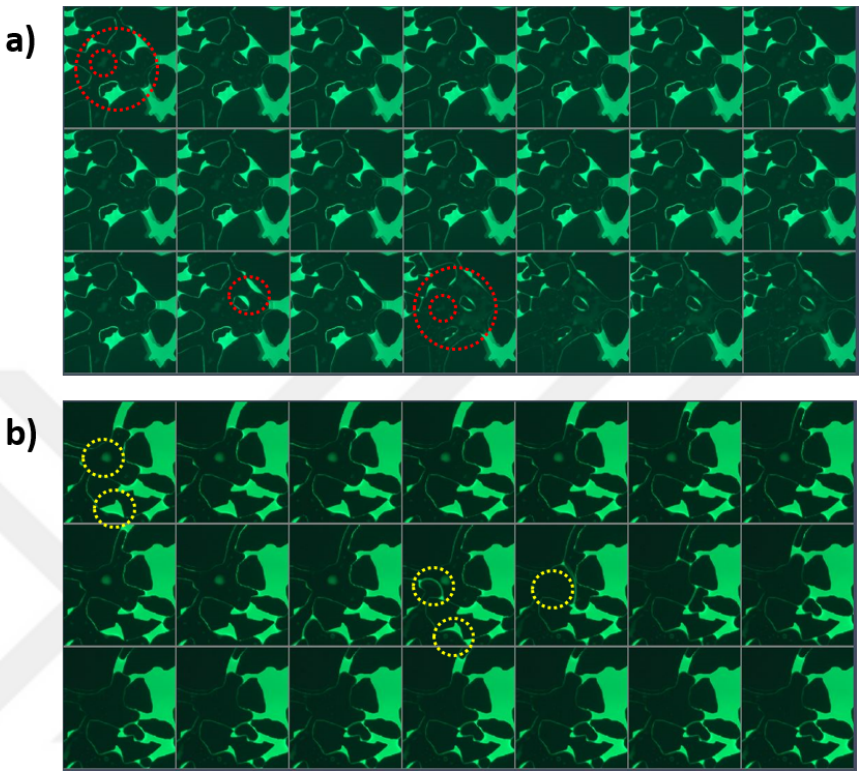

Figure 4.8: a) Adsorbed oil displacement by 30 % nanofluid (Mf) up to 21 PV after BT, b) Adsorbed oil and ganglia displacement by 30 % nanofluid (Bt) in a period of 21 PV after BT.

is illustrated, similar to 4.8b. With the injection of 11 PV, the injection fluid displaces the top layer of oil from the pore and moves it upward towards the middle of the pore, forming a visible oil film in front of injection fluid. This in results not only displaces the adsorbed oil droplet in the middle but also pushed the oil further into the pore throats in the surrounding. Overall the pore-scale analysis reveals that the injection of silver nanofluid has a potential to change the wettability and recover trapped oil under high mobility conditions.

4.2 Multiphase Displacement Application of Reconfigurable Nanoemulsions

4.2.1 Effect of pH on NPs-Surfactant Assemblies

Silica nanofluid with a concentration as low as 2 wt. % can exhibit a strong potential to detach adsorbed oil droplets because of the structural disjoining pressure [29]. Hence, the effects of SiO_2 NPs on NP-surfactants assemblies was studied. The size of LUDOX-HS- 40, SiO_2 NPs was measured to be 21 nm. NP-surfactant assemblies were investigated by generating droplets of 1 % (v/v) of SiO_2 NPs (pH: 3, 5, 6, 8) in silicon oil containing 20 % (v/v) Poly[dimethylsiloxane-co-(3-aminopropyl)methylsiloxane] copolymer in a T-shaped microfluidics platform as shown in figure 2.4a. It is anticipated that a higher NP % can potentially block the porous structure of the reservoir and could result in decreased oil recovery. Hence an optimized % of SiO_2 i.e., 1 % (v/v) was used in the study to ensure its potential for multiphase application. While, a critical micelle concentration of Poly[dimethylsiloxane-co-(3-aminopropyl)methylsiloxane], i.e., 20 % was picked from the literature [13]. Once the droplets were generated, to ensure the formation of NP-surfactant assemblies, the collected sample was kept for 1 hr before observing them under the microscope as shown in figure 2.4b.

When SiO_2 dispersion droplets are formed in silicon oil containing Poly[dimethylsiloxane-co-(3-aminopropyl)methylsiloxane] copolymer, the copolymer behaves as a surfactant forming oil-water interfacial assemblies to decrease the interfacial energy, depicted in figure 1.7. Figure 1.8 illustrates high-quality images of the buckling behavior for SiO_2 NPs at pH 3, 5, 6 and 8, captured with the Zeiss microscope. At pH 5 and 6, the copolymer acquires a positive charge and moves towards the interface. With the layer of copolymer at the interface, the negatively charged SiO_2 NPs move towards the interface and form irreversible NP-surfactant assemblies under the influence of electrostatic interaction [95]. Under the influence of external force or compression, these assemblies could wrinkle because of the NPs jamming as seen in figure 1.8 b and c. However, at pH 3 and

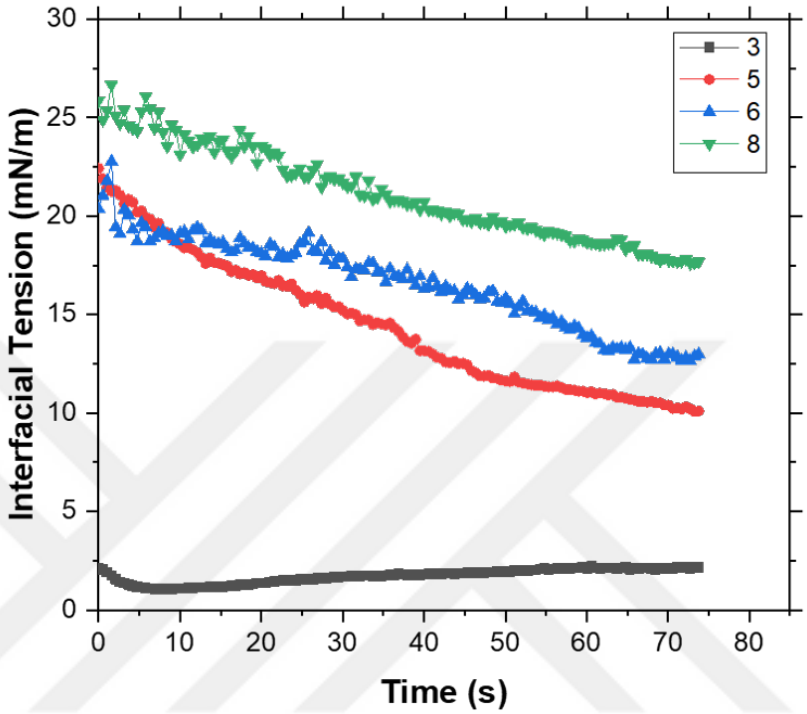

Figure 4.9: IFT measurement of 1 % SiO_2 dispersion in silicon oil containing 20% Poly[dimethylsiloxane-co-(3-aminopropyl)methylsiloxane] copolymer at pH 3, 5, 6, and 8.

8, the electrostatic interaction between copolymer and SiO_2 NPs was weakened, leading to NPs ejection from the interface under compression [95]. It can be seen that droplets or not stable under coalescence and also divide into multiple smaller droplets under compression, illustrated in figure 1.8 a and d. Hence, it was confirmed that SiO_2 NPs can form interfacial packing and reconfigurable droplets at pH 5 and 6. After attaining buckling at the desired % of reagents, the IFT between silicon oil and 1 % of SiO_2 NPs (pH: 3, 5, 6, 8) solutions was measured by pendant drop tensiometry, which varied between 2.4 mN/m and 25 mN/m as shown in figure 4.9. For pH 5 and 6, a similar IFT receding trend as reported in the literature was observed [95]. However, pH 8, also showed a similar trend yet a bit high IFT as compared to pH 5, and 6. This could be due to IFT reduction in the presence of sodium hydroxide (NaOH) (used in alkaline flooding, here used to adjust the pH) and copolymer (which also behaves as surfactant) as reported in the literature [136].

Additionally, it is widely known that NPs can enhance the water-oil emulsion stability by adsorbing to the fluid-fluid interface which reduces the droplet coalescence and minimizes the flocculation [41]. However, the advantage of NPs and the trade-off associated with using polymer as surface active agents to increase emulsification needs further investigation. Kumar et al. reported the impact of polymer (carboxyl methyl cellulose), SiO_2 NP, and surfactant (sodium dodecyl benzenesulfonate) assisted Pickering emulsions formulation with light mineral oil and successfully retrieved an additional oil recovery of 24.81 % due to enhanced rheological behavior, IFT reduction, and minimization in droplet coalescence [42]. However, a critical insight reveals that W/O emulsions receive less consideration as compared to integrated studies associated with emulsion stability and tertiary oil recovery [43]. To the best of our knowledge, the effect of pH on W/O nanoemulsions flooding in reservoir-on-a-chip remains unexplored and demands critical scrutiny to discern its impact on sweep efficiency.

4.2.2 Preliminary Investigation on the Potential EOR capacity of the Reconfigurable Nanoemulsions

To investigate the potential of reconfigurable nanoemulsions on areal sweep efficiency, a total of 12 nanoemulsion samples were prepared for injection into the microfluidic chip. We investigated 3 sets of reconfigurable nanoemulsions containing different silicon oil: NPs dispersions i.e., 80:20, 70:30 and 60:40 with 1 % SiO_2 dispersion at pH 3, 5, 6 and 8 to see their effect on displacement efficiency. For the displacement experiments, a clean microfluidic PDMS-based device mimicking reservoir-on-a-chip was filled with fluorescence-doped mineral oil (178 mPas) to age at ambient conditions for 1 hr, ensuring an oil-wet state. The initial oil in place (IOIP) and the sweep efficiency were then carefully quantified by capturing a high-quality image of the chip, following void and porosity analyses by Image J software processing. For all of the flooding experiments, a constant injection rate of 10 µl/hr was maintained to gain better injection control and accuracy due to the small size of the device.

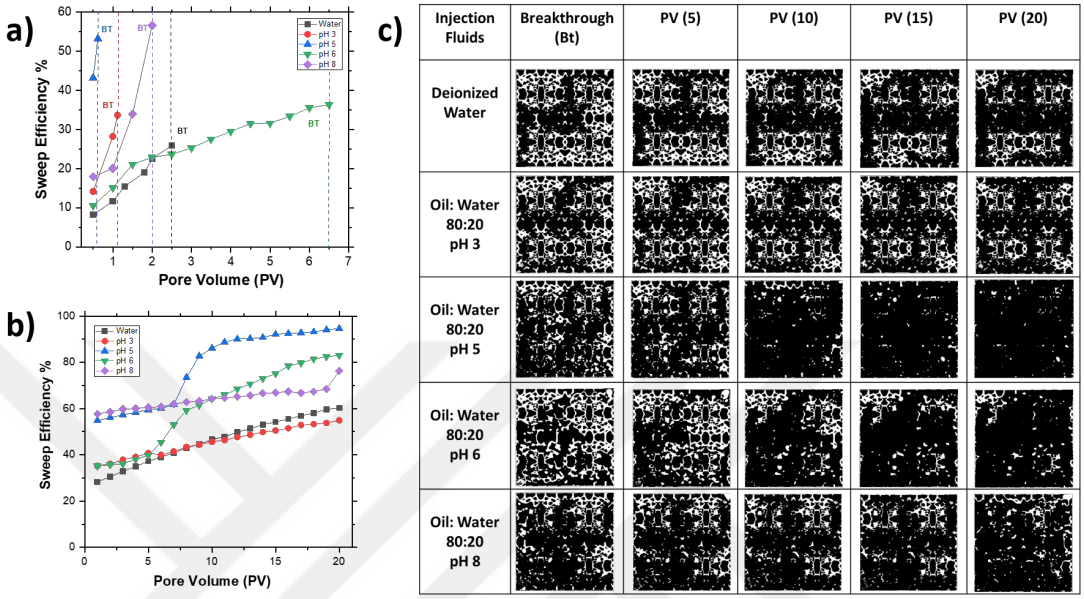

Figure 4.10: Injection fluids: deionized water, 80:20 (Oil: NPs) at pH 3, 5, 6, and 8, a) Sweep efficiencies till BT, b) Sweep efficiencies after BT, till 20 PV; c) Visual representations of fluid flow within a reservoir-on-a-chip, captured at the breakthrough point (BT) and at various PV specifically, 5, 10, 15, and 20 PV.

Then oil-aged microfluidics reservoir-on-a-chip was initially flooded by the deionized water (control group). A gradual increase in the sweep efficiency was observed till breakthrough (BT) and a small fraction was displaced. A BT period of 3 PV was observed and a sweep efficiency of 26 % was achieved. After the formation of the preferential flow pathway (at BT), 20 PV were injected and a noticeable penetration to the rest of the matrix region was observed with a 60 % sweep efficiency.

Finally, the chip was flooded with reconfigurable nanoemulsions. Figure 4.10 shows the quantified data and microscopic images of the cumulative oil recovery by 80:20 (oil: NP dispersion) emulsions as a function of the injected pore volume. A variable BT period was achieved for all samples. For nanoemulsions with pH 3, 5, 6 and 8, a sweep efficiency of 33.6 %, 53.2 %, 36.3 % and 56.6 % was achieved at BT of 1.12 PV, 0.62 PV, 6.5 PV, and 2 PV respectively. After BT, a large fraction of oil remains in the pores of the reservoir because of capillary forces and gravity effects [137]. After BT, 20 PV were injected to increase the sweep

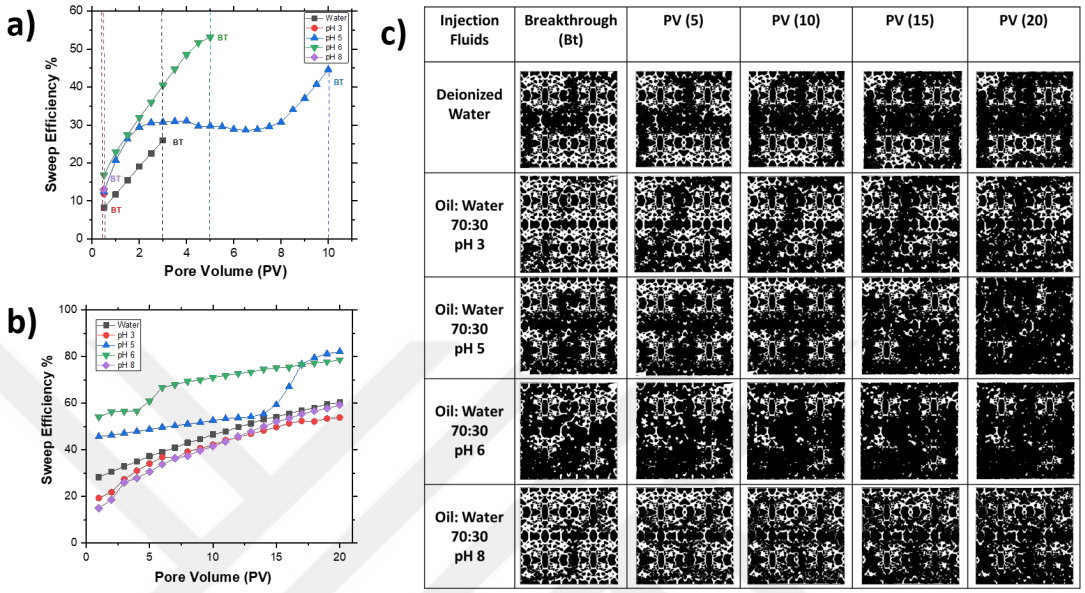

Figure 4.11: Injection fluids: deionized water, 70:30 (Oil: NPs) at pH 3, 5, 6, and 8, a) Sweep efficiencies till BT, b) Sweep efficiencies after BT, till 20 PV; c) Visual representations of fluid flow within a reservoir-on-a-chip, captured at the breakthrough point (BT) and at various PV specifically, 5, 10, 15, and 20 PV.

efficiency, a uniform curve with a gradual increment in oil recovery was achieved at 54.9 %, 94.5 %, 82.96 % and 76.26 % was achieved for nanoemulsions with pH 3, 5, 6, and 8, respectively, as shown in figure 4.10. The results indicate that the injection of O/W emulsions especially at pH 5 and 6 form reconfigurable structures which block the high permeability region by bridging or jamming and divert the flow direction to low permeable zones to improve sweep efficiency [43].

Following that, emulsions synthesized under the same reaction conditions but a different oil: NP dispersion i.e., 70:30 were injected separately into the reservoir-on-a-chip. Figure 4.11 shows the sweep efficiency as a function of pore volume with nanoemulsions at pH 3, 5, 6, and 8 (70:30). A sweep efficiency of 11.8 % (pH 3), 44.6 % (pH 5), 53.1 % (pH 6), and 13 % (pH) was achieved at a BT of 0.5 PV, 10 PV, 5 PV, and 0.5 PV respectively. After BT, a large fraction of trapped oil was displaced by injecting 20 PV. Recovery of up to 53.8 %, 82.17 %, 78.12 % and 59.23 % was observed, as shown in figure 4.11. It has been reported that emulsions can enhance the mobility ratio and increase sweep efficiency [43, 138].

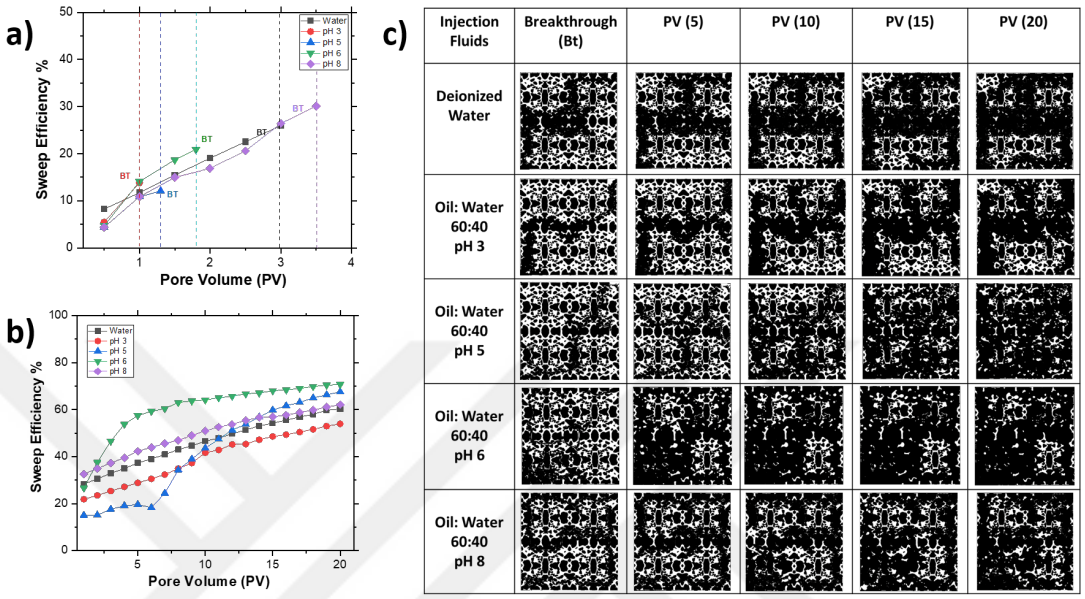

Figure 4.12: Injection fluids: deionized water, 60:40 (Oil: NPs) at pH 3, 5, 6, and 8, a) Sweep efficiencies till BT, b) Sweep efficiencies after BT, till 20 PV; c) Visual representations of fluid flow within a reservoir-on-a-chip, captured at the breakthrough point (BT) and at various PV specifically, 5, 10, 15, and 20 PV.

Lastly, 60:40 (oil: NPs dispersion) nanoemulsions were injected separately as shown in figure 4.12. A sweep efficiency of 13.8 % (1 PV), 12 % (1.5 PV), 20.9 % (1.8 PV) and 30 % (3.5 PV) were achieved at BT for nanoemulsions synthesized at pH 3, 5, 6, and 8 respectively. Following BT, a sweeping efficiency of 53.9 % (pH 3), 67.6 % (pH 5), 70.67 % (pH 6) and 62 % (pH 8) was achieved after 20 PV injection, shown in figure 4.12. It was observed that pH influenced the recovery of IOIP. As reported in the literature, W/O emulsions with higher oil percentages generally retrieve more oil because of IFT reduction between water and oil and improve the mobility ratio. Similarly, in this study, the sweep efficiency trend reveals that the highest efficiency was achieved in 80:20 nanoemulsions at pH 5 and 6. The overall sweep efficiency in all 3 sets of nanoemulsions depicted higher recovery factors by pH 5 and 6 (close to each other), following the recovery by nanoemulsions synthesized with pH 8. At a pH of 3, nanoemulsions exhibited the lowest recovery factor consistently across all scenarios This indicates the effect of NP-surfactant irreversible assemblies particularly at pH 5, and 6, forming stable reconfigurable emulsions that can reconstruct themselves in pore throats,

facilitating oil retrieval from trapped locations, as shown in figure 4.10, 4.11, and 4.12. Consequently, upon injecting W/O emulsions into the reservoir-on-a-chip, they promptly block the highly permeable areas, obstructing larger pores due to capillary pressure. Subsequently, the fluid is directed towards smaller pores with reduced resistance and enhanced sweep efficiency [108]. The results aligns with findings from existing literature on W/O core-flooding [108].

4.2.3 Distribution of the Reconfigurable Nanoemulsion in porous media

It is widely known that nanoemulsions with high kinetic stability, good mobility ratio and enhanced emulsification of trapped reservoir oil make it a promising chemical agent for multiphase displacement applications [108]. In the study, the IFT assemblies of SiO_2 and Poly[dimethylsiloxane-co-(3-aminopropyl)methylsiloxane] copolymer dispersed in silicon oil, especially at pH 5 and 6 have shown a remarkable effect on the macroscopic sweep efficiency as shown in figure 4.10, 4.11, and 4.12. Figure 2.5 shows the wide-angle view of the chip with IOIP (green) and voids (black). After BT is established (injected fluid in black), the mobilized oil is displaced in a continuous stream and collected in a vial as shown in figure 2.6.

Undoubtedly microemulsions are thermodynamically stable and can be spontaneously formed without external force. Nanoemulsions synthesized with pH 3 has less significant effects on sweep efficiency as compared to the synthesis done with other pH solutions. Hence, to confirm whether the injection fluids can generate in-situ micro or macroemulsions, a pore-scale analysis was only performed for nanoemulsions synthesized at pH 5, 6 and 8. As seen in figure 4.13a (80:20 pH 6), a collection of images up to 24 PV is provided, depicting the displacement of a large oil fraction from PV 1 to PV 24. The red arrow indicates the direction of injection fluid flow. As the injection fluid approaches, the oil fraction is emulsified into smaller oil-in-water emulsions (after PV 5), which break down the oil/water IFT and mobilize the trapped oil, indicating the effects of in-situ emulsions

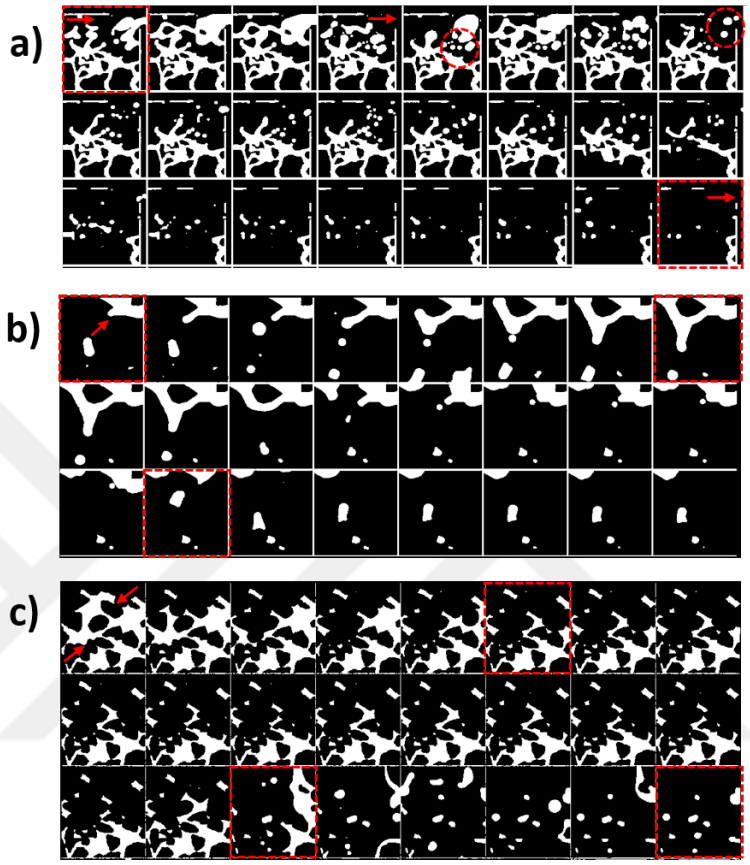

Figure 4.13: a) Displacement of oil fraction by 80:20 (Oil: NPs) nanoemulsions at pH 5 and in-situ emulsification. b) Movement of oil by in-situ emulsion 60:40 (Oil: NPs) nanoemulsions at pH 6, c) Process of oil ganglia formation and displacement by 80:20 (Oil: NPs) nanoemulsions at pH 8.

on improving sweep efficiency. These emulsions then act as a new driving fluid, which increases the areal sweep efficiency by mobilizing the trapped oil. Similar behaviour was reported in the literature for in-situ emulsion formation by surfactant flooding [99]. Figure 4.13a (80:20 pH 6) and b (60:40, pH 5) indicate the mobility of trapped oil by in-situ emulsions at another location in a microfluidic chip. In figure 4.13b (60:40, pH 5), the movement of an in-situ emulsion towards the oil fraction can be seen where the stretched droplet is moving through a pore throat. As soon as it reaches a wide pore structure, it transforms itself into a circular-shaped oil droplet due to wettability alteration and later merges with the IOIP. With the multiple in-situ emulsions approaching, the oil fraction size

increases and eventually the trapped oil is mobilized, similar to the findings reported in the literature. Additionally, if we look closely the stretched droplet in the channel has a convex shape (front and back), indicating a concave shape formed by the injected nanoemulsion (figure 4.13b). This proves the presence of local pressure difference between the two fluids. Hence, it proves the hypothesis that similar to structural disjoining pressure caused by nanofluids, the designed nanoemulsions can form a wedge film underneath the oil and effectively displace it by reconstructing themselves.

Furthermore, the effect of nanoemulsions with pH 8, on the movement of trapped oil ganglia was also investigated. As shown in figure 4.9, pH 8 has a receding impact on IFT similar to pH 5 and 6. However, because of Poly[dimethylsiloxane-co-(3-aminopropyl)methylsiloxane] copolymer surface activation between pH 5 and 6, a weak interaction at pH 8 exists and no buckling phenomena were observed [95] [13]. Figure 4.13c (80:20 pH 8) shows the process of oil ganglia formation and their displacement by reconfigurable nanoemulsions. The red arrows (1 PV) indicate the flow of nanoemulsions from diagonal positions. As seen in 6 PV (red square) the penetration of nanoemulsions causes the formation of 3 distinct oil ganglia and a large oil fraction. However, over the injection of up to 19 PV, oil ganglia and a large fraction are mobilized under the influence of IFT reduction due to the combined effect of NaOH and polymer (behaving as surfactant) by nanoemulsions with pH 8, as mentioned previously. A similar sweep efficiency behavior was noticed for the rest of the solution with varying Oil: NPs solutions at pH 5, 6, and 8.

4.2.4 Conclusion

In this work, we evaluated the sweep efficiency of green silver nanofluids (benchtop and microfluidics synthesis) and reconfigurable nanoemulsions at high mobility ratios. For the green silver-based nanofluid study, we observed a wettability shift towards intermediate from the oil-wet phase over 2 minutes. We observed that deionized water, 10 % and 20 % glycerol solutions with nanofluids displayed

49 % to 52.5 % displacement efficiency due to low viscosity and small AgNPs size, potentially limiting oil distribution via pore bridging. However, the increase in glycerol viscosity to 30 % and AgNPs size to (1.7 nm (Mf) and 3.3 nm (Bt)), led to an additional 5 % and 8 % improvement in sweep efficiency, highlighting the importance of critical glycerol viscosity and larger Ag NP size for enhanced displacement efficiency. Similarly, in second half of the study, we successfully demonstrated the synthesis of NP-surfactant stabilised W/O reconfigurable nanoemulsions using ultrasonication in a system containing SiO_2 (1 %) NPs dispersed in water and Poly[dimethylsiloxane-co-(3-aminopropyl)methylsiloxane] copolymer dispersed in silicon oil (40 mPas). The investigation included the effect of pH (3, 5, 6, and 8) and water/oil ratio (80:20, 70:30 and 60:40) as variables affecting the interfacial tension (IFT), buckling, and sweep efficiency. The flooding experiments revealed that pH 5 and 6 had shown buckling, a remarkable sweep efficiency and in-situ emulsions formation regardless of Oil: NPs concentrations. While, due to the presence of alkaline reagents (NaOH), used to adjust pH, and the presence of polymers, the pH 8 solution has also shown an increment in sweep efficiency. However, with the reduction in pH (3), a negative effect on oil recovery was observed. Overall, pH 5 and 6 in the case of 80:20 solutions, have yielded a remarkable oil recovery as compared to the rest of the nanoemulsions and silver nanofluids.

Chapter 5

Conclusions and Future Prospects

5.1 Conclusions and Future Work

The multiphase displacement in porous media is a complex process, encountered in many industrial processes [8, 9, 10]. In heterogeneous porous media, the existence of hydraulic heterogeneity causes the formation of preferential flow pathways which limits the application. In the context of multiphase displacement applications like Enhanced Oil Recovery (EOR), diverse chemicals are employed as injection fluids. These chemicals serve to alter wettability, interfacial tension (IFT), viscosity, and mobility ratios, addressing specific challenges associated with fluid displacement in porous media [8, 9, 10, 139]. In this study, we investigated the potential of silver-based nanofluids, synthesized in glycerol in benchtop and microfluidic settings, and reconfigurable nanoemulsions to investigate their effects in multiphase displacement applications in reservoir-on-a-chip. The potential of metal nanoparticles in multiphase displacement applications has not been widely investigated. Hence, we opted to synthesize a novel green nanofluid with a non-toxic and environmentally friendly reagent i,e, glycerol for the chemical synthesis of AgNPs. As compared to traditional synthesis protocols, our strategy

portrays a simple, easy, and time-efficient one-step green synthesis of AgNPs in glycerol as a solvent and reducing medium devoid of any additional conditions like high temperatures, the addition of surfactants, ultrasonication, or centrifugation. As size, polydispersity index and concentration of NPs affect the sweep efficiency in multiphase displacement applications. We did the synthesis in benchtop [5] and microfluidic settings [6]. In microfluidics synthesis, we investigated synthesis parameters and conditions such as variable glycerol percentages (10 to 80 %), *Pe* number, *Re* number, concentration of reagents, and molarity of PVP to observe the effect on the average size and size distribution of NPs [6]. The rapid mass transfer and controlled reaction kinetics in a microfluidic reactor indicate that the average size distribution of AgNPs for all reaction conditions is less than 2 nm. However, in benchtop synthesis, we were able to get a tunable size range (ultra-small to 160 nm) with a varying glycerol percentage (10 to 100 %) with a controlled polydispersity index [5].

The multiphase study on investigating Ag nanofluids efficiency, focused on synthesis done with 10 % to 30 % glycerol, to keep the application cost-effective. The study demonstrated that green silver nanofluids can be efficient for multiphase displacement applications, particularly in high mobility ratios. Deionized water, 10 %, 20 % and 30 % glycerol solutions were taken as control groups.

The following key findings were obtained after displacing a high-viscosity oil (263 mPas):

1. All nanofluids showed a wettability shift from the initial oil-wet phase towards an intermediate wettability over 2 minutes, and the wettability alteration mechanism was affected more than IFT.

2. Displacement efficiency was low for deionized water, 10 % and 20 % glycerol solutions, and their nanofluids, due to low viscosity and small AgNPs size, which possibly restrained oil distribution due to pore bridging.

3. A slight increase in glycerol viscosity (30 % gly) and AgNPs size to 1.7 nm (Mf) and 3.3 nm (Bt) resulted in a 5% and 8 % increment in sweep efficiency.

4. It was concluded that a critical glycerol viscosity (30 %) and larger AgNPs size are essential to have a positive impact on displacement efficiency.

Future flooding experiments with the combination of silver nanofluids and surfactants will help to investigate the effect of IFT on multiphase displacement.

However, in the second part of the multiphase displacement study, we investigated another common injection fluid i,e, emulsion flooding. For this, we synthesized novel nanoemulsions that could reconstruct themselves under external force. For this, we first investigated the buckling or reconfigurable phenomena at pH 3, 5, 6, and 8. The buckling phenomena were confirmed with NPs-Surfactant IFT assemblies between SiO_2 1 % (v/v) in water and 20 % Poly[dimethylsiloxane-co-(3-aminopropyl)methylsiloxane] copolymer at pH 5 and 6. Then we investigated the sweep efficiency of reconfigurable nanoemulsions synthesized with Oil: NPs; 80:20, 70:30, and 60:40 at pH 3, 5, 6, and 8 in a similar microfluidic/reservoir-on-a-chip model. Deionized water, pH 3 and 8 solutions were taken as control groups.

The following key findings were obtained after displacing mineral oil (178 mPas):

1. Displacement efficiency for deionized water was comparatively low at 60 %.
2. Nanoemulsion with pH 5 and 6, along with 80:20 (Oil: NPs), exhibited exceptional oil recovery compared to other nanoemulsions.
3. Nanoemulsion with pH 5, 6, and 8 exhibited in-situ emulsion formation, which acted as a second driving fluid to recover trapped oil.
4. A highest sweep efficiency was obtained with 80:20 and 70:30 (Oil: NPs) nanoemulsions at pH 5 and 6 solutions respectively.
5. A negative effect on oil recovery was observed at pH 3 in all Oil: NPs cases.

To recapitulate, the designed nanoemulsions have demonstrated a significant

impact on recovery efficiency. However, further investigation into the morphological characterization of reconfigurable emulsions and their effects on wettability, mobility ratios, and stability will be conducted in the future to obtain detailed information on their effects on sweep efficiency.

Bibliography

[1] J. Li, T. Zhang, S. Sun, and B. Yu, "Numerical investigation of the pod reduced-order model for fast predictions of two-phase flows in porous media," *International Journal of Numerical Methods for Heat & Fluid Flow*, vol. 29, no. 11, pp. 4167–4204, 2019.

[2] O. Tavakkoli, H. Kamyab, M. Shariati, A. M. Mohamed, and R. Junin, "Effect of nanoparticles on the performance of polymer/surfactant flooding for enhanced oil recovery: A review," *Fuel*, vol. 312, p. 122867, 2022.

[3] S. Pang, W. Pu, J. Xie, Y. Chu, C. Wang, and C. Shen, "Investigation into the properties of water-in-heavy oil emulsion and its role in enhanced oil recovery during water flooding," *Journal of Petroleum Science and Engineering*, vol. 177, pp. 798–807, 2019.

[4] A. Loiseau, V. Asila, G. Boitel-Aullen, M. Lam, M. Salmain, and S. Boujday, "Silver-based plasmonic nanoparticles for and their use in biosensing," *Biosensors*, vol. 9, no. 2, p. 78, 2019.

[5] I. Munir and G. Yesiloz, "Novel size-tunable and straightforward ultrasmall nanoparticle synthesis in a varying concentration range of glycerol as a green reducing solvent," *Acs Omega*, vol. 8, no. 31, pp. 28456–28466, 2023.

[6] R. Jahangir, I. Munir, and G. Yesiloz, "One-step synthesis of ultrasmall nanoparticles in glycerol as a promising green solvent at room temperature using omega-shaped microfluidic micromixers," *Analytical Chemistry*, vol. 95, no. 47, pp. 17177–17186, 2023.

[7] G. Kumar, E. Mani, and J. S. Sangwai, "Microfluidic investigation of surfactant-assisted functional silica nanofluids in low-salinity seawater for enhanced oil recovery using reservoir-on-a-chip," *Energy & Fuels*, vol. 37, no. 14, pp. 10329–10343, 2023.

[8] X. Lu and M. Wang, "Shape and surface property effects on displacement enhancement by nanoparticles," *International Journal of Mechanical Sciences*, vol. 255, p. 108471, 2023.

[9] W. Lei, X. Lu, and M. Wang, "Multiphase displacement manipulated by micro/nanoparticle suspensions in porous media via microfluidic experiments: From interface science to multiphase flow patterns," *Advances in Colloid and Interface Science*, p. 102826, 2022.

[10] N. Hao, Y. Nie, and J. X. Zhang, "Microfluidics for silica biomaterials synthesis: Opportunities and challenges," *Biomaterials science*, vol. 7, no. 6, pp. 2218–2240, 2019.

[11] C. Xie, W. Lei, M. T. Balhoff, M. Wang, and S. Chen, "Self-adaptive preferential flow control using displacing fluid with dispersed polymers in heterogeneous porous media," *Journal of Fluid Mechanics*, vol. 906, p. A10, 2021.

[12] Y. Khoshkalam, M. Khosravi, and B. Rostami, "Visual investigation of viscous cross-flow during foam injection in a matrix-fracture system," *Physics of Fluids*, vol. 31, no. 2, 2019.

[13] H. Zhang, T. Ramakrishnan, A. Nikolov, and D. Wasan, "Enhanced oil displacement by nanofluid's structural disjoining pressure in model fractured porous media," *Journal of colloid and interface science*, vol. 511, pp. 48–56, 2018.

[14] W. Lei, Q. Li, H.-E. Yang, T.-J. Wu, J. Wei, and M. Wang, "Preferential flow control in heterogeneous porous media by concentration-manipulated rheology of microgel particle suspension," *Journal of Petroleum Science and Engineering*, vol. 212, p. 110275, 2022.

[15] Z. Kargozarfard, M. Riazi, and S. Ayatollahi, "Viscous fingering and its effect on areal sweep efficiency during waterflooding: An experimental study," *Petroleum Science*, vol. 16, pp. 105–116, 2019.

[16] G. Rousseaux, M. Martin, and A. De Wit, "Viscous fingering in packed chromatographic columns: Non-linear dynamics," *Journal of Chromatography A*, vol. 1218, no. 46, pp. 8353–8361, 2011.

[17] R. Lenormand, "Capillary and viscous fingering in an etched network," in *Physics of Finely Divided Matter: Proceedings of the Winter School, Les Houches, France, March 25–April 5, 1985*, pp. 289–294, Springer, 1985.

[18] Z. Jeirani, B. M. Jan, B. S. Ali, C. See, and W. Saphanuchart, "Pre-prepared microemulsion flooding in enhanced oil recovery: a review," *Petroleum science and technology*, vol. 32, no. 2, pp. 180–193, 2014.

[19] S. Parsa, E. Santanach-Carreras, L. Xiao, and D. A. Weitz, "Origin of anomalous polymer-induced fluid displacement in porous media," *Physical Review Fluids*, vol. 5, no. 2, p. 022001, 2020.

[20] F. D. Curbelo, A. I. C. Garnica, D. F. Leite, A. B. Carvalho, R. R. Silva, and E. M. Paiva, "Study of enhanced oil recovery and adsorption using glycerol in surfactant solution," *Energies*, vol. 13, no. 12, p. 3135, 2020.

[21] T. K. Bradford, "Changes in interfacial tension with time in two-liquid-phase systems," tech. rep., Los Alamos National Lab.(LANL), Los Alamos, NM (United States), 2018.

[22] M. Almahfood and B. Bai, "The synergistic effects of nanoparticle-surfactant nanofluids in eor applications," *Journal of Petroleum Science and Engineering*, vol. 171, pp. 196–210, 2018.

[23] K. Wang, Q. You, Q.-M. Long, B. Zhou, and P. Wang, "Experimental study of the mechanism of nanofluid in enhancing the oil recovery in low permeability reservoirs using microfluidics," *Petroleum Science*, vol. 20, no. 1, pp. 382–395, 2023.

[24] A. Keykhosravi, M. B. Vanani, A. Daryasafar, and C. Aghayari, "Comparative study of different enhanced oil recovery scenarios by silica nanoparticles: an approach to time-dependent wettability alteration in carbonates," *Journal of Molecular Liquids*, vol. 324, p. 115093, 2021.

[25] A. L. Ogunberu and M. Ayub, "The role of wettability in petroleum recovery," *Petroleum science and technology*, vol. 23, no. 2, pp. 169–188, 2005.

[26] W. Lei, X. Lu, T. Wu, H. Yang, and M. Wang, "High-performance displacement by microgel-in-oil suspension in heterogeneous porous media: Microscale visualization and quantification," *Journal of Colloid and Interface Science*, vol. 627, pp. 848–861, 2022.

[27] J. Hou, J. Du, H. Sui, and L. Sun, "A review on the application of nanofluids in enhanced oil recovery," *Frontiers of Chemical Science and Engineering*, pp. 1–33, 2022.

[28] J. Foroozesh and S. Kumar, "Nanoparticles behaviors in porous media: Application to enhanced oil recovery," *Journal of Molecular Liquids*, vol. 316, p. 113876, 2020.

[29] K. Xu, P. Zhu, C. Huh, and M. T. Balhoff, "Microfluidic investigation of nanoparticles' role in mobilizing trapped oil droplets in porous media," *Langmuir*, vol. 31, no. 51, pp. 13673–13679, 2015.

[30] T. Nallamilli, E. Mani, and M. G. Basavaraj, "A model for the prediction of droplet size in pickering emulsions stabilized by oppositely charged particles," *Langmuir*, vol. 30, no. 31, pp. 9336–9345, 2014.

[31] W. Yu and H. Xie, "A review on nanofluids: preparation, stability mechanisms, and applications," *Journal of nanomaterials*, vol. 2012, pp. 1–17, 2012.

[32] R. R. Jalil and H. Hussein, "Influence of nano fluid on interfacial tension oil/water and wettability alteration of limestone," in *IOP Conference Series: Materials Science and Engineering*, vol. 518, p. 062004, IOP Publishing, 2019.

[33] A. Maghzi, A. Mohebbi, R. Kharrat, and M. Ghazanfari, "An experimental investigation of silica nanoparticles effect on the rheological behavior of polyacrylamide solution to enhance heavy oil recovery," *Petroleum science and technology*, vol. 31, no. 5, pp. 500–508, 2013.

[34] M. Khalil, B. M. Jan, C. W. Tong, and M. A. Berawi, "Advanced nanomaterials in oil and gas industry: Design, application and challenges," *Applied energy*, vol. 191, pp. 287–310, 2017.

[35] H. Ehtesabi, M. M. Ahadian, V. Taghikhani, and M. H. Ghazanfari, "Enhanced heavy oil recovery in sandstone cores using tio2 nanofluids," *Energy & Fuels*, vol. 28, no. 1, pp. 423–430, 2014.

[36] M. I. Pryazhnikov, A. V. Minakov, A. I. Pryazhnikov, I. A. Denisov, and A. S. Yakimov, "Microfluidic study of the effect of nanosuspensions on enhanced oil recovery," *Nanomaterials*, vol. 12, no. 3, p. 520, 2022.

[37] O. J. Emeka, A. Chikwe, I. Onyejekwe, I. Oguamah, N. Okoli, and O. C. Daniel, "Metallic oxides nanoparticles: The new frontier in eor," *American Journal of Applied Scientific Research*, vol. 6, no. 3, pp. 61–66, 2020.

[38] J. Mariyate and A. Bera, "A critical review on selection of microemulsions or nanoemulsions for enhanced oil recovery," *Journal of Molecular Liquids*, p. 118791, 2022.

[39] Y. Zhang, J. Geng, J. Liu, B. Bai, X. He, M. Wei, and W. Deng, "Direct pore-level visualization and verification of in situ oil-in-water pickering emulsification during polymeric nanogel flooding for eor in a transparent three-dimensional micromodel," *Langmuir*, vol. 37, no. 45, pp. 13353–13364, 2021.

[40] V. K. Sharma, A. Singh, and P. Tiwari, "An experimental study of pore-scale flow dynamics and heavy oil recovery using low saline water and chemical flooding," *Fuel*, vol. 334, p. 126756, 2023.

[41] R. Saha, R. V. Uppaluri, and P. Tiwari, "Silica nanoparticle assisted polymer flooding of heavy crude oil: Emulsification, rheology, and wettability

alteration characteristics," *Industrial & Engineering Chemistry Research*, vol. 57, no. 18, pp. 6364–6376, 2018.

[42] N. Kumar, T. Gaur, and A. Mandal, "Characterization of spn pickering emulsions for application in enhanced oil recovery," *Journal of industrial and engineering chemistry*, vol. 54, pp. 304–315, 2017.

[43] J. Li, W. Liu, S. Cong, Y. Li, K. Zheng, X. Luo, W. Luo, and X. Su, "The flow of water-in-oil emulsion in heterogeneous parallel model," *Journal of Petroleum Science and Engineering*, vol. 208, p. 109209, 2022.

[44] K. Takamura, H. Fischer, and N. R. Morrow, "Physical properties of aqueous glycerol solutions," *Journal of Petroleum Science and Engineering*, vol. 98, pp. 50–60, 2012.

[45] A. Hejna, P. Kosmela, K. Formela, Ł. Piszczyk, and J. T. Haponiuk, "Potential applications of crude glycerol in polymer technology–current state and perspectives," *Renewable and Sustainable Energy Reviews*, vol. 66, pp. 449–475, 2016.

[46] S. M. Hosseini-Nasab, M. Rezaee, M. Taal, and P. L. Zitha, "Investigation of foam flooding assisted by non-newtonian and novel newtonian viscosifying agents for enhanced oil recovery," *ACS omega*, vol. 8, no. 1, pp. 297–310, 2022.

[47] S. M. Hosseini-Nasab, P. L. Zitha, S. A. Mirhaj, and M. Simjoo, "A new chemical enhanced oil recovery method?," in *SPE International Conference on Oilfield Chemistry?*, p. D011S003R002, SPE, 2015.

[48] G. Ferreira, D. Souza, R. Lima, A. Lobato, A. Silva, and L. Santos, "Novel glycerin-based microemulsion formulation for enhanced oil recovery," *Journal of Petroleum Science and Engineering*, vol. 167, pp. 674–681, 2018.

[49] D. Steinigeweg and S. Schluecker, "Monodispersity and size control in the synthesis of 20–100 nm quasi-spherical silver nanoparticles by citrate and ascorbic acid reduction in glycerol–water mixtures," *Chemical Communications*, vol. 48, no. 69, pp. 8682–8684, 2012.

[50] R. Manno, V. Sebastian, S. Irusta, R. Mallada, and J. Santamaria, "Ultra-small silver nanoparticles immobilized in mesoporous sba-15. microwave-assisted synthesis and catalytic activity in the 4-nitrophenol reduction," *Catalysis Today*, vol. 362, pp. 81–89, 2021.

[51] T. M. D. Dang, T. T. T. Le, E. Fribourg-Blanc, and M. C. Dang, "Influence of surfactant on the preparation of silver nanoparticles by polyol method," *Advances in natural sciences: nanoscience and nanotechnology*, vol. 3, no. 3, p. 035004, 2012.

[52] N. T. Thanh, N. Maclean, and S. Mahiddine, "Mechanisms of nucleation and growth of nanoparticles in solution," *Chemical reviews*, vol. 114, no. 15, pp. 7610–7630, 2014.

[53] T. Liu, D. R. Baek, J. S. Kim, S.-W. Joo, and J. K. Lim, "Green synthesis of silver nanoparticles with size distribution depending on reducing species in glycerol at ambient ph and temperatures," *ACS omega*, vol. 5, no. 26, pp. 16246–16254, 2020.

[54] A. E. Díaz-Álvarez and V. Cadierno, "Glycerol: a promising green solvent and reducing agent for metal-catalyzed transfer hydrogenation reactions and nanoparticles formation," *Applied Sciences*, vol. 3, no. 1, pp. 55–69, 2013.

[55] A. Sinha and B. Sharma, "Preparation of copper powder by glycerol process," *Materials research bulletin*, vol. 37, no. 3, pp. 407–416, 2002.

[56] A. Sarkar, S. Kapoor, and T. Mukherjee, "Synthesis and characterisation of silver nanoparticles in viscous solvents and its transfer into non-polar solvents," *Research on Chemical Intermediates*, vol. 36, pp. 411–421, 2010.

[57] H. Shi, B. Song, R. Chen, Q. Zhang, G. Hu, J. Li, J. Wang, X. Meng, H. Wang, and Y. He, "Microfluidic-enabled ambient-temperature synthesis of ultrasmall bimetallic nanoparticles," *Nano Research*, vol. 15, no. 1, pp. 248–254, 2022.

[58] V. T. Noronha, A. J. Paula, G. Durán, A. Galembeck, K. Cogo-Müller, M. Franz-Montan, and N. Durán, "Silver nanoparticles in dentistry," *Dental Materials*, vol. 33, no. 10, pp. 1110–1126, 2017.

[59] S. Paul, P. Basak, R. Majumder, A. Mukherjee, J. Ghosh, S. Patra, and N. K. Jana, "Biochemical estimation of moringa oleifera leaf extract for synthesis of silver nanoparticle mediated drug delivery system," *Journal of Plant Biochemistry and Biotechnology*, vol. 29, pp. 86–93, 2020.

[60] K. Amreen and S. Goel, "Miniaturized and microfluidic devices for automated nanoparticle synthesis," *ECS Journal of Solid State Science and Technology*, vol. 10, no. 1, p. 017002, 2021.

[61] S. Bae, E. Jung, T. Yu, and T. S. Seo, "Investigation on the nucleation stage of palladium nanoparticles using a microfluidic droplet generator integrated with in situ sol-gel quencher," *Small*, vol. 14, no. 48, p. 1802851, 2018.

[62] R. Amen, A. Mukhtar, S. Saqib, S. Ullah, A. G. Al-Sehemi, S. E. H. Mehdi, M. Babar, and M. A. Bustam, "History and development of nanomaterials," in *Nanomaterials: Synthesis, Characterization, Hazards and Safety*, pp. 1–14, Elsevier, 2021.

[63] I. Lignos, S. Stavrakis, A. Kilaj, and A. J. deMello, "Millisecond-timescale monitoring of pbs nanoparticle nucleation and growth using droplet-based microfluidics," *Small*, vol. 11, no. 32, pp. 4009–4017, 2015.

[64] S. Gimondi, H. Ferreira, R. L. Reis, and N. M. Neves, "Microfluidic devices: A tool for nanoparticle synthesis and performance evaluation," *ACS nano*, vol. 17, no. 15, pp. 14205–14228, 2023.

[65] A.-G. Niculescu, C. Chircov, and A. M. Grumezescu, "Magnetite nanoparticles: Synthesis methods–a comparative review," *Methods*, vol. 199, pp. 16–27, 2022.

[66] N. E. Sunny, A. Kaviya, and S. V. Kumar, "Mechanistic approach on the synthesis of metallic nanoparticles from microbes," in *Agri-Waste and Microbes for Production of Sustainable Nanomaterials*, pp. 577–602, Elsevier, 2022.

[67] J. Polte, X. Tuaev, M. Wuithschick, A. Fischer, A. F. Thuenemann, K. Rademann, R. Kraehnert, and F. Emmerling, "Formation mechanism of colloidal silver nanoparticles: analogies and differences to the growth of gold nanoparticles," *Acs Nano*, vol. 6, no. 7, pp. 5791–5802, 2012.

[68] H. Liu, J. Huang, D. Sun, L. Lin, W. Lin, J. Li, X. Jiang, W. Wu, and Q. Li, "Microfluidic biosynthesis of silver nanoparticles: Effect of process parameters on size distribution," *Chemical engineering journal*, vol. 209, pp. 568–576, 2012.

[69] S. Gurunathan, K. Kalishwaralal, R. Vaidyanathan, D. Venkataraman, S. R. K. Pandian, J. Muniyandi, N. Hariharan, and S. H. Eom, "Biosynthesis, purification and characterization of silver nanoparticles using escherichia coli," *Colloids and Surfaces B: Biointerfaces*, vol. 74, no. 1, pp. 328–335, 2009.

[70] N. Hao, Y. Nie, and J. X. Zhang, "Microfluidic synthesis of functional inorganic micro-/nanoparticles and applications in biomedical engineering," *International Materials Reviews*, vol. 63, no. 8, pp. 461–487, 2018.

[71] J. C. Kurnia, A. Ahmadihosseini, and A. P. Sasmito, "Flow behavior and mixing of single-phase laminar newtonian miscible fluid in t-junction micromixer with twisted mixing channel-a numerical study," *Chemical Engineering and Processing-Process Intensification*, vol. 181, p. 109171, 2022.

[72] G. Yesiloz, M. S. Boybay, and C. L. Ren, "Effective thermo-capillary mixing in droplet microfluidics integrated with a microwave heater," *Analytical chemistry*, vol. 89, no. 3, pp. 1978–1984, 2017.

[73] J. Maeng, K. Yoo, S. Song, and S. Heu, "Modeling for fluid mixing in passive micromixers using the vortex index," *JOURNAL-KOREAN PHYSICAL SOCIETY*, vol. 48, no. 5, p. 902, 2006.

[74] P. R. Makgwane and S. S. Ray, "Synthesis of nanomaterials by continuous-flow microfluidics: a review," *Journal of Nanoscience and Nanotechnology*, vol. 14, no. 2, pp. 1338–1363, 2014.

[75] K.-J. Wu, G. M. D. V. Bohan, and L. Torrente-Murciano, "Synthesis of narrow sized silver nanoparticles in the absence of capping ligands in helical microreactors," *Reaction Chemistry & Engineering*, vol. 2, no. 2, pp. 116–128, 2017.

[76] D. J. Magdalene, D. Muthuselvam, and T. Pravinraj, "Microfluidics-based green synthesis of silver nanoparticle from the aqueous leaf extract of ipomea quamoclit l.," *Applied Nanoscience*, vol. 11, no. 7, pp. 2073–2084, 2021.

[77] T. Yang, J. Choo, S. Stavrakis, and A. de Mello, "Fluoropolymer-coated pdms microfluidic devices for application in organic synthesis," *Chemistry–A European Journal*, vol. 24, no. 46, pp. 12078–12083, 2018.

[78] A. Al-Halhouli, A. Alshare, M. Mohsen, M. Matar, A. Dietzel, and S. Büttgenbach, "Passive micromixers with interlocking semi-circle and omega-shaped modules: Experiments and simulations," *Micromachines*, vol. 6, no. 7, pp. 953–968, 2015.

[79] A. Toor, T. Feng, and T. P. Russell, "Self-assembly of nanomaterials at fluid interfaces," *The European Physical Journal E*, vol. 39, pp. 1–13, 2016.

[80] A. Toor, B. A. Helms, and T. P. Russell, "Effect of nanoparticle surfactants on the breakup of free-falling water jets during continuous processing of reconfigurable structured liquid droplets," *Nano letters*, vol. 17, no. 5, pp. 3119–3125, 2017.

[81] P. Pieranski, "Two-dimensional interfacial colloidal crystals," *Physical review letters*, vol. 45, no. 7, p. 569, 1980.

[82] F. Tu and D. Lee, "One-step encapsulation and triggered release based on janus particle-stabilized multiple emulsions," *Chemical Communications*, vol. 50, no. 98, pp. 15549–15552, 2014.

[83] L. Hu, M. Chen, W. Shan, T. Zhan, M. Liao, X. Fang, X. Hu, and L. Wu, "Stacking-order-dependent optoelectronic properties of bilayer nanofilm photodetectors made from hollow zns and zno microspheres," *Advanced materials*, vol. 24, no. 43, pp. 5872–5877, 2012.

[84] H. Fan and A. Striolo, "Nanoparticle effects on the water-oil interfacial tension," *Physical Review E*, vol. 86, no. 5, p. 051610, 2012.

[85] H. Hou, J. Li, X. Li, J. Forth, J. Yin, X. Jiang, B. A. Helms, and T. P. Russell, "Interfacial activity of amine-functionalized polyhedral oligomeric silsesquioxanes (poss): A simple strategy to structure liquids," *Angewandte Chemie*, vol. 131, no. 30, pp. 10248–10253, 2019.

[86] V. O. Ikem, A. Menner, A. Bismarck, and L. R. Norman, "Liquid screen: A novel method to produce an in-situ gravel pack," *SPE Journal*, vol. 19, no. 03, pp. 437–442, 2014.

[87] A. Böker, J. He, T. Emrick, and T. P. Russell, "Self-assembly of nanoparticles at interfaces," *Soft matter*, vol. 3, no. 10, pp. 1231–1248, 2007.

[88] P. Song, X. Mao, Y. Ren, H. Zeng, and Q. Lu, "Buckling effect of sole zeolitic imidazolate framework-8 nanoparticles adsorbed at the water/oil interface," *Langmuir*, vol. 36, no. 9, pp. 2322–2329, 2020.

[89] C. Huang, Z. Sun, M. Cui, F. Liu, B. A. Helms, and T. P. Russell, "Structured liquids with ph-triggered reconfigurability," *Advanced Materials*, vol. 28, no. 31, pp. 6612–6618, 2016.

[90] X. Lu and M. Wang, "High-performance nanogel-in-oils as emulsion evolution controller for displacement enhancement in porous media," *ACS Applied Materials & Interfaces*, vol. 15, no. 42, pp. 49554–49566, 2023.

[91] B. Ding, S. H. Ahmadi, P. Babak, S. L. Bryant, and A. Kantzas, "On the stability of pickering and classical nanoemulsions: Theory and experiments," *Langmuir*, vol. 39, no. 20, pp. 6975–6991, 2023.

[92] Y. Zhao, F. Peng, and Y. Ke, "Design and characterization of oil-in-water nanoemulsion for enhanced oil recovery stabilized by amphiphilic copolymer, nonionic surfactant, and laponite® rd," *RSC advances*, vol. 11, no. 4, pp. 1952–1959, 2021.

[93] A. A. Umar, I. B. M. Saaid, A. A. Sulaimon, and R. B. M. Pilus, "A review of petroleum emulsions and recent progress on water-in-crude oil emulsions

stabilized by natural surfactants and solids," *Journal of Petroleum Science and Engineering*, vol. 165, pp. 673–690, 2018.

[94] D. Arab, A. Kantzas, and S. L. Bryant, "Nanoparticle stabilized oil in water emulsions: A critical review," *Journal of Petroleum Science and Engineering*, vol. 163, pp. 217–242, 2018.

[95] A. Toor, S. Lamb, B. A. Helms, and T. P. Russell, "Reconfigurable microfluidic droplets stabilized by nanoparticle surfactants," *ACS nano*, vol. 12, no. 3, pp. 2365–2372, 2018.

[96] Y. Liu, C. Liu, Y. Li, Y. Xu, Y. Han, W. Pu, and L. Rui, "Experimental study of an amphiphilic graphene oxide based nanofluid for chemical enhanced oil recovery of heavy oil," *New Journal of Chemistry*, vol. 47, no. 4, pp. 1945–1953, 2023.

[97] Y. Zhang, G. Yesiloz, H. J. Sharahi, H. Khorshidian, S. Kim, A. Sanati-Nezhad, and S. H. Hejazi, "Geomaterial-functionalized microfluidic devices using a universal surface modification approach," *Advanced Materials Interfaces*, vol. 6, no. 23, p. 1900995, 2019.

[98] S. Betancur, C. M. Olmos, M. Pérez, B. Lerner, C. A. Franco, M. Riazi, J. Gallego, F. Carrasco-Marín, and F. B. Cortés, "A microfluidic study to investigate the effect of magnetic iron core-carbon shell nanoparticles on displacement mechanisms of crude oil for chemical enhanced oil recovery," *Journal of Petroleum Science and Engineering*, vol. 184, p. 106589, 2020.

[99] X. Zhao, F. Zhan, G. Liao, W. Liu, X. Su, and Y. Feng, "In situ micro-emulsification during surfactant enhanced oil recovery: A microfluidic study," *Journal of Colloid and Interface Science*, vol. 620, pp. 465–477, 2022.

[100] C. Mattax and J. Kyte, "Ever see a water flood," *Oil Gas J*, vol. 59, no. 42, pp. 115–128, 1961.

[101] J. Bonnet and R. Lenormand, "Constructing micromodels for study of multiphase flow in porous-media," 1977.

[102] K. Xu, P. Zhu, T. Colon, C. Huh, and M. Balhoff, "A microfluidic investigation of the synergistic effect of nanoparticles and surfactants in macro-emulsion-based enhanced oil recovery," *SPE Journal*, vol. 22, no. 02, pp. 459–469, 2017.

[103] A. Minakov, M. Pryazhnikov, Y. Suleymana, V. Meshkova, and D. Guzei, "Experimental study of nanoparticle size and material effect on the oil wettability characteristics of various rock types," *Journal of Molecular Liquids*, vol. 327, p. 114906, 2021.

[104] W. Lei, X. Lu, and M. Wang, "Multiphase displacement manipulated by micro/nanoparticle suspensions in porous media via microfluidic experiments: From interface science to multiphase flow patterns," *Advances in Colloid and Interface Science*, vol. 311, p. 102826, 2023.

[105] N. S. K. Gunda, B. Bera, N. K. Karadimitriou, S. K. Mitra, and S. M. Hassanizadeh, "Reservoir-on-a-chip (roc): A new paradigm in reservoir engineering," *Lab on a Chip*, vol. 11, no. 22, pp. 3785–3792, 2011.

[106] C. A. Conn, K. Ma, G. J. Hirasaki, and S. L. Biswal, "Visualizing oil displacement with foam in a microfluidic device with permeability contrast," *Lab on a Chip*, vol. 14, no. 20, pp. 3968–3977, 2014.

[107] C. Zhang, M. Oostrom, J. W. Grate, T. W. Wietsma, and M. G. Warner, "Liquid co2 displacement of water in a dual-permeability pore network micromodel," *Environmental science & technology*, vol. 45, no. 17, pp. 7581–7588, 2011.

[108] J. Peloquin, A. Kirillova, C. Rudin, L. Brinson, and K. Gall, "Prediction of tensile performance for 3d printed photopolymer gyroid lattices using structural porosity, base material properties, and machine learning," *Materials & Design*, vol. 232, p. 112126, 2023.

[109] H. S. Kim, J. H. Ryu, B. Jose, B. G. Lee, B. S. Ahn, and Y. S. Kang, "Formation of silver nanoparticles induced by poly (2, 6-dimethyl-1, 4-phenylene oxide)," *Langmuir*, vol. 17, no. 19, pp. 5817–5820, 2001.

[110] R. Baber, L. Mazzei, N. T. Thanh, and A. Gavriilidis, "Synthesis of silver nanoparticles in a microfluidic coaxial flow reactor," *RSC advances*, vol. 5, no. 116, pp. 95585–95591, 2015.

[111] V. Demchenko, S. Riabov, S. Kobylinskyi, L. Goncharenko, N. Rybalchenko, A. Kruk, O. Moskalenko, and M. Shut, "Effect of the type of reducing agents of silver ions in interpolyelectrolyte-metal complexes on the structure, morphology and properties of silver-containing nanocomposites," *Scientific Reports*, vol. 10, no. 1, p. 7126, 2020.

[112] Y. Nie, C. Jin, and J. X. Zhang, "Microfluidic in situ patterning of silver nanoparticles for surface-enhanced raman spectroscopic sensing of biomolecules," *ACS sensors*, vol. 6, no. 7, pp. 2584–2592, 2021.

[113] I. A. Iashchishyn, D. Sulskis, M. Nguyen Ngoc, V. Smirnovas, and L. A. Morozova-Roche, "Finke–watzky two-step nucleation–autocatalysis model of s100a9 amyloid formation: Protein misfolding as "nucleation" event," *ACS Chemical Neuroscience*, vol. 8, no. 10, pp. 2152–2158, 2017.

[114] K. Nathanael, P. Pico, N. M. Kovalchuk, A. D. Lavino, M. J. Simmons, and O. K. Matar, "Computational modelling and microfluidics as emerging approaches to synthesis of silver nanoparticles–a review," *Chemical Engineering Journal*, vol. 436, p. 135178, 2022.

[115] A. Zielińska, E. Skwarek, A. Zaleska, M. Gazda, and J. Hupka, "Preparation of silver nanoparticles with controlled particle size," *Procedia chemistry*, vol. 1, no. 2, pp. 1560–1566, 2009.

[116] L. Xu, J. Peng, M. Yan, D. Zhang, and A. Q. Shen, "Droplet synthesis of silver nanoparticles by a microfluidic device," *Chemical Engineering and Processing: Process Intensification*, vol. 102, pp. 186–193, 2016.

[117] O. Kašpar, A. Koyuncu, A. Pittermannová, P. Ulbrich, and V. Tokárová, "Governing factors for preparation of silver nanoparticles using droplet-based microfluidic device," *Biomedical Microdevices*, vol. 21, pp. 1–14, 2019.

[118] J. Sivasamy, T.-N. Wong, N.-T. Nguyen, and L. T.-H. Kao, "An investigation on the mechanism of droplet formation in a microfluidic t-junction," *Microfluidics and nanofluidics*, vol. 11, pp. 1–10, 2011.

[119] D. Liu, S. Cito, Y. Zhang, C.-F. Wang, T. M. Sikanen, and H. A. Santos, "A versatile and robust microfluidic platform toward high throughput synthesis of homogeneous nanoparticles with tunable properties," *Advanced Materials*, vol. 27, no. 14, pp. 2298–2304, 2015.

[120] M. Takesue, T. Tomura, M. Yamada, K. Hata, S. Kuwamoto, and T. Yonezawa, "Size of elementary clusters and process period in silver nanoparticle formation," *Journal of the American Chemical Society*, vol. 133, no. 36, pp. 14164–14167, 2011.

[121] X. Z. Lin, A. D. Terepka, and H. Yang, "Synthesis of silver nanoparticles in a continuous flow tubular microreactor," *Nano letters*, vol. 4, no. 11, pp. 2227–2232, 2004.

[122] S. He, T. Kohira, M. Uehara, T. Kitamura, H. Nakamura, M. Miyazaki, and H. Maeda, "Effects of interior wall on continuous fabrication of silver nanoparticles in microcapillary reactor," *Chemistry letters*, vol. 34, no. 6, pp. 748–749, 2005.

[123] P. Watts and C. Wiles, "Recent advances in synthetic micro reaction technology," *Chemical communications*, no. 5, pp. 443–467, 2007.

[124] J. Park, S. G. Kwon, S. W. Jun, B. H. Kim, and T. Hyeon, "Large-scale synthesis of ultra-small-sized silver nanoparticles," *ChemPhysChem*, vol. 13, no. 10, pp. 2540–2543, 2012.

[125] A. Prabhakar, I. Bansal, A. Jaiswar, N. Roy, and D. Verma, "A simple cost-effective microfluidic platform for rapid synthesis of diverse metal nanoparticles: A novel approach towards fighting sars-cov-2," *Materials Today: Proceedings*, vol. 80, pp. 1852–1857, 2023.

[126] D. T. Chiu, A. J. Demello, D. Di Carlo, P. S. Doyle, C. Hansen, R. M. Maceiczyk, and R. C. Wootton, "Small but perfectly formed? successes,

challenges, and opportunities for microfluidics in the chemical and biological sciences," *Chem*, vol. 2, no. 2, pp. 201–223, 2017.

[127] G. Tofighi, H. Lichtenberg, J. Pesek, T. L. Sheppard, W. Wang, L. Schöttner, G. Rinke, R. Dittmeyer, and J.-D. Grunwaldt, "Continuous microfluidic synthesis of colloidal ultrasmall gold nanoparticles: in situ study of the early reaction stages and application for catalysis," *Reaction Chemistry & Engineering*, vol. 2, no. 6, pp. 876–884, 2017.

[128] A. Soleymanzadeh, A. Rahmati, M. Yousefi, and B. Roshani, "Theoretical and experimental investigation of effect of salinity and asphaltene on ift of brine and live oil samples," *Journal of Petroleum Exploration and Production*, vol. 11, pp. 769–781, 2021.

[129] M. Adil, H. M. Zaid, and L. K. Chuan, "Electromagnetically-induced change in interfacial tension and contact angle of oil droplet using dielectric nanofluids," *Fuel*, vol. 259, p. 116274, 2020.

[130] N. Saxena, A. Kumar, and A. Mandal, "Adsorption analysis of natural anionic surfactant for enhanced oil recovery: The role of mineralogy, salinity, alkalinity and nanoparticles," *Journal of Petroleum Science and Engineering*, vol. 173, pp. 1264–1283, 2019.

[131] S. Iglauer, Y. Wu, P. Shuler, Y. Tang, and W. A. Goddard III, "New surfactant classes for enhanced oil recovery and their tertiary oil recovery potential," *Journal of Petroleum science and Engineering*, vol. 71, no. 1-2, pp. 23–29, 2010.

[132] Z. Niu, Z. Yang, Y. Chang, Y. Zhang, Y. Luo, X. Chen, and X. Zhao, "Numerical studies on displacement-imbibition process of pore-network extracted from the microfluidic chip," *Journal of Petroleum Science and Engineering*, vol. 215, p. 110686, 2022.

[133] A. Massimiani, F. Panini, S. L. Marasso, M. Cocuzza, M. Quaglio, C. F. Pirri, F. Verga, and D. Viberti, "2d microfluidic devices for pore-scale phenomena investigation: A review," *Water*, vol. 15, no. 6, p. 1222, 2023.

[134] M. Takai, T. Shirai, and K. Ishihara, "Surface functionarization of polydimethylsiloxane by photo-induced polymerization of 2-methacryloyloxyethyl phosphorylcholine for biodevices," *Journal of Photopolymer Science and Technology*, vol. 24, no. 5, pp. 597–602, 2011.

[135] R. M. Elamawi, R. E. Al-Harbi, and A. A. Hendi, "Biosynthesis and characterization of silver nanoparticles using trichoderma longibrachiatum and their effect on phytopathogenic fungi," *Egyptian journal of biological pest control*, vol. 28, no. 1, pp. 1–11, 2018.

[136] H. Zhang, M. Dong, and S. Zhao, "Experimental study of the interaction between naoh, surfactant, and polymer in reducing court heavy oil/brine interfacial tension," *Energy & fuels*, vol. 26, no. 6, pp. 3644–3650, 2012.

[137] H. Pei, G. Zhang, J. Ge, L. Jin, and X. Liu, "Analysis of microscopic displacement mechanisms of alkaline flooding for enhanced heavy-oil recovery," *Energy & Fuels*, vol. 25, no. 10, pp. 4423–4429, 2011.

[138] A. Mandal, A. Samanta, A. Bera, and K. Ojha, "Characterization of oil-water emulsion and its use in enhanced oil recovery," *Industrial & engineering chemistry research*, vol. 49, no. 24, pp. 12756–12761, 2010.

[139] P. Bedrikovetsk and M. Chumak, "Riemann problem for two-phase four-and morecomponent displacement (ideal mixtures)," in *ECMOR III-3rd European Conference on the Mathematics of Oil Recovery*, pp. cp–232, European Association of Geoscientists & Engineers, 1992.

Appendix A

Data

Appendix B

Code